*Advanced Sensor Research*

ADVANCED SENSOR RESEARCH Open Access

www.advsensorres.com

REVIEW OPEN ACCESS

# Organic and Metallacages for Chemical Sensing: Progress in Water-Compatible Systems

Rabia Zahid[1] | Martina Viola[2] | Maria Vittoria Balli[3] | Guillermo Moreno-Alcántar[4,5] | Pierre Picchetti[1]

[1]Institute of Nanotechnology (INT) Karlsruhe Institute of Technology (KIT), Karlsruhe, Germany | [2]Empa, Swiss Federal Laboratories for Materials Science and Technology, Laboratory for Biointerfaces, St. Gallen, Switzerland | [3]Department of Chemistry "Giacomo Ciamician", Alma Mater Studiorum – University of Bologna, Bologna, Italy | [4]Center for Cooperative Research in Biomaterials (CIC biomaGUNE), Basque Research and Technology Alliance (BRTA), Donostia-San Sebastian, Spain | [5]Department of Chemistry, Technical University of Munich, München, Germany

**Correspondence:** Guillermo Moreno-Alcántar (gmorenoalcantar@cicbiomagune.es) | Pierre Picchetti (pierre.picchetti@kit.edu)

**Received:** 28 September 2025 | **Revised:** 17 February 2026 | **Accepted:** 20 February 2026

**Keywords:** chemosensors | hybrid materials | metallacages | organic cages | supramolecular sensors

## ABSTRACT

Supramolecular cages are powerful tools for molecular recognition and sensing, using well-defined nanoscale cavities to encapsulate ions, small molecules, and biologically relevant guests with notable selectivity. Over the past three decades, these systems have progressed from simple conceptual assemblies to sophisticated covalent and organometallic architectures that operate in water as chemosensors, delivery vehicles, and separation p. Their analyte detection relies on diverse signal transduction mechanisms, including luminescence, circular dichroism, and Förster resonance energy transfer, enabling the sensing of anions, cations, chiral molecules, drugs, explosives, and environmental pollutants. Relative to classical receptors, cages offer notable advantages such as three-dimensional preorganization, modular functionalization, and the incorporation of multiple recognition sites within a single discrete framework. However, their broader implementation in real-world settings is still hampered, primarily by challenges in achieving sufficient stability in water and complex biological fluids. This review outlines design principles for water-stable cages, discusses analyte-specific and medium-related challenges, and surveys recent examples of water-compatible systems, including their integration into polymeric materials. Finally, we provide a perspective on next-generation cage-based chemosensors, emphasizing advanced readout strategies and potential applications in diagnostics, environmental monitoring, and biomedicine.

## 1 | Introduction

Over the last three decades, supramolecular cages have emerged as powerful platforms for host–guest chemistry [1], with applications from catalysis [2–9], sensing [10], separation [11, 12] to innovative (nano)medicines [13–16]. These well-defined three-dimensional nanoscale architectures typically consist of metal ions and organic linkers (metallacages, also referred to as metal–organic cages) or are constructed purely from covalently bonded organic linkers (organic cages), giving rise to discrete cavities. Such cavities can encapsulate ions, neutral molecules, or biologically relevant guests, enabling the design of chemosensors in which binding events are monitored or coupled to spectroscopic or electrochemical outputs. As a result, these cages have emerged as attractive candidates for synthetic chemosensor design, and, to emphasize their analogy to the receptors commonly invoked in biological recognition, we refer to the cage compounds described herein also as cagereceptors.

The use of cage-receptors for sensing applications has evolved through several distinct phases. Seminal works on synthetic macrocyclic systems, such as crown ethers, cryptates, and cavitands [17–25], as well as cyclic peptides [26–28] demonstrated the applicability of cyclic hosts for capturing and binding ions in

solution. Cage-receptor compounds offer distinctive advantages over classical synthetic receptors, including cryptands [20, 29], cyclodextrins [30–32], cucurbit [*n*]urils [33, 34], calix [*n*]arenes [35–38], pillar [*n*]arenes [39, 40], and cavitands [41–44], among others [45, 46]. Their three-dimensional cavities create size- and shape-matched environments for guest molecules, while their modular construction enables precise tuning of charge, polarity, and functionality, which clearly distinguishes them from conventional chemical probes [45, 47–49]. For example, control over the stereochemistry of metal–organic cages enables functions inherently linked to chirality, including stereoselective guest recognition and chiroptical behavior. In addition, cage-receptors can integrate multiple recognition motifs within a single architecture, allowing for cooperative binding and multifunctional sensing. Further, it is possible to further expand this design space by offering opportunities to introduce interior substituents that tailor the chemical environment of the cavity. In this review, we instead focus on systems classified as metal–organic cages and organic cages, which, among other distinctions, differ from crown ethers, cryptands or cavitands in that they form extended 3D host frameworks, metal–ligand or covalent in nature, that encapsulate guests within designable cavities through a variety of noncovalent interactions. [50, 51]

Early work in the 1980s and early 2000s established the fundamental ability of metal–organic cages to bind metal cations, anions, and neutral organic guests [52–55]. Seminal contributions, such as the dizinc bistren cages [56], highlighted the conceptual power of using a confined cavity for selective recognition in water. Subsequently, the introduction of new ligands and functional groups, such as triazolium units, porphyrins, or extended aromatic panels, expanded both the scope of detectable analytes and the range of optical signals [57–60]. Over the last decade, significant progress has been made, with cages now tailored to capture and detect cations, chiral molecules [11, 61–63], nitroaromatic compounds [64], antibiotics [65, 66], steroids [67–69], and gaseous pollutants like $SO_2$ and $CO_2$ [70]. In parallel, sensing mechanisms have expanded to include turn-on/turn-off luminescence, ratiometric emission, and circular dichroism (CD), among others, and the field has advanced to the point where cage-receptors are increasingly applied in bioimaging and therapeutic contexts [16, 71, 72]. Nonetheless, challenges remain. Many cage-receptors operate only in organic solvents or buffered aqueous mixtures, limiting direct application in biological or environmental contexts. Selectivity often diminishes in the presence of competing ions or complex sample matrices. Signal transduction is, in many instances, such as when luminescence is the main readout, prone to pitfalls including suboptimal signal-to-noise ratio, scattering, inner filter effects [73], and the possible generation of false positives, while long-term stability in physiological environments has not yet been fully established [74–77]. Furthermore, despite significant proof-of-concept demonstrations, the translation of cage-receptor-based sensors into deployable technologies, such as environmental monitoring devices or biomedical diagnostic tools, still remains to be achieved.

In 2020, an excellent review by Nitschke and co-workers highlighted design concepts for water-soluble cages in biomedical applications [78]. We aim to highlight developments since then, with a particular focus on sensing examples in which cage-receptors have been deployed for the detection of inorganic ions, biomolecules, and pollutants in water, as well as on the integration of cage-compounds into hybrid materials such as hydrogels, which have the potential to significantly enhance their stability and broaden their applicability. To this end, we first provide a brief discussion of design principles for water-soluble cage-receptors and functionalization strategies, before addressing the challenges associated with supramolecular detection in aqueous media, the interactions involved in analyte binding, and the specific difficulties encountered for the analyte classes discussed herein. We then present a selection of cage-receptors reported in recent years that are applicable in water or that exhibit promising features for future cage-receptor-based assays. Cage-receptors that have been employed to construct hybrid macroscale materials for sensing applications are also discussed. Finally, we offer a critical outlook on the progress achieved to date and on future directions for cage-receptors applicable in water, while highlighting current limitations.

## 2 | Design Principles for Recognition in Water

Molecular cage-receptors have been identified early in the development of supramolecular chemistry as discrete entities, which delimit a 3D cavity [50, 51]. This broad definition leaves enough space to include a wide variety of systems from the frontier of cryptands (initially studied by Jean-Marie Lehn) [20] to the size and complexity record-breaking metallacages of Fujita [79]. Commonly, the broad spectrum of systems that can be classified as cages is divided into two large categories, encompassing, on the one hand, purely organic structures and, on the other, metal-organic structures. These two categories have their extended reticular parallels in the covalent organic frameworks (COFs) [80, 81] and the metal-organic frameworks (MOFs) [82–90], respectively, but are clearly differentiated from them by being discrete entities rather than extended materials. The vast design and synthesis strategies that are available for both families, and comprehensive analyses of the structural features emerging from them, have been thoroughly revised [51, 91–97]. This section provides an overview of these strategies, highlighting systems applicable to sensing in water, and is complemented by a schematic summary in Scheme 1.

Disregarding their composition, the molecular design of most of the systems relies on the connection of strategically positioned union points by directional nodes (Figure 1) [98–100]. In the case of organic cages, the union points and nodes present complementary geometry in shape-persistent building-blocks and matching reactivity (i.e., alkyne-azide, amine-carboxyl, amine-carbonyl, boronic acid-diol, etc.), which allows the construction of the cage structure by the formation of a set of new covalent bonds [101]. Metallacages, in exchange, exploit the well-defined coordination geometry of metal ions, which are used as nodes to connect polytopic organic ligands with strategically positioned donor atoms [98]. In any case, the topologies of the building blocks will get combined to define the geometry of the obtained assembly with virtually an unlimited number of possibilities. Importantly, the successful formation of the cage structure, which is often the thermodynamically preferred product, is conditioned on the self-correction capabilities of the systems that allow the escape from kinetically trapped off-target structures. [102, 103] This process is

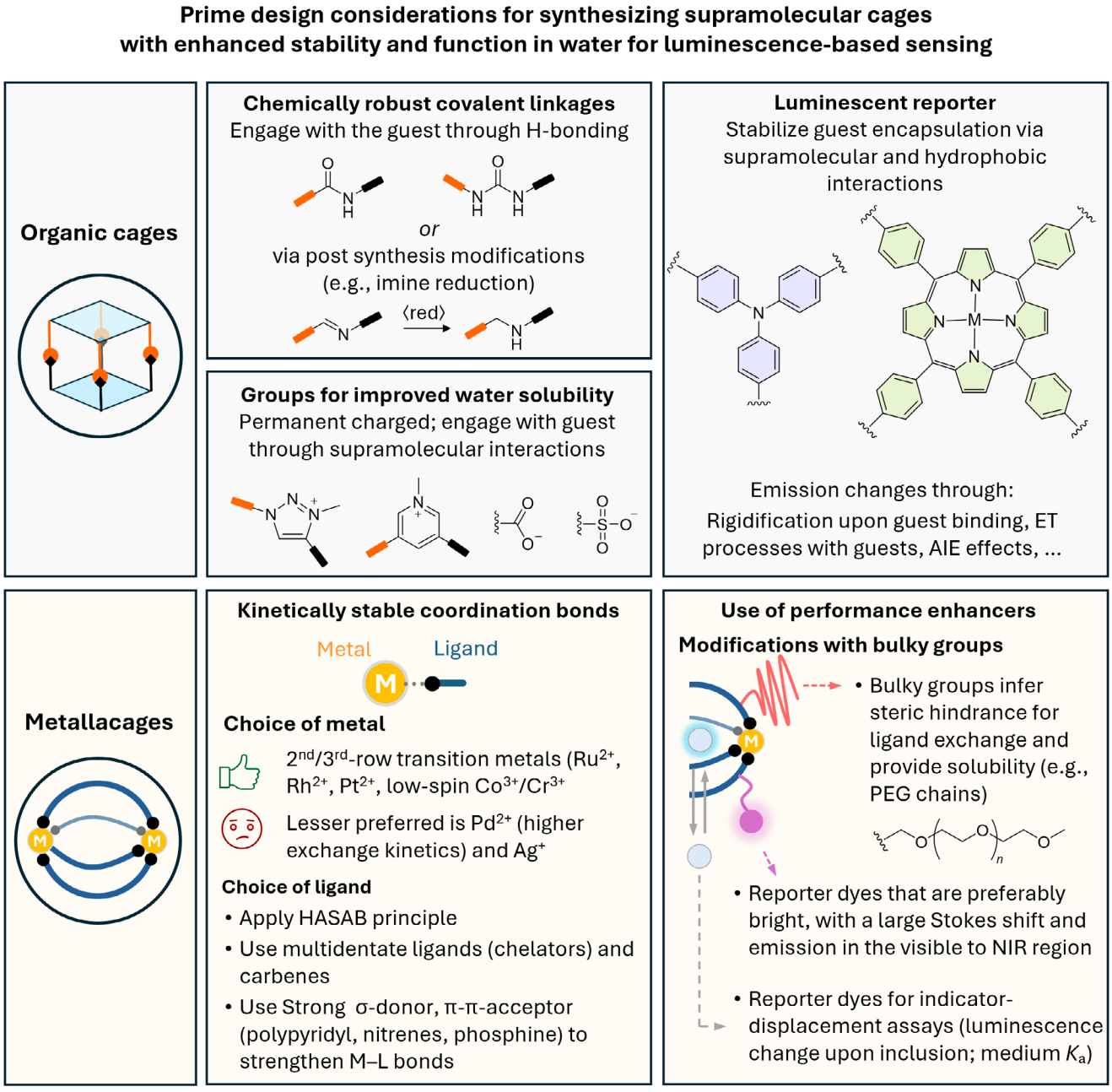


**SCHEME 1** | Design considerations for preparing cage receptors that are chemically robust in water and enable luminescence-based analyte detection.

granted by the use of dynamic reversible bonds. Thus, besides the basic design principles, cages intended to sensing applications in aqueous media must be engineered, balancing this self-corrective requirement with the need for stability not only toward water but also toward functional groups present in potential analytes and their matrices. Additionally, the cavity design for analyte-directed tuning, and the introduction of readout signals increase the complexity of the systems, which remains a challenge.

## 2.1 | Organic Cages

Organic cages are typically built via covalent chemistry and while this fact provides them in many cases with enhanced stability, making them capable of standing water environments, harsh temperatures, and a wide pH range [94, 95], the direct formation of covalent robust bonds via common synthetical methodologies, such as copper-catalyzed alkyne-azide cycloaddition (CuAAC) click reactions [104], nucleophilic substitutions [105], and amide bond formation (Figure 2a) [95] has the disadvantage of avoiding the self-correction of the structures, and off-path defective structures and undesired assemblies are often formed, decreasing the yield of the desired cage structures and requiring their purification via chromatographic methods. To decrease the formation of off-path structures, a strong preorganization should be imprinted in the building blocks either by the rigidification of the structures or by templating strategies (Figure 2b) [106–108].

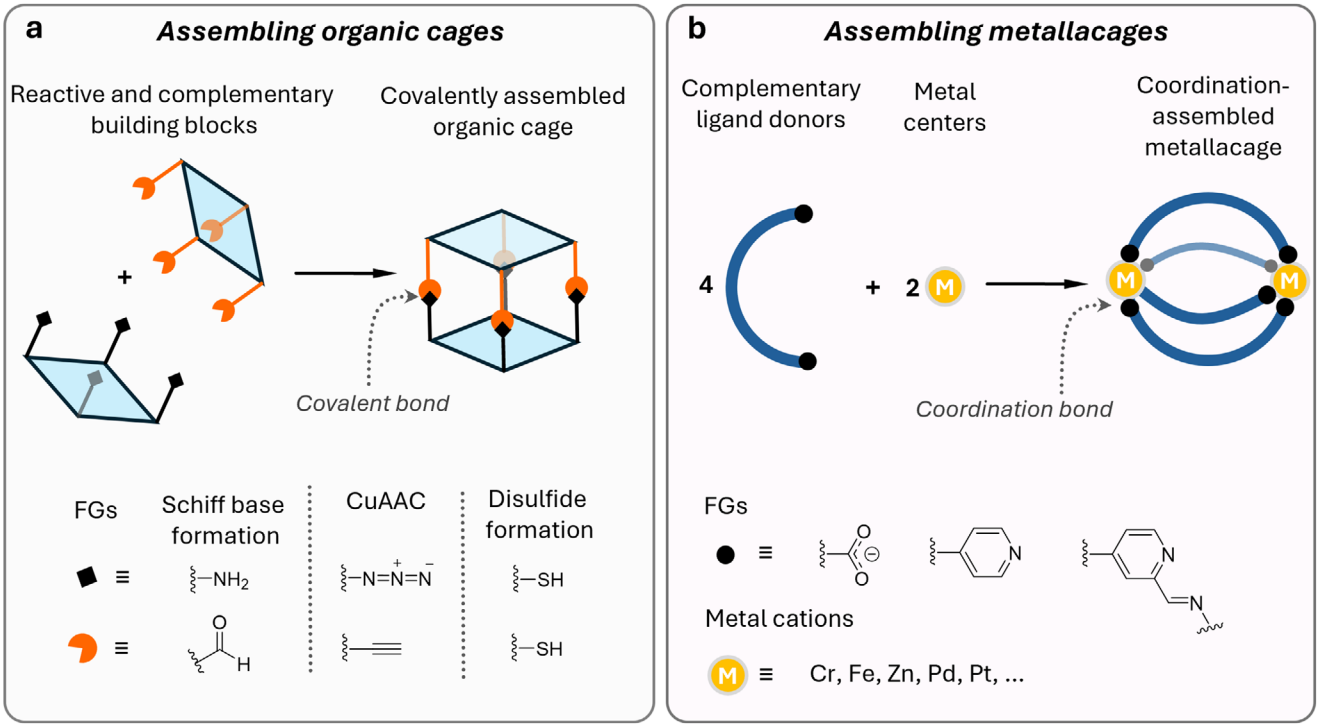


**FIGURE 1** | Schematic representation of the main synthetic strategies for organic cages and metallacages. (a) Organic cages are obtained via reactions between complementary organic panels that form covalent linkages, which can be under thermodynamic or kinetic control, to yield discrete covalently assembled cages. A broad range of reactive functionalities can be employed, including amines, aldehydes, azides, alkynes, and thiols. (b) Metallacages are constructed through coordination-driven self-assembly between electron-donating ligands and metal cations that act as Lewis-acidic acceptors. Typical ligands include pyridyl donors, Schiff-base motifs, and carboxylate groups, combined with a wide variety of transition-metal cations to afford well-defined supramolecular cages.

Reversible covalent linkages such as imines, boronic esters, or disulfide bridges have shown greater effectiveness in the selective formation of covalent cages. In particular, the combinatorial imine chemistry has been extensively applied to form dynamic and responsive cage structures. [111] Although these systems cannot be directly applied for sensing in aqueous conditions due to the favored imine hydrolysis, particularly under acidic regimes, strategies to lock the cages after formation (hence increasing their stability) have been developed, allowing the formation of covalent cages in high yields. For example, reduction to amines (Figure 2c) [109, 112] and Pinnick oxidation to amides [113], allow chemically robust and water-compatible systems which can be initially synthesized in non-aqueous media, profiting from dynamic bonds and later, after locking, transferred to aqueous environments for the final application.

Besides optimizing the synthesis of water-compatible systems with high yields, the low water solubility of purely covalent organic cages is often an issue. To address this, it is necessary to introduce high polarity or charged groups into the structure, which requires post-assembly modifications [114].

Besides purely organic structures, non-covalent linkage via highly directional interactions such as hydrogen-, halogen-, and chalcogen bonding interactions, have also been reported. While these interactions can stabilize cage-like structures in apolar solvents, they are much less prevalent in polar protic solvents, limiting the applicability of these systems without additional stabilization sources. H-bonding self-complementarity has been applied to assemble capsules following the work of Rebek on the homodimerization of glycourils [115]. This approach has been used with monomers including amides [116], ureas [117], and resorcinarenes [118]. However, this type of assembly is highly sensitive to competing H-bonding solvents and thus incompatible with water. A variation of this strategy is the assembly of heteromeric cages containing H-bond donors (e.g., carboxylic acids, alcohols, amines) and H-bond acceptors (e.g., amines, pyridines, carbonyls) in different building blocks. Charge-assisted hydrogen-bonded assemblies [119, 120] can also be formed, increasing the stability of the systems thanks to the electrostatic contribution to the overall building-block interaction, which competes more effectively with solvation, even achieving assemblies with considerable association constants in water ($\sim 10^4$ $M^{-1}$) as for the calix [4]arene capsule reported by Reinhoult (Figure 3a) [121]. Importantly, further stabilization can be promoted by the encapsulation of host molecules either by the recognition of additional interaction motifs within the cavity or by the release of high-energy water molecules and hydrophobic effects (Figure 3b) [122]. A similar approach has been proposed to stabilize chalcogen-bonded structures in an aqueous environment [123]. Recently, anion-coordination assemblies have also appeared as a special class of charge-assisted hydrogen-bonded structures. Nevertheless, the application of such systems as receptors in water remains challenging, as anion solvation energies preclude the formation of such assemblies [124].

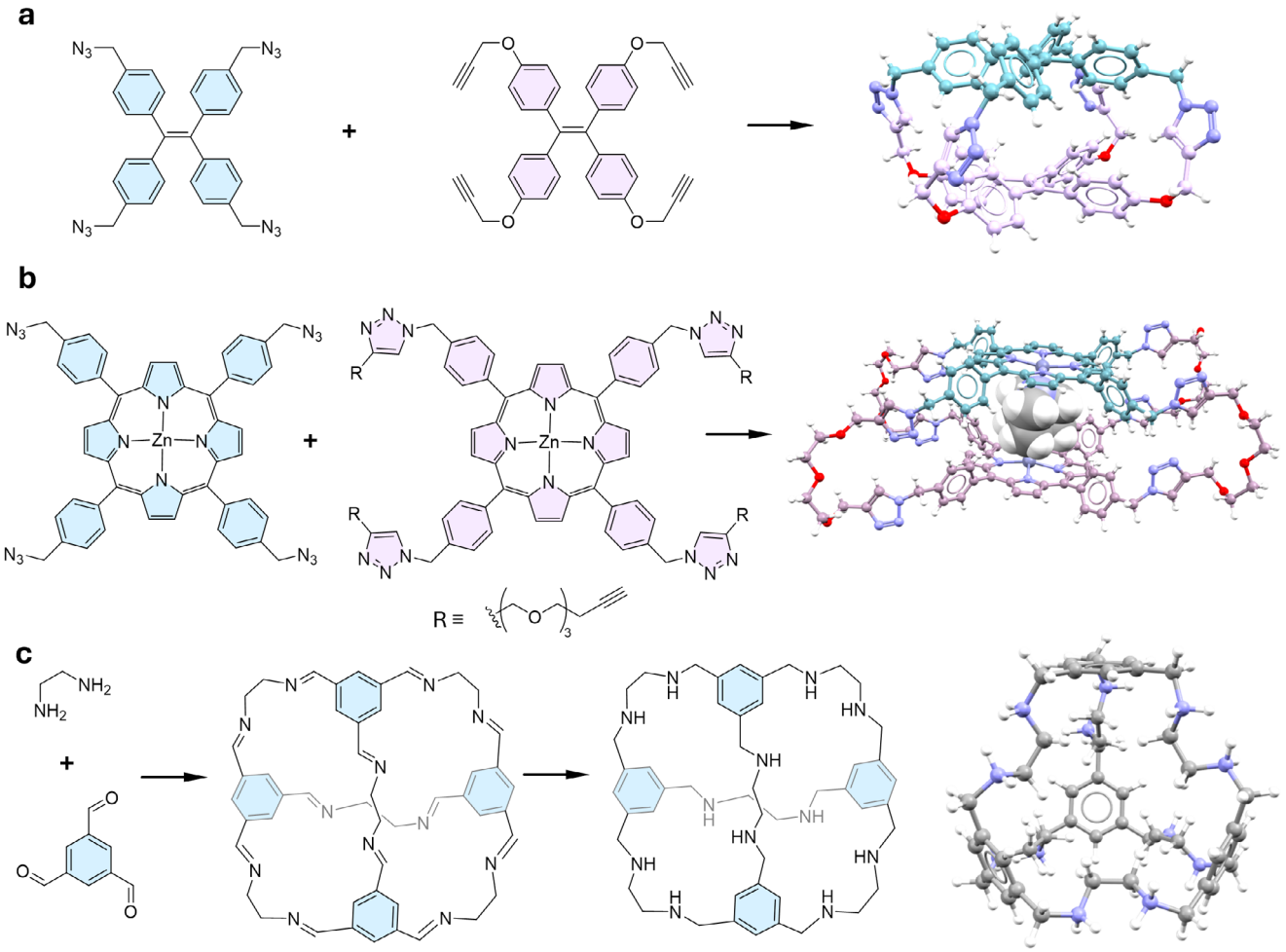


**FIGURE 2** | (a) Organic cage synthesis via heterodimerization of same-core building blocks bearing complementary reactive substituents, followed by CuAAC to form the cage structure (CCDC 2271519) [104]. (b) Templated CuAAC synthesis of a porphyrin organic cage, in which 1,4-diazabicyclooctane acts as a template during the click reaction (CCDC 1535914) [108] (c) Imine-condensation synthesis of a purely organic cage via dynamic self-assembly, followed by reduction to lock the cage structure (CCDC 800538) [109]. The molecular structures derived from X-ray crystallographic analysis were rendered using Mercury [110].

## 2.2 | Metallacages

Metallacages are built using coordination-driven self-assembly. This principle exploits the defined geometry of metal ions in coordination and organometallic compounds, combining them with predesigned ligands that place donor atoms in strategic positions. Overall, the combination of metal ions and ligands opens a huge area of the chemical space, making metallacages attractive when it comes to the exploration of newer applications. The design of metallacages that function effectively in aqueous media requires careful consideration of several structural features. First, although metal coordination generally meets the self-correction requirements of coordination-driven self-assembly, highly dynamic coordination cages can lack sufficient robustness for use in water and complex media. In general, when considering monodentate coordination, first-row transition metal centers display lower thermodynamic stability and [125], even more importantly, much higher kinetic lability than their 4d and 5d family members. Thus, not many examples of metallacages using monodentate coordination to first-row building motifs exist, and those available are not compatible with an aqueous environment. Instead, following the approach by Raymond [126], chelating ligands (O^O, N^O, N^N, etc.) are combined with octahedral first-row and even representative metal centers (e.g., Ga(III), Al(III), Ge(IV), Ti (IV)) to generate kinetically inert arrangements that have shown potential to be used in aqueous media [78]. These types of octahedral metal ions can be used to form tetrahedral or cubic cages, depending on the ligand coordination topology (Figure 4a,b) [127].

On the other hand, mono-coordinating ligands can be more favorably used to generate water-compatible metallacages when combined with heavier metals, as a clear example, N-heterocyclic ligands (pyridine, imidazole, triazole, quinoline, etc.) coordinate with square-planar Pd(II) centers, generating a vast structural diversity in size, shape, symmetry, and even component nature. [99] [129] Generally, Pd(II) cages are sufficiently stable in water. Although the typical polyaromatic nature of the ligands commonly used in this family of cages limits their solubility, new functionalization strategies and modifications to the cage composition that promise higher solubility are being explored. For example, water-soluble and stable $Pd_2L_4$ peptide cages (L = polyproline-based ligand; Figure 4c) have recently been synthesized [128, 130]. Although Pd(II) presents relatively high thermodynamic

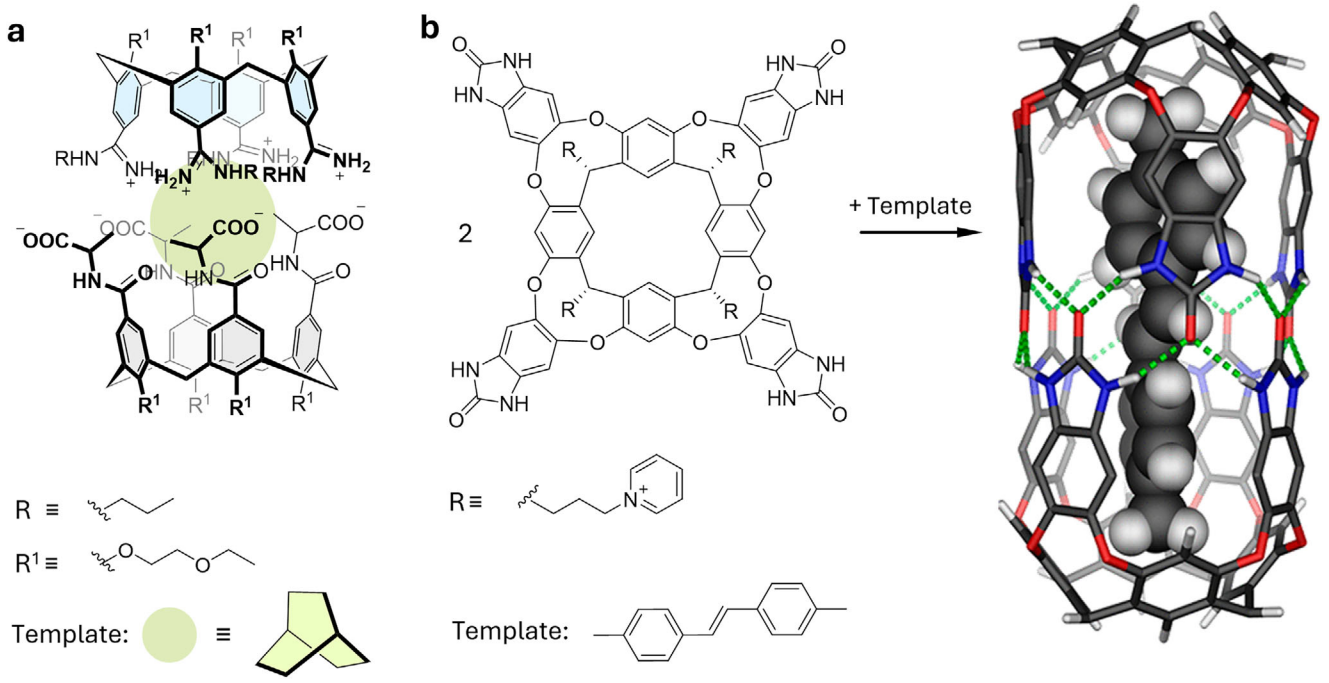


**FIGURE 3** | (a) Calix [4]arene capsule assembled via charge-assisted hydrogen bonding in water [121]. (b) Guest encapsulation-aided formation of a hydrogen-bonded cage-like structure in an aqueous environment. The shown 3D structure is a semi-empirical optimization of the host-guest complex, hydrogen bonds are displayed as green dotted lines. Adapted with permission [121]. Copyright 2013, American Chemical Society.

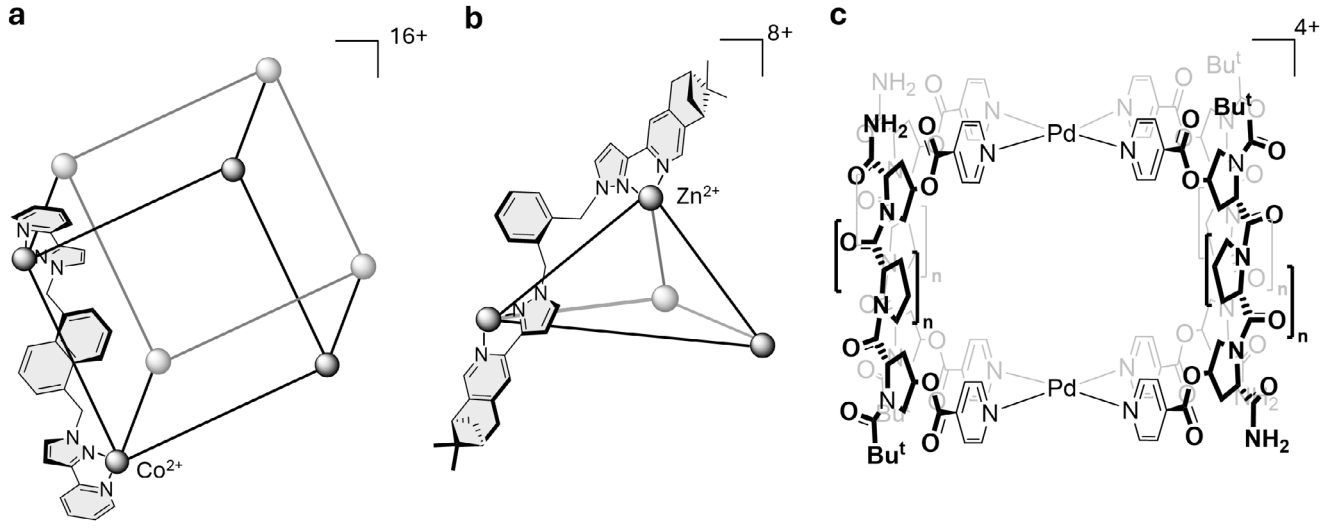


**FIGURE 4** | Common metallacage architectures using octahedral coordination nodes. (a) A cubic $Co^{2+}$-based arrangement and (b) a tetrahedral $Zn^{2+}$ cages [91]. (c) Polyproline-based $Pd_2L_4$ metallacages, which produce anisotropic cavities [128].

stability, giving good water compatibility, it is kinetically prone to ligand exchange reactions in the presence of nucleophiles bearing soft Lewis bases (as defined in Pearson's classification). Thiols, in particular, which are ubiquitous in biologically relevant environments, are strong scavengers of Pd(II), can rapidly disrupt the cage structure and limit its scope of application in biological samples. Pt(II) is an obvious isostructural alternative for directly translating the extensive knowledge available for generating complex and diverse Pd(II)-based self-assembled structures [131] in the development of broadly applicable sensor platforms. However, the enhanced kinetic stability of Pt(II) compounds necessitates high temperatures and long reaction times to allow structural self-correction in cage synthesis [132]. This compromises the compatibility of the process with certain ligands that would be of particular interest for sensing applications in water (such as the previously mentioned peptides or nucleic acids). Thus, alternative or optimized synthetic protocols need to be generated in this area. Additionally, as recently pointed out by Furukawa and coworkers [99], coordination cages based on square-planar metal centers and N-heterocyclic ligands find

parallels developed in the area of metal-organic cages (MOCs or metallacages; Figure 4b), which, instead of single metal ions, use secondary building units (SBUs) based on carboxylate-metal clusters, particularly the Cu(II) paddlewheel structure. However, this motif has only limited stability in water [133], and thus migrating to more water-stable SBUs is needed for the application of metallacages in aqueous sensing. From the expertise gained with water-compatible MOFs, which, unlike MOCs, are extended, crystalline, infinite coordination networks, one can propose the use of Zr(IV) oxoclusters as particularly suitable synthons, since their highvalent, hardacid character and robust metal–oxygen connectivity confer outstanding resistance to hydrolysis under demanding aqueous conditions [133]. Comparable stability can be achieved using Al(III)based trimeric or rodlike SBUs, as well as Cr(III) and Fe(III) $\mu_3$-oxo-centered clusters, which similarly combine strong metal–carboxylate bonding with high coordination connectivity to preserve integrity in water and even under extreme pH [133, 134], yet the application of these types of SBUs in the construction is scarce [135, 136].

Many other metallacage designs are available, including heteroleptic approaches combining binuclear metal-arenes to clip panel ligands [137], as well as strategies that exploit the charge-separation preferences of metal ions to form heteroleptic cages [138]. In all cases, similar thermodynamic and kinetic stability considerations have to be taken into account to ensure water compatibility. Recently, organometallic assemblies have attracted attention for medical-related applications [139], as organometallic bonds are kinetically inert and the higher covalent character of C—M bonds provides additional stabilization toward biological nucleophiles, providing a new platform for the development of sensors in aqueous and biological environment.

Solubility in water is not an issue only for organic cages that needs to be solved. Although most metallacages are intrinsically charged species, in many cases displaying high-charge density, their charged nature is insufficient to confer water solubility, as, owing to the common use of aromatic building blocks, the resulting structures also exhibit high hydrophobicity. While this characteristic may be positive to the inclusion of certain guests, it overall causes many of the available designs to display limited or no solubility in aqueous media, yet some of the less aromatic-extended systems, or those containing polar ligands, can also have appropriate solubility [78]. Functionalization of the cages' exterior (exo-functionalization) with diverse charged (e.g., R-$SO_3^-$) [140] or polar (alcohols [141, 142], polyethyleneglycol [141–143], peptides [144], carbohydrates) [145] groups to favor the solubility of the cage has been explored with positive outcomes.

### 2.3 | Cavity Design, Guest-Inclusion and Other Related Considerations

When compared to other receptors widely used in sensing applications (e.g., macrocycles or chelators), molecular cages offer the potential to design tailored cavities that increase affinity for analytes of different sizes, shapes, and properties [146]. However, to achieve this tuning of the cage receptor capabilities, fine synthetic strategies have to be developed [147]. Several avenues are currently being explored to achieve this aim. First, many available synthetic approaches employ high-symmetry synthons to increase assembly precision and minimize off-pathway products. An active trend in cage synthesis deals with the generation of higher-complexity assemblies with anisotropic and low-symmetry cavities [148, 149], achieved by the precise assembly of heteroleptic [150–153] (and heterometallic) [154] cages. These systems should ultimately recognize guests with the specific characteristic of biological systems. An advance in this direction is the use of peptides (Figure 4c) as building blocks in the construction of cages, which provide anisotropic cavities with potential specific recognition capabilities [155, 156].

A second avenue in cavity design is the development of functionalization methodologies [114]. Two general scenarios are possible. In the pre-assembly functionalization (PrAF), the building blocks used in the assembly of the cages are synthesized with functional units that will be included in the cage after the assembly. This approach has the advantage of having a broad set of organic synthesis tools that can be applied for the inclusion of such groups. However, pre-assembly modified synthons have higher complexity, many times including additional functional groups that may disturb the self-assembly of the cage structure by generating competing reactive paths or by simple steric effects, which are particularly important when the cavity is to be functionalized. Moreover, the functionalities included in the building blocks need to be stable to the reaction conditions required in the assembly process. This last consideration is of special importance in the case of peptides or other biomolecular-related functionalities, which are not necessarily compatible with high temperatures usually applied to favor the cage assembly self-correcting processes. On the other hand, post-assembly modification (PAM), i.e., functionalization of the cage after the self-assembly process, has the advantage of not compromising the self-assembly process itself. However, to be successful, the cage structure should be robust enough to withstand the chemical processes used for post-functionalization. While this is, in general, a minor issue in purely covalent organic cages without reversible bonds and has indeed been applied to increase cage stability, just a limited number of metallacages are suitable for PAM, and the possible reactions applicable to these scaffolds are also limited due to the incompatibility of metallacages with extreme conditions of pH and temperature, particularly in the presence of nucleophiles or additional metal ions [157, 158]. Thus, PAM of metallacages is limited to reversible processes, such as metal coordination and imine formation, or, in some cases, reactions with soft synthetic requirements (i.e., normal or inverse electron-demand Diels–Alder reactions, or click chemistry) [159].

For water-based sensing applications, metallacage cavities require functionalization to enable selective host–guest interactions, which can be achieved via PrAF or PAM, each presenting distinct challenges. PrAF leverages organic synthesis to incorporate functional groups into ligands before assembly but risks disrupting self-assembly through steric hindrance or competing coordination, particularly for cavity-targeted modifications, and demands compatibility with assembly conditions [158, 160]. On the other hand, PAM avoids these issues by modifying robust cages post-assembly [112, 157, 158], yet the chemical instability of metallacages to harsh conditions (pH, nucleophiles, competing metals) limits it to reversible chemistries (e.g., metal coordination, imine exchange) or

mild reactions (click chemistry, or inverse electron-demand Diels-Alder reactions). [159]

Ultimately, the main challenge in the application of cages in sensing in aqueous media relies, perhaps, in the matching of the adequate cage system to the targeted analyte. There is not, of course, a universal solution. While sensing in water (Section 3) has to overcome the large enthalpic stabilization granted by their favorable hydration [161, 162], which is hard to equal within common organic cavities via fewer hydrogen bonding or even electrostatic interactions. The detection of organic entities, such as neurotransmitters or drugs, which is favored by strong hydrophobic effects, requires mostly increased selectivity and fine design of receptor-like pockets capable of binding the desired target [163, 164].

## 3 | Aspects of Analyte Detection in Water

### 3.1 | Water—A Non-Innocent Solvent

Before examining specific examples of detection in solution, this chapter outlines the general aspects and challenges of sensing in aqueous media using cage-receptors. Many biologically relevant analytes occur in water and biofluids as ions, whose detection remains one of the major challenges in supramolecular receptor chemistry [165–167]. This arises for several reasons. From an analyte perspective, anions and cations in aqueous solutions are surrounded by hydration shells that are dynamic but strongly stabilizing, significantly masking interactions between the analyte and the receptor. For example, the relatively high dielectric constant of water ($\varepsilon \approx 78$ at 25°C) [168] can effectively screen ionic charges, thereby weakening Coulombic interactions. For a cage-receptor to bind such hydrated ions, forming, for example, a host-guest inclusion complex, without relying also on hydrophobic, $\pi$–$\pi$, dispersion, or hydrogen-bonding interactions, a large hydration energy must be overcome, and remains a challenging task (Figure 5a).

From the standpoint of the cage-receptor, several specific challenges arise when attempting detection in water, which affect not only the binding strength and selectivity toward analytes but also the chemical stability and solubility of the receptor itself. First, water solvates not only the analytes but also the receptor itself. Consequently, purely ionic cage–analyte interactions show limited affinity in water. Many receptor designs studied in organic solvents that rely on hydrogen bonding between the cage-receptor and analyte perform poorly in water, as strong competition from water molecules greatly weakens these interactions and limits their effectiveness for high-affinity binding [169, 170]. Earlier attempts to enhance H-bonding by installing quaternary ammonium groups into cage-receptor frameworks gave only modest affinities [171]. More effective designs increasingly rely on charge-assisted hydrogen bonding, using protonated ammonium, guanidinium, or amidinium donors to strengthen interactions with hydrogen-bond-accepting anions. [172–175] Additional interaction motifs that can be exploited for anion detection in water include halogen [176, 177] and chalcogen bonding [178], cation/anion–$\pi$ interactions [179, 180], amongst others. Several recent reviews provide comprehensive discussions of these interaction types, and readers seeking further detail are directed to those publications [166, 170, 181–183]. Despite these challenges, water is not merely an "adversary". The classical and non-classical hydrophobic effect [184, 185], for instance, can drive weakly interacting molecules in organic solvents to associate strongly in water, a principle effectively exploited by many synthetic macrocyclic receptors.

From the standpoint of the receptor, chemical stability in water, solubility, and, most importantly, from a detection-performance perspective, obtaining specificity represents a major challenge (Figure 5b). Chemical stability becomes an issue when the cage-receptor constitutes a framework containing hydrolysable linkages such as imines or hydrazones, which indeed are prominent motifs in organic cages. In this context, the use of intrinsically more resilient analogues, such as oximes or trialkylhydrazonium derivatives [186], offer a valuable strategy to improve hydrolytic stability. Other weak points can be metal centers that are prone to ligand-exchange reactions, particularly with biomolecules such as thiols, if the metal–ligand bonds are not kinetically stable enough. As in the case of metallacages, the use of kinetically more stable metal–ligand linkages is therefore an important design consideration. For this reason, second- and third-row d-block elements are often preferred as metal centers, as they can form stronger coordination bonds, according to the hard–soft acid–base principle (HSAB) [187], between soft metal ions (e.g., $Pt^{2+}$, $Pd^{2+}$) and soft donor ligands (e.g., phosphines, pyridines) [78]. Such interactions lead to slower exchange kinetics and thus higher kinetic stability, although achieving complete inertness remains an unresolved challenge to date.

Aqueous and biological samples contain many competing ions at substantially high micro- and millimolar concentrations, while the analytes of interest may be present only in the nanomolar to micromolar range. This means that extraordinarily high binding affinities from the cage-receptor and selectivity are required, levels that are rarely achievable with current receptor designs in water.

### 3.2 | Analyte Specific Challenges

#### 3.2.1 | Inorganic Analytes

Only a limited subset of metal cations is essential for human physiology. The major electrolytes $Na^+$, $K^+$, $Ca^{2+}$, and $Mg^{2+}$ govern osmotic balance, membrane potentials, and cellular signaling, and typically occur at millimolar concentrations in the human body [45]. Trace metals such as $Mn^{2+,3+,4+}$, $Fe^{2+,3+}$, $Co^{2+,3+}$, $Cu^{+,2+}$, $Zn^{2+}$, and $Mo^{4+,6+}$ function as enzymatic cofactors and are generally present only in the micro- to nanomolar range [188–190], with Fe representing a notable exception due to its higher abundance in blood and typically found in mM concentratons [45]. Perturbations in the levels of either group are closely linked to electrolyte disorders and metal-homeostasis diseases. By contrast, metal cations such as $Hg^{2+}$, $Pb^{2+}$, $Cd^{2+}$, and $As^{3+}$ are intrinsically toxic, owing to their strong affinity for thiol, phosphate, and amide groups, which disrupts protein structure and enzyme function and leads to severe neurotoxic, nephrotoxic, or carcinogenic effects [191]. $Al^{3+}$ is similarly monitored because of suspected neurotoxicity [192]. Overall, alkali and alkaline-earth cations are simple, hard Lewis acids with closely similar radii

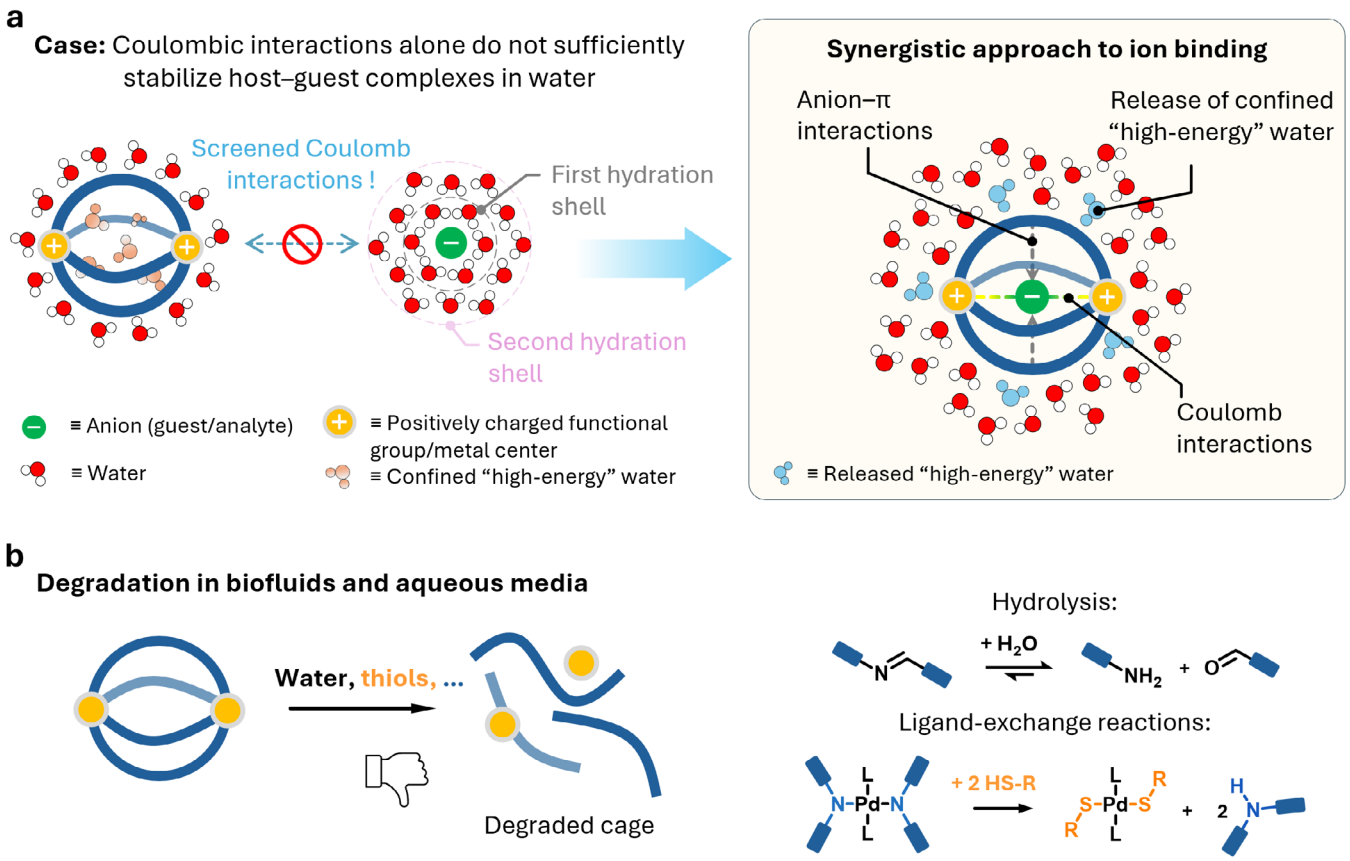


**FIGURE 5** | (a) Schematic representation of the synergistic design principle in supramolecular ion recognition, highlighting the introduction of multiple noncovalent interactions within a cage-receptor for anion binding. For anion-encapsulating cages operating in aqueous media, Coulombic interactions alone are typically insufficient to afford a stable host–guest complexes, because hydration shells strongly attenuate purely electrostatic binding. By contrast, receptors engineered to engage a combination of interactions, for example, anion–$\pi$, electrostatic, and the (non)classical hydrophobic effect, can achieve markedly enhanced binding strength and selectivity. Such cooperative interplay between distinct supramolecular forces translates into higher apparent binding affinities and, consequently, improved performance in ion sensing applications. (b) Another persistent limitation arises from the chemical instability of cage-receptors in aqueous and biological environments. For instance, imine-based cages are prone to hydrolysis in water, while metal–ligand cages may undergo ligand exchanges (e.g., with thiols), ultimately compromising structural integrity and binding function.

and hydration energies within each group. As for the selectivity, cage-receptors generally struggle to discriminate between ions of similar size and charge density (e.g., $K^+$ vs. $Na^+$ or $Cl^-$ vs. $Br^-$) in aqueous solution (Figure 6a). As a result, receptors that rely primarily on electrostatic attraction and size/shape complementarity often struggle to differentiate between, for example, $Na^+$ and $K^+$ or $Mg^{2+}$ and $Ca^{2+}$ in water. For first-row transition metal cations, the richer coordination chemistry, defined by preferred geometries, ligand-field stabilization, HSAB matching, and distinct redox behavior, provides additional design handles that can be exploited to achieve much higher selectivity than is typically possible for s-block cations. Soft, highly polarizable heavy-metal cations such as $Pb^{2+}$, $Hg^{2+}$, and $Cd^{2+}$ display distinct coordination and reactivity preferences compared to hard or borderline metal ions, as shown for example by their pronounced thiophilicity with a tendency to form thermodynamically robust complexes in aqueous media with sulfur ligands.

Among inorganic anions of biomedical relevance, $Cl^-$ is the principal extracellular species (present at high mM concentrations) and a key indicator of renal and acid–base balance [193]. $HS^-$ contributes to vascular and neural signaling [194], while $NO_3^-$ and $NO_2^-$ regulate NO availability in the body [195], influencing blood-flow regulation and cell signaling and serving as biomarkers of oxidative stress. Phosphates are especially important: present at ~1 mM in serum [196], essential for energy metabolism and nucleic acids, dysregulated in renal and bone disease [197], and a major environmental pollutant driving eutrophication [198]. Its strong hydration and multiple protonation states make selective binding in water particularly difficult for cage-receptors (Figure 6a). Highly toxic anions such as $CN^-$ and the related biomarker $SCN^-$ [199], as well as $F^-$ [200], which is beneficial only at low concentrations, further demonstrate the analytical need for receptors capable of distinguishing closely related inorganic anions in complex aqueous settings.

### 3.2.2 | Organic Analytes

Detection of organic analytes in aqueous and biological media poses distinct analytical challenges yet is generally more straightforward than the determination of inorganic cations and anions. In living systems, a vast array of organic molecules, ranging from metabolites such as neurotransmitters to steroid hormones,

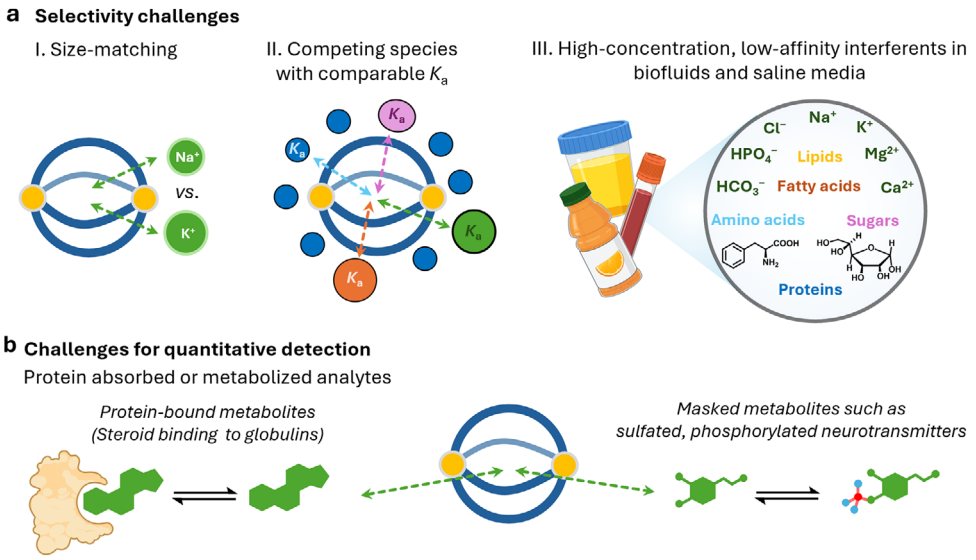


**FIGURE 6** | Schematic representation of key performance-limiting challenges encountered by cage-receptors in sensing applications using real-world samples. (a) Cage-receptors often face selectivity issues due to matrix components that share similar size, charge, or binding affinity with the target analyte. This problem becomes particularly pronounced in complex biological matrices such as blood or serum, where numerous interferents, often present at much higher concentrations than the analyte, significantly hamper reliable detection. (b) Quantitative analysis is further complicated by the fact that cage-receptors are typically designed to bind the "free" analyte species. In practice, however, many targets, such as steroids bound to transport proteins or neurotransmitters present as phosphorylated or sulfated derivatives, exist in chemically modified or sequestered forms, reducing effective receptor binding.

are present only in trace amounts, often at low-nanomolar concentrations [45, 201]. This imposes stringent performance requirements on cage-receptors, which must combine high affinity with high selectivity for analytes (Figure 6a). The catecholamine neurotransmitters serotonin, dopamine, adrenaline, and norepinephrine exemplify this issue as their close structural resemblance severely restricts the number of discriminating interactions available to a cage-receptor [202–205]. From a supramolecular perspective, such narrow physicochemical differences limit the design space for differential binding motifs. Adding further complexity for reliable detection with cage-receptors is the fact that many intracellular metabolites and drugs exist in phosphorylated or glycosylated forms, or undergo additional metabolic transformations such as sulfation or acetylation, among others (Figure 6b) [206–208], which increase their charge density, hydration, and steric bulk. This highlights two relevant cases for important biomarkers, as dopamine in human serum circulates predominantly as dopamine-4-sulfate [209–211], and estrogens are likewise largely absent in their free form, with roughly 97% of circulating estrogen bound to plasma proteins [212]. Furthermore, metabolites and drugs, as well as clinically relevant toxins, pesticides, and illicit drugs, must be detected with high fidelity in complex matrices such as blood, saliva, wastewater, or plant samples. Their metabolic transformation further complicates analysis and poses a significant challenge for cage-receptors, which must distinguish between parent molecules and their often abundant, structurally altered derivatives to achieve accurate detection. Many organic analytes also occur at low-nM to low-μM concentrations and reside in protein-rich environments that markedly attenuate host–guest interactions.

Organic ions often feature aromatic rings, alkyl chains, heteroatoms, or other functional groups that provide multiple interactions for supramolecular recognition. These moieties enable receptors to exploit $\pi$–$\pi$ stacking, cation–$\pi$ and anion–$\pi$ interactions [213], hydrogen bonding [214, 215], and dispersion interactions [216, 217], which can occur either inside the cavity of a cage or along its external walls. Importantly, the classical hydrophobic [184] effect plays a central role by providing strong entropic contributions to the binding event with the cage-receptor. Beyond the classical hydrophobic effect, the binding of organic ions often displaces structured water molecules, providing enthalpic stabilization through favorable analyte–receptor interactions and an entropic gain from water release [185]. Together, these contributions lower the energetic cost of desolvation and can confer both higher affinity and improved selectivity. Consequently, organic cations and anions, particularly those with aromatic or lipophilic moieties, are often more effectively recognized by cage-receptors in aqueous solutions, making them attractive targets for sensing applications. Carbohydrates constitute another important class of molecular targets that remain challenging for cage-receptors to bind selectively in water, owing to their complex and highly diverse chemical structures. As a consequence, association constants in aqueous media are typically modest (often not exceeding the $10^3$ $M^{-1}$ range) [218], and luminescent sensing systems for carbohydrates are correspondingly scarce, particularly those that operate reliably in biofluids. Effective strategies for carbohydrate recognition in water by supramolecular receptors commonly combine extended aromatic surfaces, capable of hydrophobic and CH-$\pi$ interactions, with polar functionalities that engage in hydrogen bonding. Electrostatic interactions and hydrophobic effects can also play significant roles. In this context, the cage-receptor reported by the Davis group, which incorporates six N-H···O hydrogen-bond donor urea or amide units within the cage pillars, achieves relevant saccharide binding in aqueous solution [219–221]. Comprehensive reviews on biomimetic car-

bohydrate recognition and synthetic receptors for saccharides by Prof. Anthony Davis [218], as well as Tan and coworkers [222], will therefore not be discussed in detail here, and interested readers are referred to the reviews cited herein. Instead, only the most recent designs featuring a luminescent readout are presented in this review.

Finally, non-canonical nucleic acid structures have recently emerged as an additional analyte class for detection with metallacages as they can stabilize DNA junctions and G-quadruplexes (G4s) through electrostatic attraction to the phosphate backbone, $\pi$-stacking with exposed bases or G-tetrads, hydrogen bonding, and shape-complementary encapsulation of the nucleic acid motif. A more detailed discussion of these systems will be presented in Section 5.

## 4 | Sensing Examples in Water Using Synthetic Cage-Receptors

Supramolecular chemistry [223] offers substantial promise for the development of new analytical tools that enable rapid, cost-effective sensing technologies [224], with the potential to simplify both signal readout and sample preparation for practical point-of-care applications. This promise stems from the use of synthetic, "designer" receptors, which can be prepared entirely in the laboratory, from receptor synthesis to the implementation of sensor assays that are, in principle, compatible with large-scale production and commercialization. Compared with established analytical techniques such as high-performance liquid chromatography, these receptor-based sensing platforms can markedly reduce preparation costs and operational complexity, allowing their use by non-specialized personnel [45]. In this context, synthetic cage-receptors can make a significant contribution to the realization of truly affordable point-of-care diagnostics. If successfully translated, such systems could rapidly provide a broad range of low-cost sensors for analyte detection at the presumptive screening level [225], for example in emergency or control settings. Potential applications include the rapid identification of illicit explosive substances in law-enforcement contexts, first-aid scenarios involving unconscious individuals suspected of drug overdose, or the on-site detection of hazardous drug adulterants such as fentanyl [226]. Beyond these immediate applications, cage-receptors are also expected to advance biomedical diagnostics more broadly, as already exemplified by crown-ether-based sensor cassettes for ion detection in blood that have successfully reached the market [227]. Beyond biomedical uses [16, 78, 228], this aspect is particularly important in the field of environmental sensing [201, 229]. Preventing disease caused by pollutants that enter the food chain through human activity remains both urgent and highly challenging [201]. Destructive agricultural practices and poorly managed or inadequately regulated industrial waste discharges highlight the pressing need for new sensors that are simple, robust, and effective, offering accessible technologies for real-world monitoring. Finally, advances in sensing technologies are expected to substantially benefit plant sciences, from the detection of pesticides to the development of luminescent tools for live-cell imaging in plants [201]. These approaches can support comprehensive environmental monitoring of ecosystems, enable the visualization of plant processes relevant to biotechnology, and aid in uncovering new metabolic pathways and metabolite transport mechanisms within plant systems.

The examples discussed herein are summarized in Table 1, which reports their analyte scope and key performance parameters, including the type of targeted analyte, binding affinities, detection range, limit of detection achieved, solvent system used, and primary detection mode. Table 2, instead, highlights representative optical cage-receptor systems featuring absorbance or luminescence-based readouts, detailing their chromophoric units, photophysical properties, targeted analyte classes, and the major underlying binding interactions.

### 4.1 | Sensing Inorganic Species

#### 4.1.1 | Inorganic Anions

Luminescence-based readouts are generally favored in chemical sensing, as they typically provide superior sensitivity, lower limits of detection, and the capability for ratiometric or time-resolved measurements that reduce background interference. Nonetheless, optical sensors that rely on analyte-induced color changes in the porphyrin Soret band [230] remain promnent [231], since the large molar absorption coefficient (up to $10^5$ $M^{-1}{\cdot}cm^{-1}$) [232] and distinct spectral shifts enable straightforward, rapid, and even naked-eye detection using simple instrumentation. In this respect, Beer and co-workers, introduced triazole- and triazolium-functionalized $Zn^{2+}$ metalloporphyrin cages (**R1** and **R2** in Figure 7) that achieve effective anion binding through a combination of C–H···anion hydrogen bonding and the Lewis acidity of the $Zn^{2+}$ centers. The binding event is monitored via shifts in the Soret band of the absorption spectrum. The neutral receptor **R1** binds hard/basic anions in organic media ($F^-$, $Cl^-$, $AcO^-$, $H_2PO_4^-$, $SO_4^{2-}$), whereas heavier halides show only weak responses. This selectivity reflects the strong polarization-dependent interaction between the porphyrin core and charge-dense anions. Introducing cationic triazolium units in **R2** significantly enhances anion binding under aqueous conditions. For example, at 15% water content in acetone, sulfate binding is retained with minimal competition from monovalent anions.

The design of luminescent cage receptors often employs triphenylamine moieties, [233] which show reduced luminescence when coordinated to transition-metal ions but become emissive upon release from the assembly. Yu and co-workers reported luminescent hexanuclear $Pd^{2+}$ cages (**R3**, Figure 8) constructed from tris(4-(1H-pyrazol-3-yl)phenyl)amine and dipalladium(II, II) nodes to give water-compatible assemblies $[(N^{\wedge}N)_6Pd_6L_2]^{6+}$ [234]. Coordination to $Pd^{2+}$ quenches the emission of the triphenylamine moieties, creating a low-background system suitable for turn-on sensing. In ACN/$H_2O$ (1:2, *v*/*v*), the cages displayed a strong luminescence enhancement (~30-fold) upon addition of $HSO_3^-$. Other anions, including $SO_4^{2-}$, $HSO_4^-$, $NO_2^-$, $NO_3^-$, $F^-$, $Br^-$, $I^-$, and $SCN^-$, induce negligible changes, confirming high selectivity for $HSO_3^-$. Excess bisulfite eventually causes quenching, consistent with competitive $Pd^{2+}$ coordination and partial cage decomposition. The water compatibility of **R3** was attributed to the intrinsic robustness of their coordination framework, where strong Pd—N bonds, multidentate chelation, and the stabilizing influence of the bimetallic Pd(II, II) corners

**TABLE 1** | Representative cage-receptors discussed in this review are summarized, together with their reported binding affinities toward the respective analytes, detection ranges, limits of detection, solvents or solvent mixtures employed, and the detection methods used to generate a diagnostic signal for analyte sensing.

| Cage-receptor | Analyte and Binding affinities ($K_a$) | Conc. range | LoD | Solvent | Main detection method | Reference |
|---|---|---|---|---|---|---|
| **R1** and **R2** | Fluoride ($F^-$), chloride ($Cl^-$), bromide ($Br^-$), iodide ($I^-$), acetate ($AcO^-$), dihydrogen phosphate ($H_2PO_4^-$), sulfate ($SO_4^{2-}$); $K_a$: $10^4$–$10^5$ $M^{-1}$ | at 2.0 μM | n.a. | Acetone/$H_2O$ (1:1) | Absorption | [311] |
| **R3** | Bisulfite ($HSO_3^-$) | 10.0–200.0 μM | n.a. | ACN/$H_2O$ (1:2) | Luminescence | [234] |
| **R4** | Acetate ($AcO^-$), phosphate ($PO_4^{3-}$), hydroxide ($OH^-$) | 200.0–800.0 μM | n.a. | DMSO | Absorption, luminescence | [235] |
| **R5** | Oxalate ($C_2O_4^{2-}$), sulfate ($SO_4^{2-}$), acetate ($AcO^-$); $K_a$: $2\times10^6$ $M^{-1}$ ($C_2O_4^{2-}$), $2\times10^4$ $M^{-1}$ ($SO_4^{2-}$), $1.5\times10^3$ $M^{-1}$ ($AcO^-$) | n.a. | n.a. | $H_2O$ | NMR | [237] |
| **R6** | Sulfate ($SO_4^{2-}$), selenate ($SeO_4^{2-}$), hydrogen phosphate ($HPO_4^{2-}$), oxalate ($C_2O_4^{2-}$), chloride ($Cl^-$); $K_a$: $>5\times10^9$ $M^{-1}$ ($SO_4^{2-}$ in DMSO); $3.8\times10^4$ $M^{-1}$ ($SO_4^{2-}$ in 50% $H_2O$); 66 $M^{-1}$ ($SO_4^{2-}$ in $H_2O$) | n.a. | n.a. | $H_2O$ and DMSO/$H_2O$ mixtures | NMR | [238] |
| **R7** | Fluoride ($F^-$) | 300.0 μM | n.a. | Chloroform | Absorption | [239] |
| **R8** | Acetate ($AcO^-$), azide ($N_3^-$), fluoride ($F^-$), chloride ($Cl^-$); | 0.052 – 5770.0 μM | n.a. | ACN | Absorption, luminescence | [241] |
| **R9** | Fluoride ($F^-$), chloride ($Cl^-$), acetate ($AcO^-$), azide ($N_3^-$), nitrate ($NO_3^-$); $K_a$: $10^4$ $M^{-1}$ | n.a. | n.a. | ACN-$d_3$/DCM-$d_2$ with added $H_2O$, lipids | NMR and luminescent ion transport assays | [242] |
| **R10** | Chloride (Cl–) $K_a$: ~$10^5$ $M^{-1}$ (in HEPES buffer) | mM range | n.a. | HEPES buffer | NMR | [244] |
| **R11** | Lanthanum(III) ($La^{3+}$) | 10.0–100.0 μM | n.a. | $H_2O$ | Luminescence | [245] |
| **R12** | Iodide ($I^-$), copper(II) ($Cu^{2+}$); | $I^-$: 0.0–150.0 μM, $Cu^{2+}$: 0.0–500.0 μM | $I^-$: 43.55 μM | ACN | Absorption, luminescence | [247] |
| **R13** | Silver(I) ($Ag^+$) | 0.0–200.0 μM | n.a. | $CHCl_3$/ACN (20:1) | Luminescence | [249] |
| **R14** | Gold(III) ($Au^{3+}$) | 1.0–60.0 μM | 0.008 μM | $H_2O$, PBS (10 mM) | Luminescence | [250] |
| **R15** | Aluminum(III) ($Al^{3+}$), nitrofurantoin; | Aluminum Ion ($Al^{3+}$): 18.7–75.0 μM Nitrofurantoin: 0.0–50.0 μM | Aluminum Ion ($Al^{3+}$): 0.016 μM Nitrofurantoin: 1.6 μM | ACN | Absorption, luminescence | [251] |
| **R16** | Cadmium(II) ($Cd^{2+}$) | 0.0–15.0 μM | n.a. | $CHCl_3$/ACN (10:1 v/v) | Luminescence | [252] |

(Continues)

**TABLE 1** | (Continued)

| Cage-receptor | Analyte and Binding affinities ($K_a$) | Conc. range | LoD | Solvent | Main detection method | Reference |
|---|---|---|---|---|---|---|
| **R17** | Gold bisdithiolene complexes | 3400 μM | n.a. | ACN | Absorption | [253] |
| **R18** | Chiral guests (α-ammonium esters, amongst others) | 0.06–6.0 μM | n.a. | $H_2O$ | Circular dichroism | [61] |
| **R19** | N-Boc amino acids | 10.0–100.0 μM | Below 100 μM for N-Boc-Asp | MeOH, $H_2O$ | Luminescence, circular dichroism | [255] |
| **R20** | Dicarboxylate guests (C4–C8) | μM-range | n.a. | $H_2O$ | Circular dichroism | [256] |
| **R21** | Deoxynucleotides $K_a$: $10^3$–$10^5$ $M^{-1}$ | μM-range | n.a. | $H_2O$ | Circular dichroism and CPL | [258] |
| **R22** | Cysteine (Cys) | n.a. | 5.91 μM | $H_2O$ | Luminescence | [261] |
| **R23** | Glutathione (GSH), cysteine (Cys) | 2.0–80.0 μM | Glutathione: 0.19 μM, Cysteine: 0.28 μM | MeOH/$H_2O$ (1/1) | Luminescence | [262] |
| **R24** | Adenosine triphosphate (ATP) $K_a$: $1.3\times10^7$ $M^{-1}$ – $5.9\times10^6$ $M^{-1}$ | n.a. | In buffer: PCC·Cl: 2.8 nM, BCC·Cl: 5.7 nM ATP in serum: PCC·Cl: 151.0 nM, BCC·Cl: 270.0 nM | HEPES buffer (10 mM, pH 7.4); 10% Human sDerum in HEPES buffer (10 mM, pH 7.4) | Luminescence | [263] |
| **R25** | Lithocholic acid, cholic acid (CA), ursodeoxycholic acid (UDCA), chenodeoxycholic acid (CDCA), deoxycholic acid (DCA), progesterone; | n.a. | CDCA (15 nM), DCA (13 nM), UDCA (25 nM) | n.a. | Luminescence | [264] |
| **R26** | Scopolamine | 0.0–2.500 μM | 135 μM | DMSO/$H_2O$ (2:8) | Luminescence | [265] |
| **R27** | Iron(III) ($Fe^{3+}$), dichromate ($Cr_2O_7^{2-}$), antibiotics (NFT, NFZ, MNZ, ONZ); | $Fe^{3+}$: 0.0-10 000 μM, $Cr_2O_7^{2-}$: 0.0–10 000 μM, Antibiotics: 0–1000 μM | $Fe^{3+}$: 4.1 μM, $Cr_2O_7^{2-}$: 3.1 μM, NFT: 0.53 μM, NFZ: 0.52 μM, MNZ: 1.24 μM, ONZ: 1.62 | $H_2O$ | Absorption, luminescence | [267] |
| **R28** | Nitrotyrosine $K_a$: ~$10^4$ $M^{-1}$ (in THF/$H_2O$), ~$10^3$ $M^{-1}$ in diluted blood | 0.0–1400 μM | 3 μM (in aqueous media), 23 μM in diluted blood | THF/$H_2O$ (2:8) | Luminescence | [268] |
| **R29** | D-glucose $K_a$: ~50 $M^{-1}$ (in $D_2O$) | 0.0–2000 μM | n.a. | Phosphate buffer | Luminescence | [269] |
| **R30** | D-glucose $K_a$: ~218 $M^{-1}$ (in $D_2O$) | 0.0–4500 μM | n.a. | $H_2O$ | Luminescence | [270] |
| **R31** | Picric acid (PA), trinitrotoluene (TNT); | PA: 0.0–45.8 μM, TNT: 0.0–150.0 μM | n.a. | MeOH | Absorption, luminescence | [271] |

(Continues)

**TABLE 1** | (Continued)

| Cage-receptor | Analyte and Binding affinities ($K_a$) | Conc. range | LoD | Solvent | Main detection method | Reference |
|---|---|---|---|---|---|---|
| **R32** | Electron deficient nitroaromatic compounds (Picric acid (PA), 1-methyl-4-nitrobenzene, 1-(4-nitrophenyl) ethanone, 1,3-dinitrobenzene, 1-methyl-2,4-dinitrobenzene) | 10.0–300.0 μM | Picric acid: 1.41 μM | ACN | Luminescence | [272] |
| **R33** | Picric acid (PA) | 10 000.0 μM | n.a. | ACN | Luminescence | [273] |
| **R34** | Picric acid (PA) $K_a$: $1.8{\cdot}10^6$ $M^{-1}$ | 10.0–30.0 μM | n.a. | ACN | Luminescence | [274] |
| **R35** | Picric acid (PA) | 1000.0 μM | 345 nM | DMSO | Luminescence | [275] |
| **R36** | Picric acid (PA) | 0.0–40.0 μM | 2.0 μM | Acetone/$H_2O$ (80/20) | Absorption, luminescence | [276] |
| **R37** | Picric acid (PA) $K_a$: $1.7{\times}10^5$ $M^{-1}$ | n.a. | n.a. | ACN | Luminescence | [277] |
| **R38** | Fluorinated corticosteroids | n.a. | n.a. | ACN | NMR | [280] |
| **R39** | Short-chain perfluoroalkyl carboxylates (PFAS): trifluoroacetate ($TFA^-$), pentafluoropropionate ($C_2F_5COO^-$), heptafluorobutyrate ($C_3F_7COO^-$), nonafluoropentanoate ($C_4F_9COO^-$); $K_a$: $3.5{\times}10^4$ $M^{-1}$ (TFA); $10^3$ $M^{-1}$ (for other TFAs) | mM-range | n.a. | $CD_3NO_2$, HEPES buffer (50 mM, pH 7.5) | NMR | [281] |
| **R40** | BODIPY, coumarin 153, Nile red; | 80.0 μM | n.a. | $H_2O$ | Absorption, luminescence | [282] |
| **R41** | Tetraazaporphyrine (TAP) | mM-range | n.a. | $H_2O$ | Luminescence | [283] |
| **R42** | Nitric oxide (NO) $K_a$: $6{\times}10^4$ $M^{-1}$ | 100.0–450.0 μM | 5.0 nM | DMF/$H_2O$ (9:1), cell culture medium | Luminescence | [284] |
| **R43** | 2,6- dichloro-nitroaniline (DCN) | 0.0–100.0 μM | 8.0 μM | ACN | Luminescence | [286] |
| **R44** | Intracellular $Pd_2L_4$ metallacage | μM-range | n.a. | PBS, ell culture media | Luminescence | [308] |
| **R45** | G-quadruplex (G4) | 0.4–11.0 μM | n.a. | IDTE buffer and in cells | Luminescence | [309] |
| **R46** | Tumor cell targeting and imaging | n.a. | n.a. | Cell culture media and in vivo | Luminescence | [310] |

**TABLE 2** | Representative cage-receptors enabling spectrophotometric detection of analytes by UV–vis absorption, circular dichroism, and photoluminescence. Also highlighted are the chromophoric units employed, the excitation and emission wavelengths, the targeted analyte classes, and the dominant host–guest interactions involved in analyte binding.

| Cage-receptor | Chromophore and signal readout | Luminescence $\lambda_{ex}/\lambda_{em}$ | Analyte class | Major binding interactions | Reference |
|---|---|---|---|---|---|
| **R1** | Porphyrins (absorption) | — | Inorganic anion | $Zn^{2+}$ Lewis acidity enable interactions with anions | [311] |
| **R2** | Porphyrins (absorption) | — | Inorganic anion | C–H···anion hydrogen bonds combined with $Zn^{2+}$ Lewis acidity enable interactions with anions | [311] |
| **R3** | Tris(4-(1*H*-pyrazol-3-yl)phenyl)amine coordination to $Pd^{2+}$ (luminescence) | 320;420 | Inorganic anion | Analyte engages in ligand exchange reaction with $Pd^{2+}$ nodes. | [234] |
| **R9** | Indirectly through luminescence assays for liposome membrane permeability assays (luminescence) | various | Anion transport through liposome membranes | Multivalent N–H···anion interactions | [242] |
| **R17** | 5,10,15,20-tetrakis(4-carboxyphenyl)porphyrin complexation with $Pd^{2+}$ (absorption) | — | Transition-metal bis-dithiolene complexes | $\pi$–$\pi$- and electrostatic interactions | [253] |
| **R18** | Trisacylhydrazone ligand coordination to $Ga^{3+}$ (CD spectroscopy) | — | | Hydrophobic effects in combination with electrostatic interactions, together with $\pi$-type dispersion and CH–$\pi$ interactions. | [61] |
| **R19** | Tetraaza-12-crown-4) coordination to $Eu^{3+}$ or $Tb^{3+}$ (luminescence) | 254; 545/615 | N-protected amino acids | Amino acid derivatives coordinate and exchange with lanthanide ions. | [255] |
| **R20** | *Tris*(2-pyridylmethyl)amine units (CD spectroscopy) | — | Dicarboxylates | Carboxylate to metal coordination as well as cavity size matching | [256] |
| **R25** | Indicator displacement assay using the reporter sulforhodamine 101 (luminescence) | 475;606 | Bile acids | Hydrophobic confinement combined with cooperative interguest hydrogen bonding | [264] |
| **R26** | Fluoresceine as reporter dye (luminescence) | 470;535 | Biogenic amine | Size-fitting, dispersion interactions | [265] |
| **R27** | Phenanthroline dibenzoic acid-based ligand coordination to $Cd^{2+}$ (luminescence) | 320;535 | Inorganic anions and cations; Antibiotics | $\pi$–$\pi$ interactions in combination with electrostatic interactions | [267] |
| **R28** | Tetraphenylethene (luminescence) | 375;450 | Nitro-containing amino acid | Cation–$\pi$ interactions | [268] |
| **R29** | Anthracene-panels (luminescence) | 394;423 | Saccharides | NH···O hydrogen bonds as well as CH-$\pi$ contacts | [269] |
| **R30** | Pyrene-based panels (luminescence) | 420;499 | Saccharides | C-H···$\pi$ and C-H···O interactions | [270] |

(Continues)

**TABLE 2** | (Continued)

| Cage-receptor | Chromophore and signal readout | Luminescence $\lambda_{ex}/\lambda_{em}$ | Analyte class | Major binding interactions | Reference |
|---|---|---|---|---|---|
| **R31** | 1,3,5-tris(4-pyridylethynyl)benzene coordination to $Ru^{2+}$ (luminescence) | 280;350 | Nitroaromatics | $\pi$–$\pi$ donor–acceptor interactions | [271] |
| **R32** | Oxazoline-based ligand coordination to $Eu^{3+}$ (luminescence) | 350;615 | Nitroaromatics | $\pi$–$\pi$ interactions | [272] |
| **R33** | (4,4′,4′′,4′′′-(ethene-1,1,2,2-tetrayl)tetrakis(benzene-4,1-diyl))tetrakis(methylene)tetrapyridin-4(1H)-one ligand complexation to Ln3+ nitrate (luminescence) | 356;1058 | Nitroaromatics | n. a. | [273] |
| **R34** | Zinc(II)–bipyridine carbazole complex (luminescence) | 400;608 | Nitroaromatics | $\pi$–$\pi$ interactions | [274] |
| **R35** | Carboxylate-functionalized tris(triazamacrocyclic) ligand complexation with $Co^{2+}$ and $Ln^{3+}$ ions (luminescence) | 280; ~370 | Nitroaromatics | $\pi$–$\pi$ stacking and H-bonding interactions | [275] |
| **R36** | Tetraphenylpyrazine-based tetraimidazole complexation with $Pt^{2+}$ (luminescence) | 350; ~425 | Nitroaromatics | $\pi$–$\pi$ stacking and H-bonding interactions | [276] |
| **R37** | Dipyridyl-phenoxazine $Zn^{2+}$ complexes (luminescence) | 400;568 | Nitroaromatics | $\pi$–$\pi$ interactions | [277] |
| **R40** | Bispyridine ligand coordinated to $Pt^{2+}$ whereas BODIPY was used as luminophore (luminescence) | ~495; ~535 | Aromatic compounds (anthracene derivatives) | $\pi$–$\pi$ stacking and dispersion interactions | [282] |
| **R41** | 2,4,6-tri(pyridin-4-yl)-1,3,5-triazine panels and pyrazine pillar coordination to $Pt^{2+}$ (luminescence) | ~500;630 | Azaporphyrin | Electrostatic interactions at basic pH combined with $\pi$–$\pi$ interactions | [283] |
| **R42** | Triphenylamine-based tris(salicylhydrazone) ligand coordination to $Ce^{3+}$ (luminescence) | 350;470 | Nitronyl nitroxide | N–H···O interactions as well as electrostatics | [284] |
| **R43** | Tetraimidazolium ligand (luminescence) | 358; ~475 | Pesticide | n.a. | [286] |
| **R44** | 3,5-bis(3-ethynylpyridine)phenyl ligand coordinated to $Pd^{2+}$ (luminescence) | 290/ 525; 544 | Cell imaging / Cis-platin delivery | Encapsulation; BODIPY emission | [308] |
| **R45** | Biphenyl-bridged bis(pyridinium) ligand (luminescence) | 360;445 | G-quadruplex | Stacking interactions on the guanine quartets | [309] |
| **R46** | Tetraphenylethene (luminescence) | ~430;525 | Cells | Biotin-receptor binding | [310] |

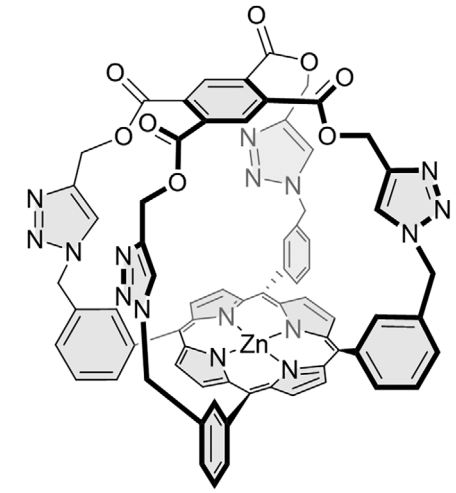


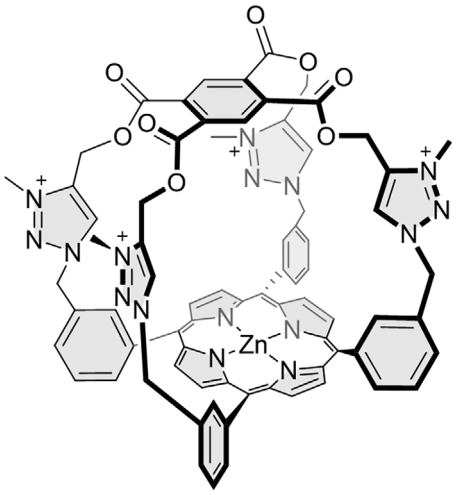


**FIGURE 7** | Chemical structures of R1 and R2 employed in the UV–vis-based detection of $F^-$, $Cl^-$, $AcO^-$, $H_2PO_4^-$, $SO_4^{2-}$ in aqueous–organic solvent mixtures.

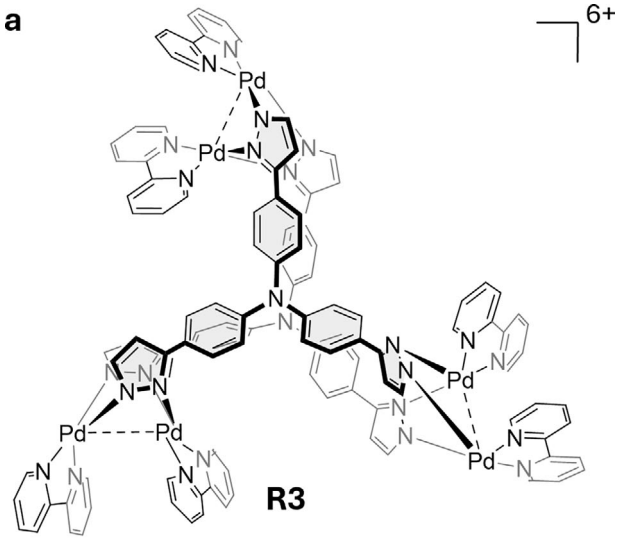


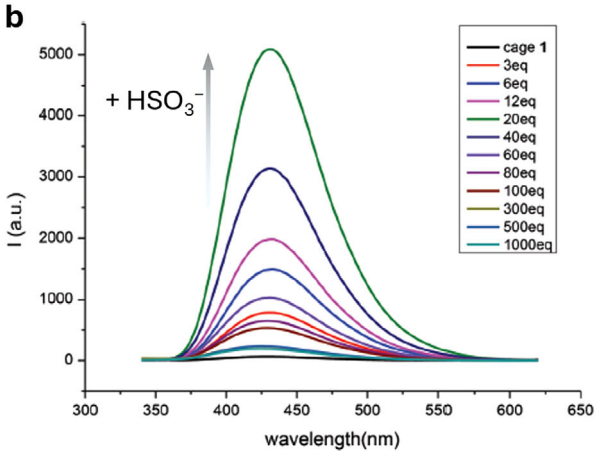


**FIGURE 8** | (a) Chemical structure of the cage-receptor R3 used for the detection of $HSO_3^-$ in aqueous media. (b) The luminescence response of R3 exhibits an $HSO_3^-$-dependent increase in emission, whereas an excess of bisulfite eventually leads to decreased emission due to decomposition of the cage. Adapted with permission. [234] Copyright 2017, The Royal Society of Chemistry.

collectively suppress hydrolysis and preserve structural integrity in aqueous media. At the same time, their reliance on an organic cosolvent indicates limited intrinsic solubility in pure water, which may constrain their applicability in fully aqueous sensing environments.

Anthracenes are well-known luminescent moieties that exhibit decreased luminescence upon aggregation [233]. In this context, a more recent example involves an anthracene-functionalized $Pd^{2+}$ metallacage (**R4**, Figure 9) assembled from 4-(anthracen-9-yl)-N,N-bis(4-(pyridin-3-yl)phenyl)aniline and $Pd(NO_3)_2$ [235]. In dimethyl sulfoxide (DMSO), the cage displays strongly quenched emission relative to the free ligand, consistent with $Pd^{2+}$-mediated excited-state quenching. Addition of $OH^-$, $PO_4^{3-}$, or $AcO^-$ triggers cage disassembly, releasing the emissive ligands and producing a pronounced luminescence turn-on response. Other anions, including $BF_4^-$, $PF_6^-$, $F^-$, $Cl^-$, $Br^-$, $I^-$, $NO_3^-$, $CO_3^{2-}$, $SO_4^{2-}$, $HPO_4^{2-}$, and $H_2PO_4^-$, do not induce comparable changes, either because they fail to promote disassembly or undergo simple nitrate exchange without restoring ligand emission. Although the system was evaluated exclusively in DMSO, its behavior in aqueous media remains uncertain, and possible limitations in solubility, which were not addressed in the original study, may further restrict its applicability.

Building on the 3,5-dicarboxamide pyridinium motif previously used by the Beer group for anion-binding interlocked structures in organic media [176, 236], Liu and co-workers developed a water-soluble bicyclic amide cage incorporating the same recognition element (**R5**, Figure 10). [237] The cage-receptor was obtained by imine condensation of (2,4,6-triethylbenzene-1,3,5-triyl)trimethanamine with pyridine-3,5-dicarbaldehyde, followed by conversion of the intermediate imine cage into the amide-based cage-receptor via Pinnick oxidation. **R5** combines charge-assisted hydrogen bonding with a triply cationic scaffold, enabling strong electrostatic attraction to hydrated anions while providing a convergent array of amide NH and pyridinium C–H donors for selective cavity binding. In water, **R5** binds hydrophilic

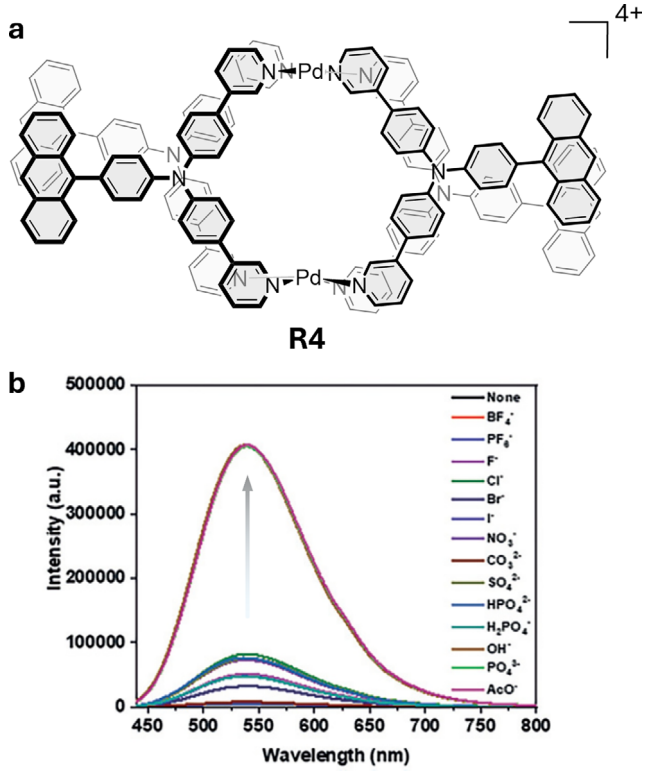


**FIGURE 9** | (a) Chemical structure of R4 used for luminescence-based detection of $OH^-$, $PO_4^{3-}$, and $AcO^-$. (b) Luminescence response curves of R4 toward different anions, where binding of $OH^-$, $PO_4^{3-}$, and $AcO^-$ induces disassembly of the cage-receptor, thereby restoring the luminescence of the anthracene-based ligands. Adapted with permission. [235] Copyright 2024, Thieme.

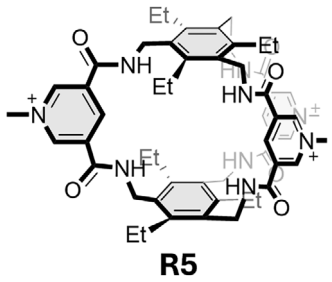


**FIGURE 10** | (a) Chemical structure of R5 capable of binding $SO_4^{2-}$ and $C_2O_4^{2-}$ in water.

oxoanions with high affinity, with $SO_4^{2-}$ and oxalate showing favorable enthalpic contributions and substantial desolvation gains. Other anions bind only weakly to **R5**, with affinities decreasing in the order $I^-$, $NO_3^-$ > $AcO^-$, $NO_2^-$ ≫ $Br^-$, $Cl^-$.

A recently reported, impressively selective $SO_4^{2-}$ cage-receptor was developed by Wu, Deplazes, and co-workers, who used a neutral [2.2.2] urea cryptand (**R6**), achieving high-affinity sulfate recognition in water using only NH hydrogen bonds, closely mimicking biological sulfate-binding proteins (Figure 11) [238]. Prepared through a one-pot, sulfate-templated assembly, **R6** encapsulates $SO_4^{2-}$ via twelve convergent NH···O hydrogen bonds, as confirmed by X-ray crystallography and molecular dynamics simulations. In DMSO containing 0.5 vol% $H_2O$, **R6**

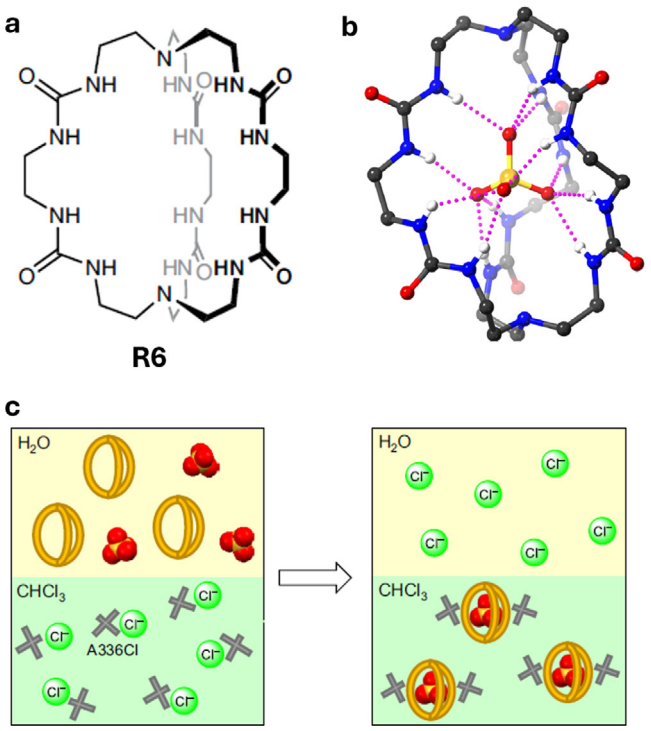


**FIGURE 11** | (a) Chemical structure of R6 and (b) Molecular structure of the R6⊃$SO_4^{2-}$ complex derived from X-ray analysis in the solid state. (b) Schematic representation of $SO_4^{2-}$ extraction by R6, omitting $Na^+$ counterions in the aqueous phase. Adapted with permission. [238] Copyright 2024, Springer Nature.

binds $SO_4^{2-}$, four orders of magnitude stronger than an acyclic tris-urea control, while displaying only modest affinity for $Cl^-$. Selectivity studies revealed more than a 10-fold preference for sulfate over other oxoanions and halides. The receptor's high sulfate affinity stems from a preorganized cluster of six urea groups whose twelve NH donors create a hydrogen-bonding pocket precisely complementary to $SO_4^{2-}$. Incorporating the receptor into cetyltrimethylammonium bromide micelles enhances sulfate extraction by locally concentrating $SO_4^{2-}$ at the positively charged micellar surface, while the phase-transfer counterion methyltrialkyl $C_{8\text{-}10}$-ammonium chloride (A336Cl) enables the anion to migrate into the micellar interior and, subsequently, into the organic phase.

Leveraging the ease of functionalization of calix [*n*]arenes, Yang and co-workers synthesized a cage receptor (**R7**) composed of both oxa- and aza-calixarene units, a hybrid of three azacalixarenes and two oxacalixarenes (Figure 12) [239]. Absorption studies of **R7** showed that addition of $Bu_4N^+F^-$ (30 eq) diminishes the higher-energy absorption band and generates a new visible absorption band, producing a brown-colored solution. **R7** showed good selectivity, as the addition of other anions such as $Cl^-$, $Br^-$, $I^-$, $PF_6^-$, $BF_4^-$, $H_2PO_4^-$, $AcO^-$, $NO_3^-$, $HSO_4^-$, $SO_4^{2-}$, and $PO_4^{3-}$ yield no detectable spectral changes. Fluoride selectivity was ascribed to its capacity to deprotonate the receptor's NH groups, which in turn generated a detectable color change in the aromatic framework bearing the dinitrophenylene substituents.

Boron-dipyrromethene (BODIPY) dyes are widely used fluorophores valued for their sharp, intense absorption, high

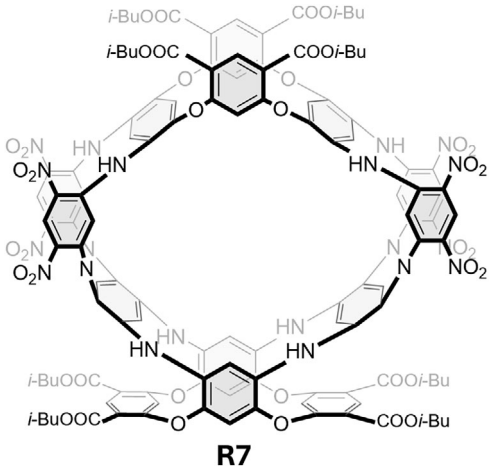


**FIGURE 12** | Chemical structure of R7 used for the UV–vis-based detection of $F^-$.

fluorescence quantum yields, and excellent photochemical stability [240]. With this in mind, Nitschke and co-workers developed a family of luminescent $M_4L_6$ tetrahedral cages (**R8**, Figure 13) incorporating BODIPY and pyrene fluorophores, assembled from bis(aminophenyl)BODIPY and pyrene-substituted formylpyridines with $Fe^{2+}$ or $Zn^{2+}$ ions [241]. The $Zn^{2+}$ cage lacking pyrene pendants shows optical responses to certain anions in ACN. For example, binding $AcO^-$ or $N_3^-$ induces bathochromic absorption shifts and up to a 25-fold enhancement of its red emission. Smaller but discernible responses occur for $F^-$ and $Cl^-$, while $Br^-$, $I^-$, $NO_3^-$, $BF_4^-$, $PF_6^-$, and $ClO_4^-$ elicit minimal changes. Spectroscopic analyses confirmed that the tetrahedral framework remained intact, and recognition was attributed primarily to electrostatic attraction and anion–$\pi$ interactions, with absorption red-shifts arising from perturbation of ligand $\pi$ orbitals. A colorimetric test strip was developed for detecting aqueous $AcO^-$, $N_3^-$, $F^-$, and $Cl^-$ (1 mM). Interestingly, amino acids such as cysteine induce cage disassembly through imine exchange with the linkers, releasing the BODIPY units and forming mononuclear $Fe^{2+}$ amino-acid complexes. This process enables luminescence-based detection through distinct changes in color and emission intensity. The authors also reported a pyrene derivative capable of white-light emission, offering an additional sensing modality.

Peptide-based recognition motifs offer a promising approach to designing water-compatible cage receptors. Peptide-derived capsule hemispheres assemble through directional hydrogen bonding to form a spherical supramolecular cage, whose internal hydrogen-bonding network encapsulates and stabilizes anions in aqueous solution. Granja and co-workers reported peptide-based capsules (**R9**) that recognize anion–water clusters rather than bare anions, establishing a distinct binding mode for operation in aqueous environments (Figure 14) [242]. The capsules form by dimerization of $\alpha,\gamma$-cyclic hexapeptides capped with tris(triazolylethyl)amine groups yielding $C_3$-symmetric hydrogen-bonded assemblies. X-ray structures revealed that **R9** encapsulates hydrated clusters such as $3F^-{\cdot}8H_2O$ and $3Cl^-{\cdot}4H_2O$, stabilized through a network of amide hydrogen bonds and hydrophobic leucine pockets. Water plays an indispensable role, as drying the samples released the guests, and rehydration

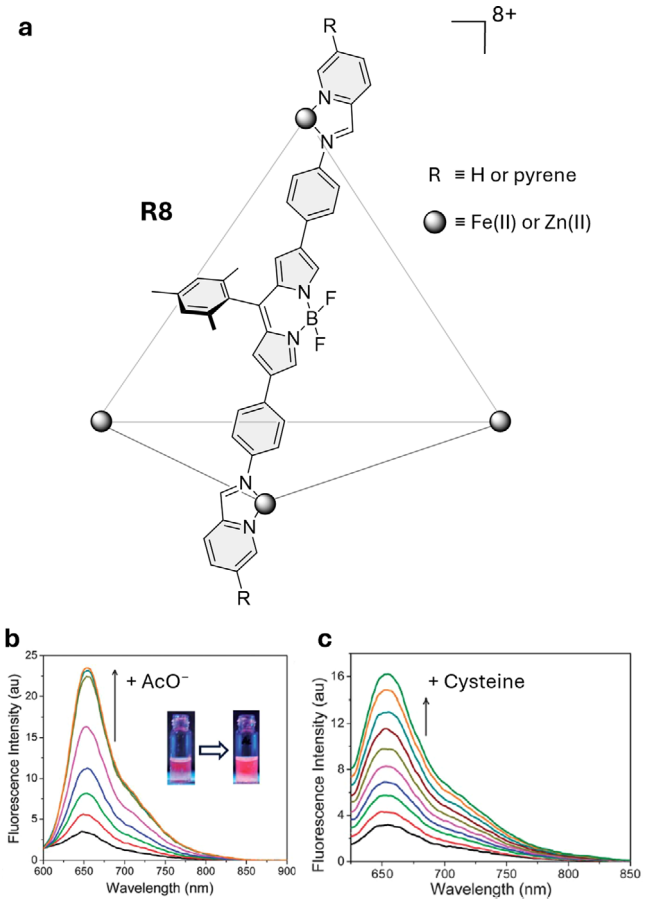


**FIGURE 13** | (a) Truncated chemical structure of cage-receptor R8 used for the detection of acetate anions and amino acids. (b) Luminescence spectra of R8 upon addition of tetrabutylammonium acetate in ACN, and (c) in response to cysteine in ACN/$H_2O$ (1:1, v/*v*). Adapted with permission. [241] Copyright 2014, The Royal Society of Chemistry.

restored the complexes, demonstrating that recognition targets the hydration sphere itself. Correspondingly, **R9** favors small, strongly hydrated anions ($F^-$, $Cl^-$, $AcO^-$, $N_3^-$, $NO_3^-$) and excludes larger, weakly hydrated ones ($Br^-$, $I^-$, $PF_6^-$). The capsules also mediate anion transport across lipid bilayers with $Cl^-/H^+$ symport or $Cl^-/OH^-$ antiport, and the transport can be monitored because the liposomes contain luminophores (e.g., the lucigenin assay [243]) that become emissive upon anion uptake into their inner cavity.

As mentioned above, the detection of small inorganic anions such as $Cl^-$ imposes very stringent physicochemical requirements on receptor cages for achieving selectivity. Remarkably, the detection of $Cl^-$ in aqueous solution has recently been demonstrated using a $Pd^{2+}$-based metallacage constructed from $Pd(NO_3)_2$ and a 1,3-di(pyridin-3-yl)benzene ligand (L2) bearing a short polyethylene glycol chain, leading to $[Pd_2(L2)_4(NO_3)]^{3+}$ (**R10**, Figure 15) [244]. These cages exhibit micromolar binding affinity toward chloride ions. In this case, the $Cl^-$ binding interactions were attributed to eight C—H···$X^-$ hydrogen bonds involving the pyridyl NCH protons, in addition to electrostatic interactions with the $Pd^{2+}$ nodes within the cage framework. Interestingly, the binding of $Cl^-$ occurs via an anion exchange mechanism, converting **R10** into $[Pd_2(L2)_4Cl]^{3+}$. Notably, these interactions persist in

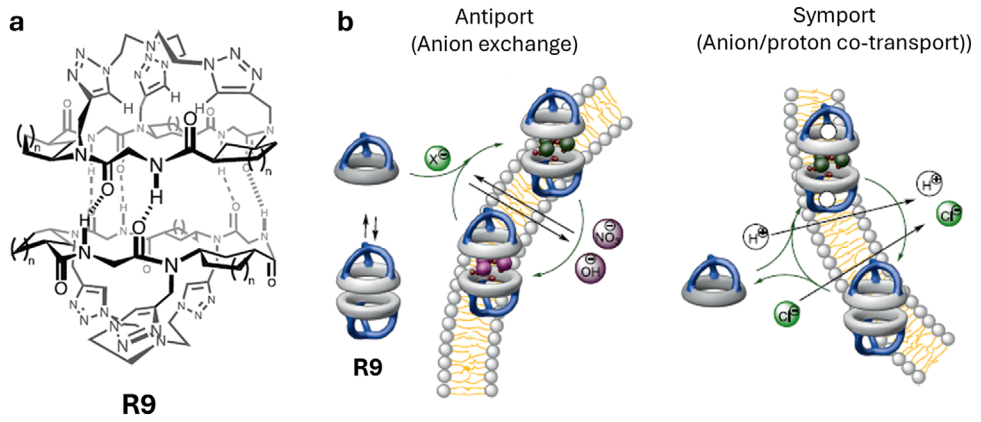


**FIGURE 14** | (a) Chemical structure of **R9** ($n$ = 1, 2), which, in combination with a luminescent assay such as the lucigenin assay, can be used to detect and enable anion transport through lipid bilayer membranes. (b) Schematic representation of the transport mechanisms facilitated by **R9** in liposomal systems. Adapted with permission. [242] Copyright 2024, Springer Nature.

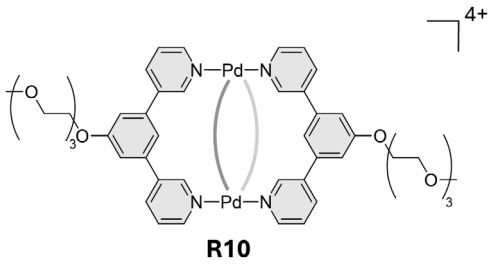


**FIGURE 15** | Chemical structure of cage-receptor R10 (lacking $NO_3^-$ in its cavity), which exhibits binding of $Cl^-$ ions in water.

water, resulting in measurable binding affinities suitable for chloride capture. Future investigations should aim to evaluate potential cross-selectivity with competing anions and to incorporate into the receptor design an appropriate reporter unit for chloride detection beyond nuclear magnetic resonance (NMR) spectroscopy, which would enhance the applicability of cage-receptor.

### 4.1.2 | Cation Sensing

Peptide-based receptors have been used, for example, in liposome-based assays, [243] where peptide–receptor assemblies capture analytes and, due to their lipophilicity, facilitate anion transport across membranes by acting as anion carriers. However, peptide-based cages can also be assembled to enable direct luminescence sensing. For example, Stefankiewicz and co-workers developed water-soluble pseudopeptide cage-receptors (**R11**) assembled through reversible disulfide exchange of three trifunctional thiol building blocks derived from benzene-1,3,5-tricarboxamide, triphenylamine-triamide, and trisphenylbenzene-triamide, each bearing three L-cysteine residues (Figure 16) [245]. Under oxidative conditions, the monomers assemble into homodimeric tris-disulfide cages, and mixtures give both homo- and heterodimers through size- and symmetry-driven self-sorting. The triphenylamine cage 2-2 (**R11**) displays strong aggregation-induced emission (AIE). Addition of $La(NO_3)_3$ produced a 1:1 $La^{3+}$–**R11** adduct in $H_2O$ that precipitates as an amorphous solid and shows a shifted emission

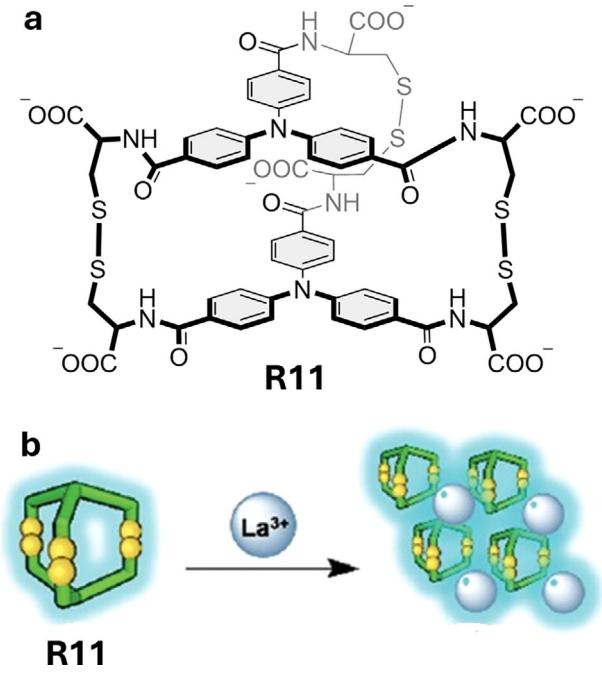


**FIGURE 16** | (a) Chemical structure of R11, which can be used for the detection of $La^{3+}$ ions in water via (b) luminescence, as the cage aggregates in the presence of these ions, where aggregation-induced luminescence enhancement can be observed. Adapted with permission. [245] Copyright 2021, American Chemical Society.

maximum compared to the amorphous **R11** solid alone. $La^{3+}$ binding reorganizes the cage and limits intramolecular motion, resulting in intense luminescence that increases with $La^{3+}$ concentration. This coordination is enabled by the polyanionic framework of **R11**, where six carboxylates and the rigid, electron-rich triphenylamine core provide an effective multidentate O-donor site for hard metal cations.

Triazine-based moieties are attractive structural components because they enable energy-transfer processes within cage receptors, such as intraligand charge-transfer (ILCT) sensitization in combination with lanthanide ions [246]. Sun and co-workers described $Eu_4L_4$ tetrahedral cages (**R12**) assembled from $C_3$-

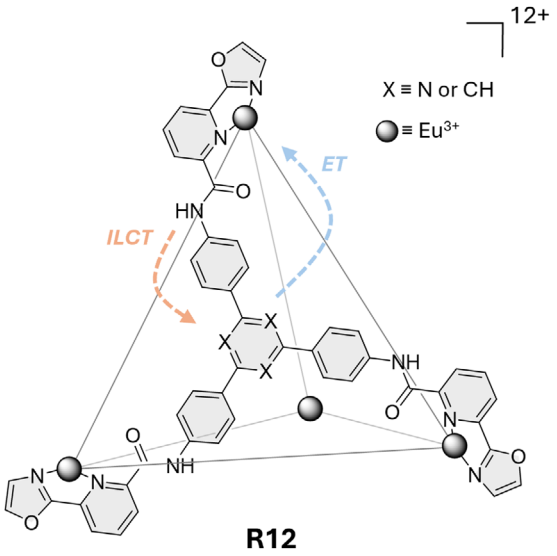


**FIGURE 17** | Chemical structure of R12, which, upon iodide addition, showed strong emission quenching, whereas $Cu^{2+}$ induced a pronounced luminescence turn-on response.

symmetric oxazoline ligands, including a triazine-containing variant that enabled efficient ILCT sensitization (Figure 17) [247]. The cages were stable in ACN and enabled dual-mode luminescent sensing as anions such as iodide strongly quench the emission, whereas $Cu^{2+}$ produces a pronounced turn-on response of up to 40-fold with over five-fold selectivity versus other divalent cations. This $Cu^{2+}$-induced enhancement was attributed to strengthened ILCT sensitization via cation–$\pi$ interactions with the triazine units, while other divalent cations have only minor effects.

Compared to fluorescence, phosphorescence is advantageous for sensing because its lower-energy and long-lived emission enables time-resolved, background-suppressed, and highly sensitive measurements that are robust to intensity fluctuations and efficiently quenched by target analytes [248]. In this respect, the Yam group developed Au(I)-containing metallacages (**R13**) and related two-dimensional assemblies $[Au_8L_2]_n$ ($n$ = 1 or $\infty$) formed from tetrakis-dithiocarbamato-calix [4]arene deep-cavitand ligands that organize into octanuclear Au(I) motifs (Figure 18) [249]. These systems display green phosphorescence in deoxygenated dichloromethane, arising from mixed metal-centered and ligand-to-metal charge-transfer excited-state character modulated by Au···Au interactions, with possible contributions from dithiocarbamate-centered states. A key sensing feature is their pronounced response to $Ag^+$. In DCM/ACN mixtures, addition of $AgPF_6$ induced large red shifts in the luminescence, attributed to formation of Au(I)···Ag(I) metallophilic contacts and Ag(I)···$\pi$ interactions that extend the Au(I)···Au(I) network and generate new three-center ligandtometal–metal charge transfer emissive states, *i.e.*, Au(I)···Au(I)···Ag(I). NMR data supported a reorganization of the distorted dimeric cage into a more symmetric structure upon $Ag^+$ interaction, consistent with the observed photophysics, although a discrete $Ag^+$ complex could not be definitively assigned. Other metal ions ($Zn^{2+}$, $Hg^{2+}$, $Cd^{2+}$, $Ni^{2+}$, $Pb^{2+}$, $Co^{2+}$, $Mn^{2+}$, $Fe^{3+}$, $Cu^{2+}$) produced no comparable luminescence changes.

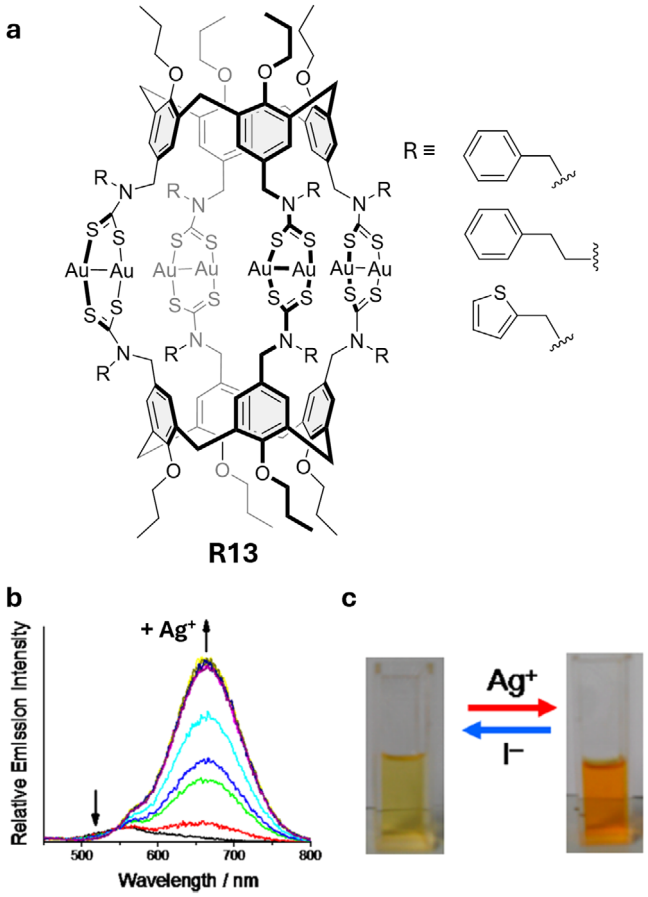


**FIGURE 18** | (a) Chemical structure of R13, which can be used for the detection of $Ag^+$ ions via luminescence. (b) Luminescence response curves showing the increase in the emission band intensity of R13 upon addition of $Ag^+$ ions to a solution of the receptor-cage. (c) Images of cuvettes containing R13 in solution, showing the distinct optical changes exhibited by the cage-receptor in the presence of $Ag^+$ or upon addition of $I^-$. Adapted with permission. [249] Copyright 2014, American Chemical Society.

Ratiometric luminescent sensors offer inherent self-calibration by relying on the ratio of two emission signals rather than a single intensity, thereby minimizing interferences and enhancing both accuracy and sensitivity. Dai and co-workers developed a water-soluble organic cage (**R14**) that acts as a ratiometric luminescent probe for $Au^{3+}$ (Figure 19) [250]. The receptor was obtained by reduction of an imine cage formed from (1R,2R)-cyclohexane-1,2-diamine and 2-hydroxybenzene-1,3,5-tricarbaldehyde. In PBS buffer, **R14** displays dual emission. Upon addition of $Au^{3+}$, a ratiometric response to $Au^{3+}$ was possible, achieving a limit of detection (LoD) in the nM range. The assay maintains good selectivity toward common ions, while stronger interferents, including $Fe^{3+}$, $Cu^{2+}$, $Zr^{4+}$, $Pb^{2+}$, and $Ag^+$, were efficiently suppressed by trapping them via ethylenediaminetetraacetic acid complexation. Mechanistic studies support a redox process in which **R14** is oxidized to a dimer as $Au^{3+}$ is reduced to $Au^+$ or $Au^0$ nanoparticles, and subsequent coordination stabilizes these assemblies and drives the ratiometric response. The method performed reliably in real matrices, yielding accurate recoveries for $Au^{3+}$ spiked into domestic wastewater and human serum, in agreement with atomic absorption measurements.

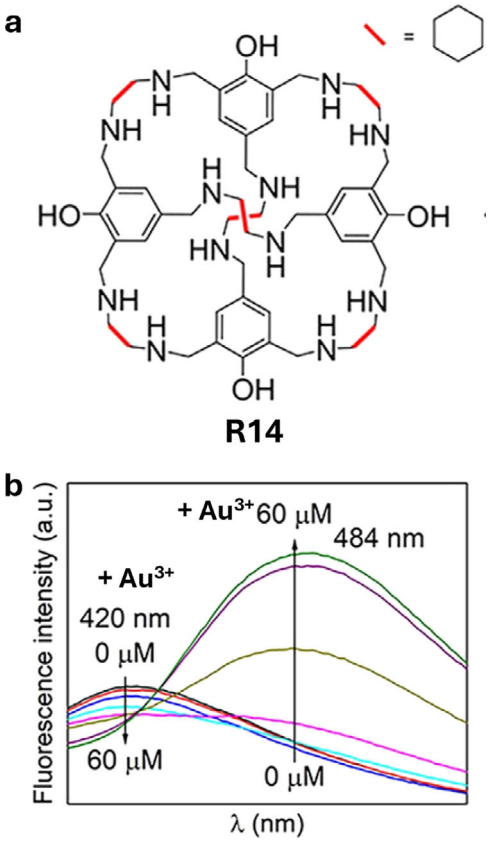


**FIGURE 19** | (a) Chemical structure of R14 used for the detection of $Au^{3+}$ ions in buffered solution. (b) Corresponding luminescence changes of R14 upon addition of $Au^{3+}$. Adapted with permission. [250] Copyright 2022, Elsevier.

Leveraging the functionalization possibilities of calix[*n*]arenes, Dai and co-workers introduced a triphenylamine-functionalized Ni-based coordination cage (**R15**) with octahedral geometry, assembled from 4,4′,4″-nitrilotribenzoic acid, *p*-*tert*-butylsulfonylcalix [4]arene, and $Ni^{2+}$ (Figure 20) [251]. In ACN, **R15** is weakly emissive, but the addition of $Al^{3+}$ produces a selective turn-on response, yielding more than a 500-fold luminescence increase accompanied by a red-shift, achieving μM detection limits even in simulated sewage. It was proposed that $Al^{3+}$ binding restricts phenyl rotation, suppressing nonradiative decay and enhancing intermolecular charge transfer to the triphenylamine units. Interestingly, the $Al^{3+}$@**R15** complex also functions as a secondary probe for the antibiotic nitrofurantoin, as its presence induces complete quenching, enabling μM-level detection within seconds (~40 s).

Zeng and co-workers developed a benzothiadiazole-based [3 + 2] imine cage (**R16**) prepared by condensing 4,4′-(benzothiadiazole-4,7-diyl)dibenzaldehyde with tris(2-aminoethyl)amine (TREN) in chloroform (Figure 21) [252]. Luminescence screening of **R16** showed a pronounced and selective response to $Cd^{2+}$. In fact, the addition of 10 eq produced nearly seven-fold emission enhancement, visible by eye under UV illumination. $Ag^{+}$ and $Cu^{2+}$ induced slight quenching, while other metal ions ($Co^{2+}$, $Ba^{2+}$, $Pb^{2+}$, $Mg^{2+}$, $Zn^{2+}$, $Fe^{2+}$, $Ni^{2+}$) caused only minor changes. NMR titrations revealed downfield shifts in cage proton signals and partial release of TREN, indicating that the sensing mechanism involves $Cd^{2+}$-induced cage decomposition, with the liberated fluorescent components responsible for the turn-on signal.

## 4.2 | Detection of Bioactive Organic Molecules

Detection of anticancer drugs with simple synthetic receptors enables rapid, cost-effective, and minimally invasive quantification of drug levels in patient samples, pharmaceutical formulations, and environmental matrices, surpassing the practical accessibility of many conventional analytical platforms. An optical cage receptor for detecting gold-based anticancer bisdithiolene-type metal complexes was developed by Rivas, Costas, and co-workers. They designed a tetragonal prismatic cage (**R17**, Figure 22) with an $A_4B_2$ architecture, where the A units are dipalladium hexaazamacrocyclic complexes and the B units are the tetraanionic form of palladium tetrakis(4-carboxyphenyl)porphyrin [253]. Although **R17** was not evaluated in water, in ACN it acted as a selective host for planar anionic guests with extended $\pi$ conjugation. Gold bisdithiolene complexes such as TBA [$Au(tdas)_2$] (tdas [2]$^{-}$ = 1,2,5-thiadiazole-3,4-dithiolate), bound in a 1:1 stoichiometry, as shown by light absorption titrations of **R17** with up to 20 eq of guest. Complexation generated characteristic spectral changes, notably reduced bathochromically shifted and less intense absorption maxima. Other bisdithiolene complexes, as well as the corresponding Pt, Pd, and Ni analogues, were likewise encapsulated with 1:1 stoichiometry. In this cage-receptor design, host–guest binding was enabled by $\pi$–$\pi$ stacking between the planar aromatic guest cores and the porphyrin panels, supplemented by metallophilic Pd-Au interactions.

For the detection of bioactive compounds, chiral recognition, that is, the ability to distinguish between enantiomers, is highly important. To achieve this, chiral information must be encoded into the receptor cage itself, so that it can provide energetically more favorable binding for one enantiomer over the other. Li and co-workers reported an anionic, homochiral octahedral cage (**R18**) formed from $Ga^{3+}$ ions and tris-acylhydrazone benzene ligands, providing a water-stable platform for the potential detection of chiral guests (Figure 23) []. The cage, formed by condensing a tris-acylhydrazide with salicylaldehyde sulfonic acid in the presence of $GaCl_3$, is obtained as a racemic mixture of two homochiral enantiomers. With twelve sulfonate groups, **R18** is highly water-soluble and remains stable in $D_2O$ for at least one month. Binding is driven largely by the hydrophobic effect, supplemented by electrostatic attraction toward cationic guests. Adding chiral substrates to **R18** generated strong CD signals, and their intensity varied linearly with enantiomeric excess, enabling accurate enantiomeric excess (*ee*) determination. Although CD is not the most sensitive detection method, **R18** is notable for its full water compatibility. Fluorescence-detected CD, already effective for macrocyclic systems, [254] could further enhance sensitivity for aqueous chiral sensing.

Ito and co-workers reported chiral dimeric lanthanide macrotricyclic complexes (*R*/*S*-receptor-Ln; Ln = $Eu^{3+}$, $Tb^{3+}$) that act as chirality sensors for *N*-Boc-protected amino acid anions in polar media (**R19**, Figure 24) [255]. The complexes were assembled from chiral bisoctadentate cyclen ligands and $LnCl_3$, giving stable dinuclear structures that retain one coordinated solvent molecule

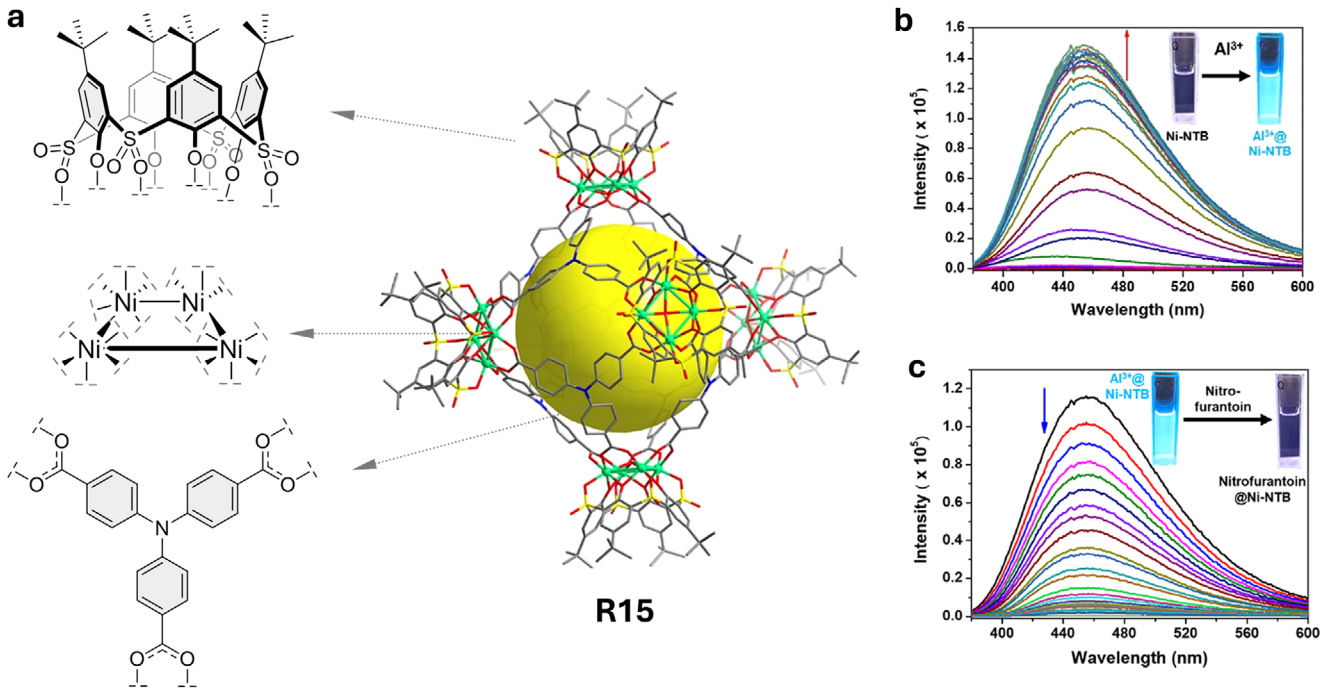


**FIGURE 20** | (a) Chemical structures of the components of R15. Luminescence response curves of R15 in the presence of (b) $Al^{3+}$ and (c) nitrofurantoin. Adapted with permission. [251] Copyright 2023, American Chemical Society.

per metal center. In methanol, the $Eu^{3+}$ and $Tb^{3+}$ receptors display strong red and green emissions, which are modulated when the coordinated solvent is displaced by the carboxylate group of an *N*-Boc amino acid anion. Luminescence titrations showed clear enantioselective sensing of *N*-Boc-aspartate, and competition experiments demonstrated that the aspartate dianion binds preferentially, indicating that both its charge and length are recognized. Combining (*S*)-receptor and (*R*)-receptor with $Tb^{3+}$ enabled simple visual discrimination of *N*-Boc-*D*- and *L*-aspartate through a red/green luminescence color change, detectable at low micromolar concentrations.

Zonta and co-workers developed a family of chiral supramolecular cages (**R20**) constructed from $Zn^{2+}$– tris(2-pyridylmethyl)amine (TPMA) complexes linked by enantiopure diamines, designed as diastereodynamic probes that assemble around dicarboxylate templates and thereby operate as molecular-length sensors (Figure 25) [256]. Dicarboxylates from succinate ($C_4$) to sebacate ($C_{10}$) direct cage formation, giving well-defined host–guest complexes. CD spectroscopy showed that the chiroptical response correlates directly with guest length as short dicarboxylates (C4, C5) induced negative CD bands, whereas longer guests ($C_7$, $C_8$) produce positive, red-shifted bands. These opposite signals reflect a helicity inversion of the TPMA stereodynamic units, triggered by conformational adjustments of the diamine linkers that modulate the Zn···Zn distance within the cage. This length-dependent self-assembly effectively converts an achiral structural parameter, guest chain length, into a chiroptical output with a resolution of two methylene units. Although the presence of imine linkages renders these cages unstable in water, subsequent studies have shown that cage stability can be modulated by the identity of the bound dicarboxylate [257], suggesting opportunities to refine this dynamic architecture for more robust sensing designs and potentially adapt it for aqueous environments.

Cheng and co-workers introduced an achiral tetraphenylethene (TPE)-based octacationic cage (**R21**) that acquires induced chirality upon binding deoxynucleotides in water, giving both CD and circularly polarized luminescence (CPL) signals [258] (Figure 26) [259]. The highly water-soluble cage (≈22 mM) stabilizes two hydrogen-bonded nucleotides inside its hydrophobic cavity with medium binding constants, whereas recognition is driven by electrostatic attraction to phosphate groups and base-pair hydrogen bonding. Luminescence titrations of the cage-receptors with deoxynucleotides in water revealed emission enhancement for adenosine monophosphate (A), thymidine monophosphate (T), and cytidine monophosphate (C), but strong quenching for guanosine monophosphate (G), reflecting a balance between restricted intramolecular rotation (RIR), which increases emission, and photoinduced electron transfer (PET), which quenches it. For the nucleotides A/T/C, RIR dominates upon guest binding, whereas guanine's stronger electron-donor character shifts the equilibrium toward PET, producing net quenching. Chiroptical studies revealed efficient chirality transfer from the ribose units to the cage, giving induced CD bands and CPL.

Most known molecular probes for amino acids operate through a chemical reaction with their nucleophilic functionality, with thiol-containing amino acids being prominent targets and biomarkers [260], as their nucleophilic thiol group can trigger a response in cage receptors by inducing their disassembly. For example, Han and co-workers reported emissive poly-NHC organometallic cages from a sulfonate-pendant TPE-bridged tetrakis(1,2,4-triazolium) ligand and $Ag_2O$, yielding a water-soluble $Ag_8L_4$ cage (**R22**) in $H_2O$ (Figure 27) [261]. The cage-

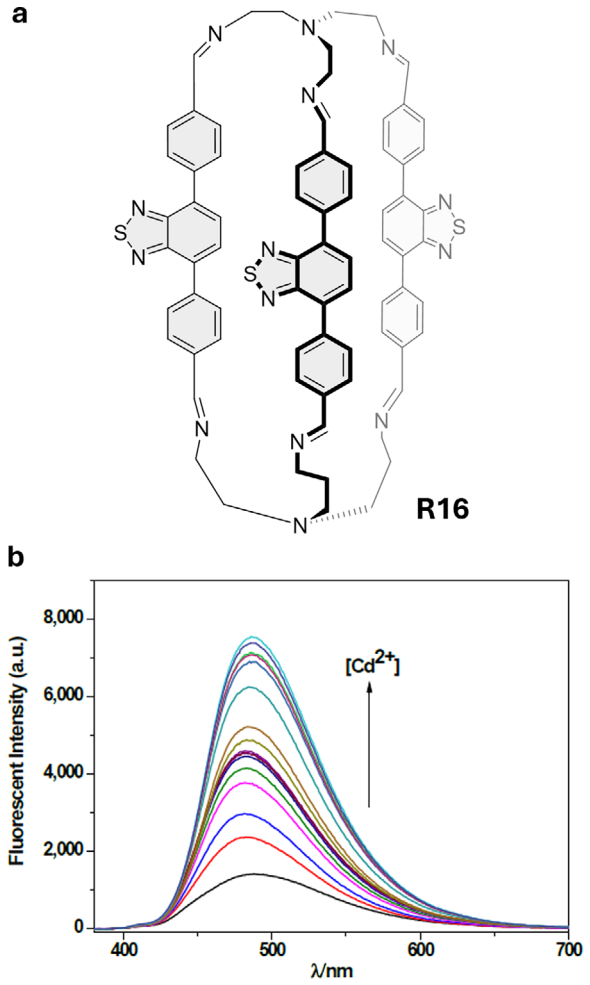


**FIGURE 21** | (a) Chemical structure of R16 used for luminescence-based detection of $Cd^{2+}$. (b) Changes in the emission spectra of R16 upon addition of $Cd^{2+}$ ions in $CHCl_3$/ACN. Adapted with permission. [252] Copyright 2023, MDPI.

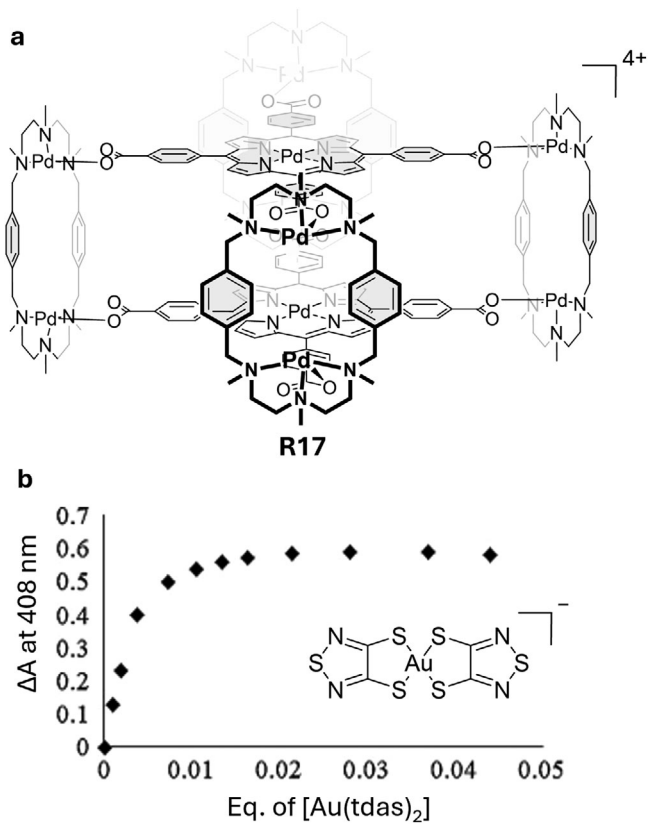


**FIGURE 22** | (a) Truncated chemical structure of R17 used for UV–vis-based detection of bisdithiolene-type metal complexes. (b) UV-vis monitoring of the titration of R17 with $[Au(tdas)_2]^-$ and the corresponding absorbance variation at the Soret band as a function of substrate concentration. Adapted with permission. [253], Copyright 2013, Wiley-VCH.

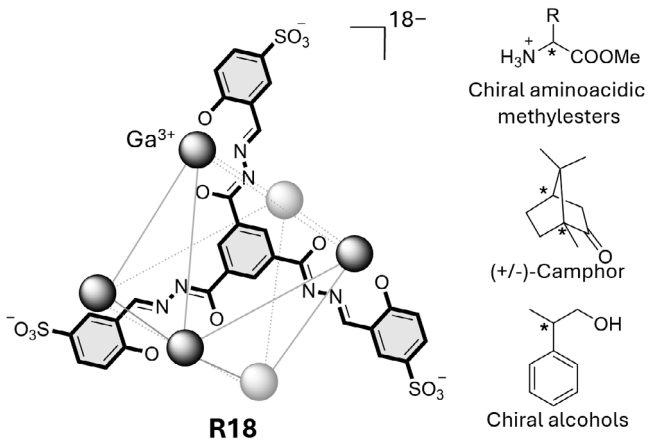


**FIGURE 23** | Truncated chemical structure of R18 and representative chiral organic and bioactive molecules detected through CD measurements in water.

receptor shows AIE features, where **R22** acts as a selective luminescence turn-off sensor for thiol-containing amino acids in water, as cysteine addition causes progressive luminescence quenching with μM-level detection limits, whereas other amino acids produce negligible interference. Mechanistic studies showed that cysteine triggers decomposition of **R22** into the free TPE ligand. Beyond sensing, **R22** enabled lysosome-targeted imaging in A549 cells displayed strong antibacterial activity against *Staphylococcus aureus*, and showed selective anticancer activity.

Zhang, Stang, and co-workers reported emissive tetragonal prismatic Pt(II) cages (**R23**) assembled from eight Pt(II) acceptors, four dipyridyl ligands, and two TPE-based sodium benzoate ligands (Figure 28) [262]. Cages incorporating 1,2-di(4-pyridyl)ethylene pillars displayed TPE-based emission and acted as turn-on luminescence sensors for thiol-containing amino acids in MeOH/$H_2O$ (1:1, *v*/*v*). Although non-emissive in this solvent system, addition of cysteine or glutathione generates strong, linear luminescence responses with nM detection limits, while other amino acids produce negligible effects. NMR studies indicated that thiols decompose the cage through preferential Pt–S coordination, releasing the AIE-active TPE ligand that accounts for the turn-on signal. Notably, the cage can be regenerated by adding $Pt^{2+}$ acceptors, enabling reversible and stimuli-responsive assembly.

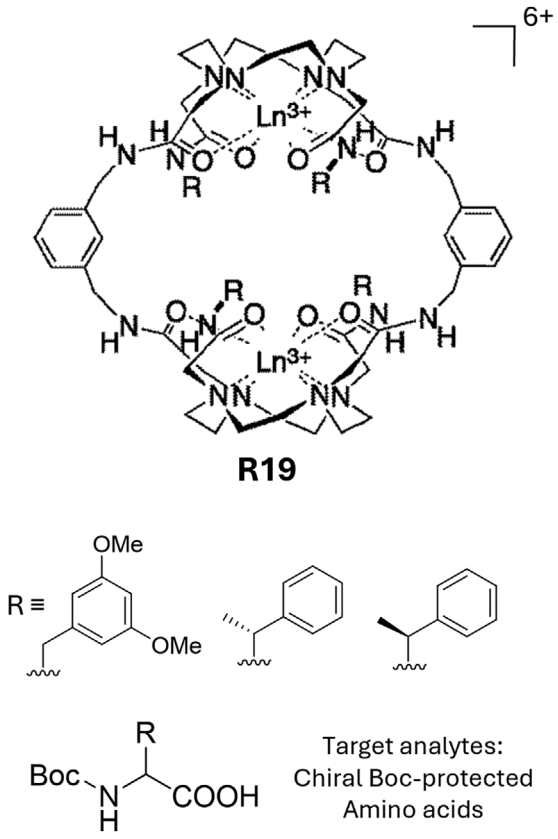


**FIGURE 24** | Chemical structure of the bis(octadentate cyclen)-based cage-receptor R19, functioning as a chirality sensor for *N*-Boc-protected amino acids.

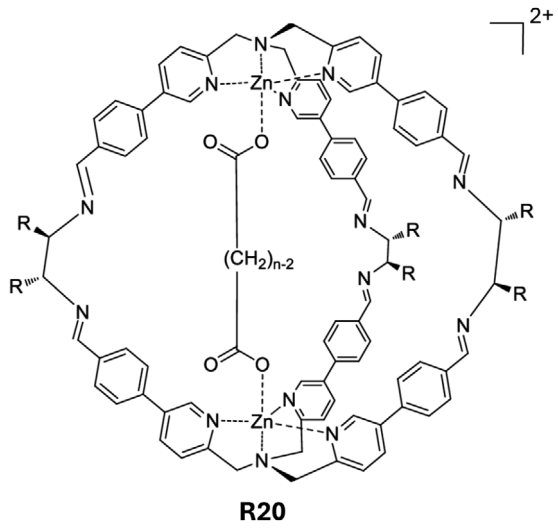


**FIGURE 25** | General structure of the R20 receptor with a dicarboxylic acid bound inside the cage-receptor's cavity, detected via changes in the CD signal.

The application of cage receptors in indicator displacement assays (IDAs) is well developed for synthetic macrocyclic chemosensors but remains comparatively underexplored for discrete cage-receptors [45, 46]. IDAs are particularly attractive because they provide a straightforward strategy to harness spectroscopically silent cage receptors for analyte detection by employing a

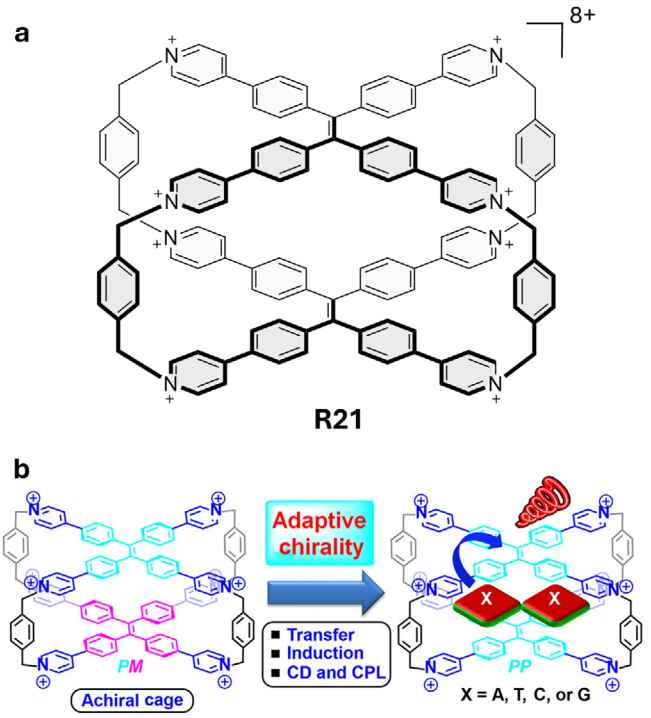


**FIGURE 26** | (a) Chemical structure of R21, which hosts two nucleotides, while host–guest complex formation with the cage-receptor produces measurable (b) changes in luminescence emission intensity and induces chiroptical responses such as CD and CPL signals. Adapted with permission. [258] Copyright 2021, Chinese Chemical Society.

reporter dye whose optical properties change upon encapsulation within the cage cavity or displacement by a more strongly binding analyte. Natarajan and co-workers developed two water-soluble triazolium covalent cages (**R24**), prepared by a CuAAC click approach followed by triazole *N*-methylation and chloride exchange (Figure 29) [263]. Their rigid hydrophobic cavities, cationic surfaces, and hydrogen-bonding triazolium sites make these cages well-suited for adenosine triphosphate (ATP) sensing via an IDA format in HEPES buffer using 8-hydroxypyrene-1,3,6-trisulfonic acid trisodium salt (HPTS) as the reporter dye. ATP binding displaces HPTS, whose emission intensifies once free in solution because it is no longer quenched by charge-transfer processes inside the cage. This IDA achieved nM detection limits and over 90-fold signal enhancement. The cages show strong selectivity for ATP over adenosine diphosphate (ADP), adenosine monophosphate (AMP), nicotinamide adenine dinucleotide (NAD), and thymidine monophosphate (TMP), while partial responses to guanosine triphosphate (GTP), cytosine triphosphate (CTP), uridine triphosphate (UTP), and pyrophosphate ($PP_i$) reflect contributions from phosphate charge density and adenine $\pi$-stacking. NMR and computational studies confirmed adenine encapsulation through $\pi$-stacking and triazolium–triphosphate hydrogen bonding. Interestingly, the sensing platform remains effective across pH 3–11 and in complex media, including 10% bovine serum albumin, human serum albumin, and human serum, where ATP binding is still detectable at μM concentrations with LoDs in the nM regime.

The same group also reported two $Pd^{2+}$ coordination cages (**R25**) for the luminescent-based detection of bile acids in water

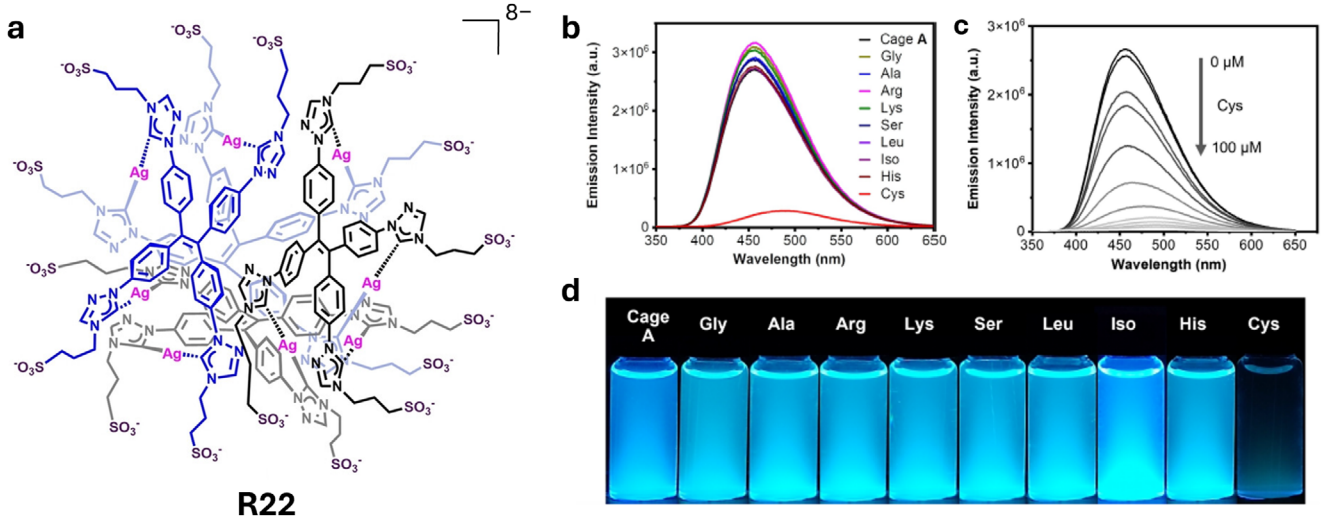


**FIGURE 27** | (a) Chemical structure of R22 in water, used for luminescence-based detection of thiols such as cysteine. (b) Fluorescence spectra of R22 upon the addition of different amino acids. (c) Fluorescence spectra of R22 with increasing concentrations of cysteine. (d) Photograph showing the fluorescence response of amino acid solutions in the presence of R22 in water under UV excitation. Adapted with permission. [261] Copyright 2023, Wiley-VCH.

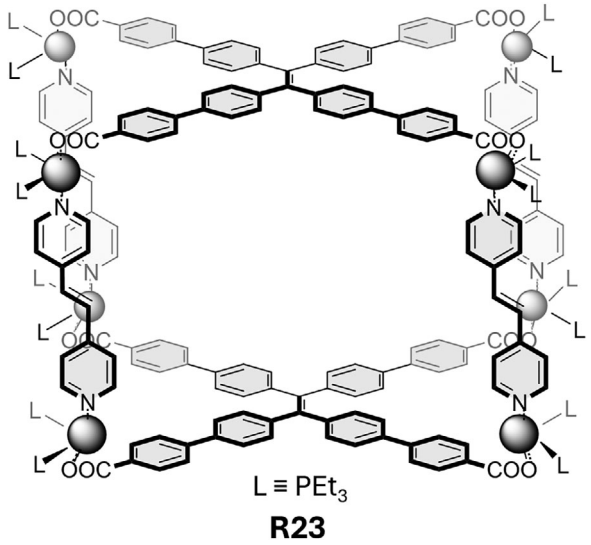


**FIGURE 28** | Chemical structure of R23, used for luminescence-based detection of cysteine or glutathione in aqueous media, which triggers cage disassembly and thereby restores the luminescence of TPE. Schematic representation of the self-assembly process of R23.

(Figure 30) [264]. Specifically, inspired by the Fujita-type cage design, the authors employed an expanded analogue derived from a conformationally flexible triazine–pyridine ligand. The larger triazine–pyridine cage accommodates two amphiphilic bile acids in a 1:2 stoichiometry, stabilized by cooperative interguest hydrogen bonding. Importantly, this analogue enables luminescence-based detection of chenodeoxycholic acid (CDCA), deoxycholic acid (DCA), and ursodeoxycholic acid (UDCA), achieving nM detection limits when sulforhodamine 101 (SR101) is used as the indicator dye.

A more recent example utilizing an IDA-based detection method was reported by Martínez-Máñez, Martí-Centelles, and co-workers, who employed a Pd-based molecular cage for scopolamine detection using an IDA format with luminescent readout with fluorescein (FL) [265]. The cage, formed by reacting a 4,4′-oxydi(benzohydrazide) linker with $[Pd(3\text{-pyridinecarboxaldehyde})_4](NO_3)_2$, yielded the receptor **R26** (Figure 31), previously developed by the group for doxorubicin delivery [266]. A preassembled **R26**⊃$(FL)_2$ complex containing two encapsulated dye molecules served as the sensor. Upon addition of scopolamine, FL was displaced, forming a new 1:2 scopolamine–**R26** complex (**R26**$_2$⊃scopolamine), accompanied by a detectable increase in the emission of the displaced fluorescein. This enabled detection at diagnostically relevant low-micromolar limits of detection. Other drugs, such as ecstasy or ketamine, have been shown to cause a moderate increase in luminescence and could therefore potentially interfere with scopolamine detection.

Yuan and co-workers reported a phenanthroline-based trefoil-shaped metal–organic cage (**R27**) that functions as a multifunctional fluorescent sensor for $Fe^{3+}$, $Cr_2O_7^{2-}$, and nitrofuran/nitroimidazole antibiotics (Figure 32) [267]. The receptor $[Cd_3L_3{\cdot}6MeOH{\cdot}6H_2O]$, synthesized through a solvothermal method from a phenanthroline-derived ligand ($H_2L$) and $CdI_2$, is water-stable and microporous. Luminescence studies in aqueous solution revealed strong quenching upon addition of $Fe^{3+}$ or $Cr_2O_7^{2-}$, with LoDs in the low μM range. The quenching mechanism was attributed to resonance energy transfer, supported by spectral overlap between the analytes' absorption and the cage excitation band. Importantly, the sensing response was reversible and retained after five cycles without structural degradation. For antibiotics, the cage-receptor displayed efficient fluorescence quenching with nitrofurazone (NFZ), nitrofurantoin (NFT), metronidazole (MNZ), and ornidazole (ONZ), with detection limits as low as 0.52 μM.

Pushing the application further toward blood detection, Carillo, Lahoz, and co-workers utilized TPE units within a covalent

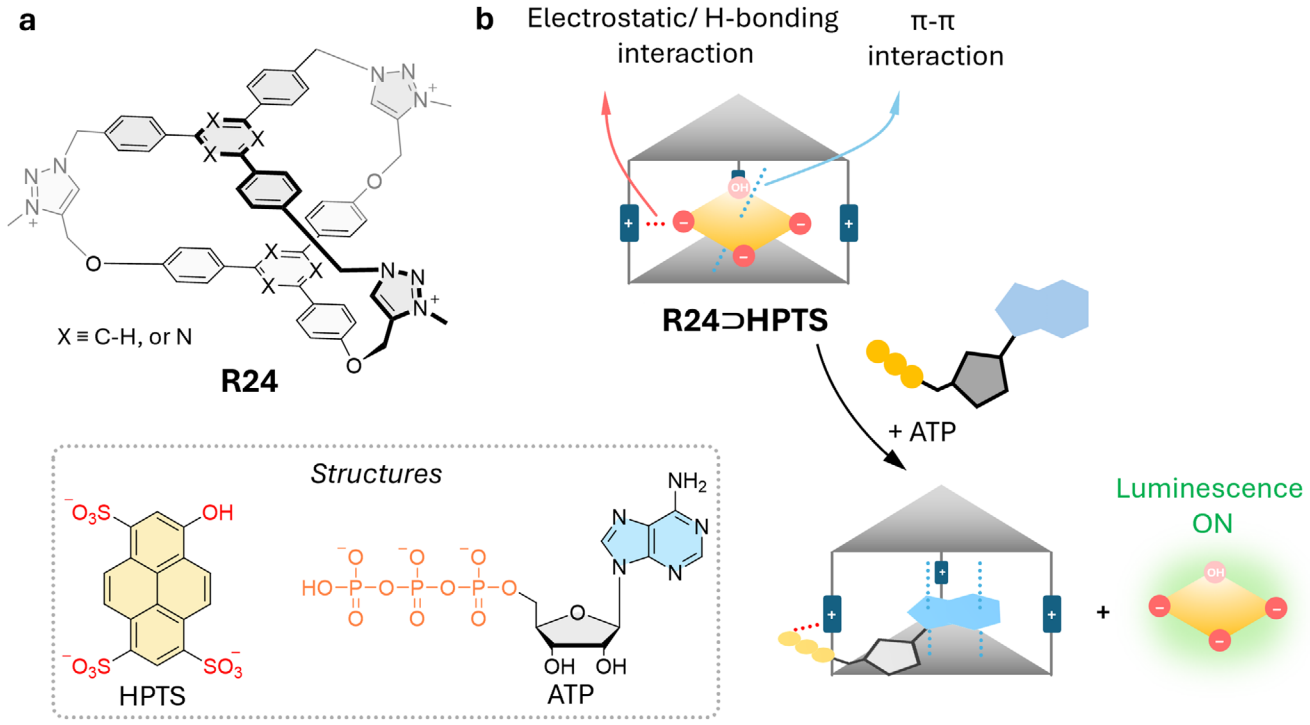


**FIGURE 29** | (a) Chemical structures of the receptors R24 used for IDA-based detection of ATP in buffered solutions. (b) Working principle and structure of HPTs used in the IDA for luminescence-based detection of ATP.

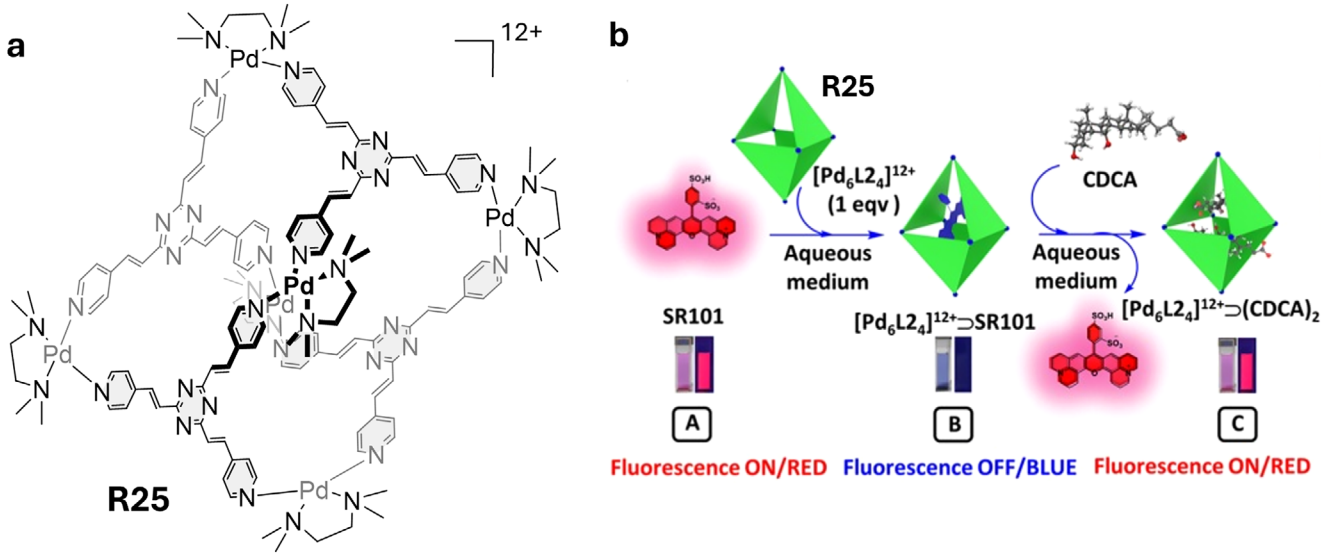


**FIGURE 30** | (a) Chemical structure of R25 used as a cage-receptor for the detection of bile acids in water through an IDA format. (b) Schematic representation of the working principle of the IDA for luminescence-based detection of CDCA. Adapted with permission. [264] Copyright 2024, American Chemical Society.

cage, in which a thiol–Michael addition provides stable thioether pillars supporting the TPE top panels, albeit with yields that remain amenable to future optimization [268]. One isomer of the resulting cage-receptor (**R28**, Figure 33) was found to be luminescent, and in the presence of 3-nitrotyrosine, an important kidney disease marker, the luminescence was quenched, enabling its detection in aqueous solutions at low micromolar concentrations and, more importantly, in diluted blood samples spiked with 3-nitrotyrosine, achieving low micromolar LoDs. Because of its limited solubility, the cage-receptor necessitates the use of an organic co-solvent (e.g., DMSO) for effective operation. Despite this requirement, its demonstrated performance in blood samples provides a compelling illustration of its practical applicability and diagnostic potential.

In 2012, the Davis group reported a bisanthracenyl-based cage-receptor that enables fluorescence-based detection of glucose in water through the anthracene panels incorporated into the recep-

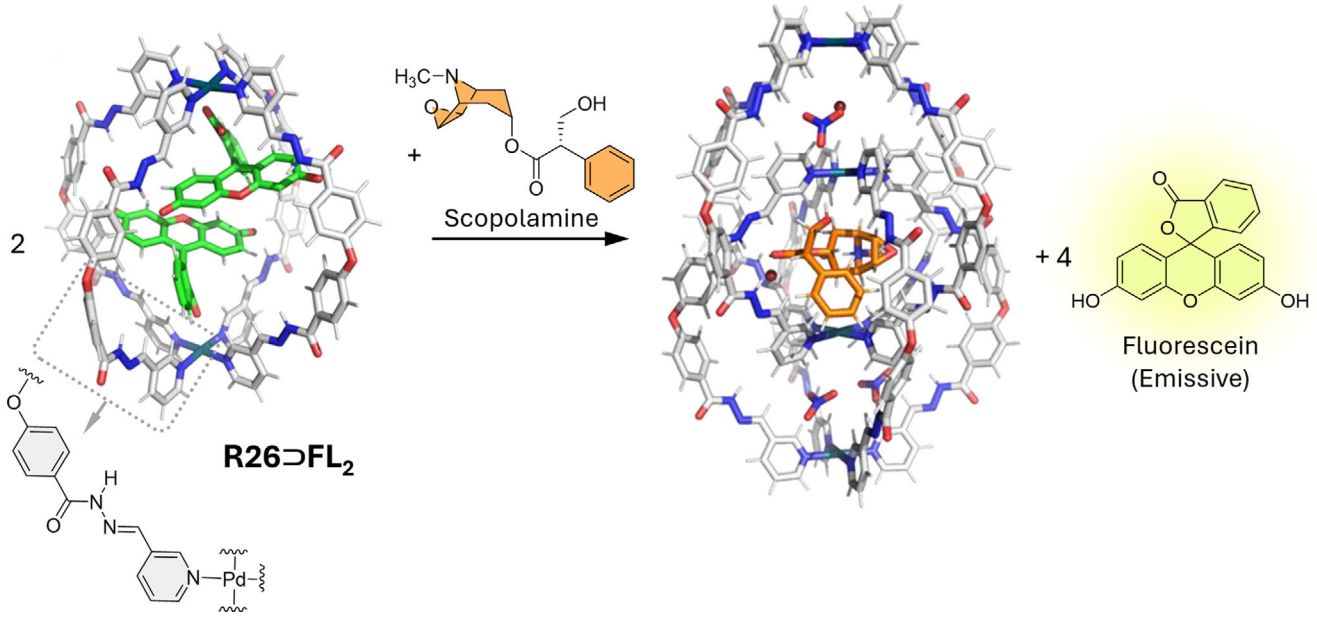


**FIGURE 31** | Molecular structure of R26 derived from X-ray analysis and its assembly with the FL reporter dye to form [R26⊃$FL_2$], which enables scopolamine detection in an IDA format, as the analyte displaces FL from the cage-receptor, rendering the free dye emissive. Adapted with permission. [265] Copyright 2025, Wiley-VCH.

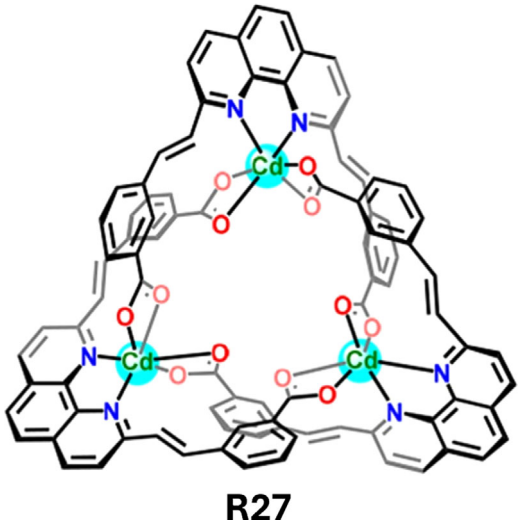


**FIGURE 32** | Chemical structure of R27 used for the luminescence-based detection of antibiotics, such as MNZ, in water. Adapted with permission. [267] Copyright 2023, American Chemical Society.

tor design [269]. Importantly, the cage-receptor (**R29**, Figure 34) bears six carboxylate pendants, which confer millimolar water solubility. The binding affinity for $\beta$-glucose is moderate (56 $M^{-1}$), yet millimolar concentrations of this analyte could be detected, as binding to the receptor led to quenched anthracene emission in phosphate buffer. Although some in vivo applications have been explored, the binding affinities of such cages must be further increased to render them suitable for practical use.

Instead of employing the established C—H···$\pi$ and N-H···O interactions used by the Davis group, Tan, Stoddart, and their coworkers utilized C—H···$\pi$ and C—H···O interactions for glucose binding. They introduced two pyrene-based molecular cages (**R30**, Figure 35) [270], where the pyrene panels act as the roof and floor of the structure, providing flat, electron-rich surfaces for interaction with all-axial C—H bonds of glucose in its chair conformation. Four para-xylylene pillars regulate the distance between the roof and floor. The polarized C—H bonds function as hydrogen-bond donors, forming multiple C—H···O hydrogen bonds with the hydroxyl groups of glucose. Upon glucose binding, these receptors exhibit enhanced fluorescence intensity, making them effective for glucose sensing in water.

### 4.3 | Detection of Environmental Pollutants

Environmentally relevant nitroaromatic pollutants are attractive guests for molecular cages because their electron-poor aromatic rings engage in strong $\pi$–$\pi$ stacking, charge-transfer, and hydrogen-bonding interactions with electron-rich, shape-matched cavities, leading to favorable interactions accompanied by a luminescence change of the cage-receptor. Stang, Chi, Mukherjee, and co-workers reported $M_3L_2$ trigonal cages assembled from preorganized metalloligands bearing octahedral Al(III), Ga(III), or R(II) centers and Pt(II) acceptors, yielding trigonal-bipyramidal and trigonal-prismatic architectures (**R31**, Figure 36) [271]. Two $Ru^{2+}$-based trigonal–prismatic cages, assembled from 1,3,5-tris(4-pyridylethynyl)benzene and half-sandwich arene-Ru acceptors, were designed with electron-rich ethynyl linkers that impart intrinsic luminescence. Their electron-rich framework promotes strong donor–acceptor interactions with electron-deficient nitroaromatics. In MeOH, luminescence was efficiently quenched by trinitrotoluol (TNT) and picric acid (PA). TNT induced clear quenching of **R31**, enabling μM-level detection, while PA produced even stronger quenching consistent with its higher electron deficiency. Selectivity studies showed that

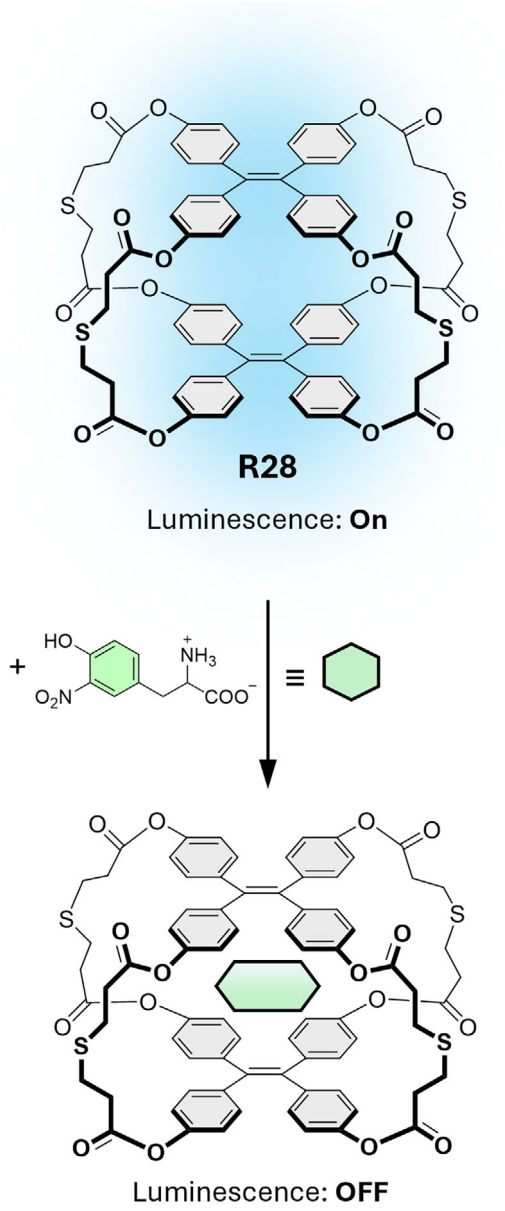


**FIGURE 33** | Chemical structure of the cage-receptor R28 used for the detection of the chronic kidney disease biomarker 3-nitrotyrosine in aqueous solution and in diluted blood samples via luminescence-quenching-based detection upon host–guest binding.

only nitroaromatics caused substantial quenching, supporting an excited-state electron-transfer or charge-transfer mechanism.

Sun and co-workers reported luminescent lanthanide cages that undergo a concentration-controlled helicate-to-tetrahedron transformation using oxazoline-based bis(tridentate) ligands and $Eu(OTf)_3$ (Figure 37) [272]. The $Eu_4(L1)_6$ cage-receptor (**R32**) exhibited enhanced red luminescence, and the addition of several nitroaromatics led to emission quenching, with PA producing the strongest response and enabling detection in the micromolar range. UV–vis titrations and lifetime measurements indicated that quenching arises from ground-state charge-transfer complex formation between the $\pi$-rich oxazoline ligands and electron-poor nitroaromatics, disrupting the $Eu^{3+}$ antenna effect.

Near-infrared (NIR) emission is particularly valuable in sensing because it penetrates deeper into samples and experiences much lower background autofluorescence, which together provide higher signal-to-noise ratios and enable more sensitive detection in complex environments. Pan and co-workers developed the first NIR-emissive lanthanide cage for nitroaromatic sensing, a $Nd^{III}$-based binuclear assembly (**R33**) formed from the (4,4′,4′′,4′′′-(ethene-1,1,2,2-tetrayl)tetrakis(benzene-4,1-diyl))tetrakis(methylene)tetrapyridin-4(1*H*)-one (TPE-4PO) ligand [273]. In DMSO, **R33** shows characteristic $Nd^{3+}$ NIR emission that is selectively and strongly quenched by P, with negligible response to other nitroaromatics. Time-resolved photoluminescence and NMR studies reveal a predominantly static quenching mechanism arising from specific host–guest interactions. Li and co-workers reported a carbazole-based $M_2L_3$ cage (**R34**, $Zn_2(L1)_3(NTf_2)_4$) designed for cavity-directed sensing of nitroaromatic explosives (Figure 38) [274]. The cage, which is assembled from a V-shaped carbazole ligand and $Zn(NTf_2)_2$ in ACN, shows strong carbazole-centered emission. PA induces up to 55% quenching with 1:1 host–guest binding and a high affinity, whereas other nitroaromatics produce much weaker responses. Isothermal titration calorimetry

(ITC) revealed enthalpy-driven binding, and mass spectrometry analysis confirmed the formation of the inclusion complex $[PA\subset\mathbf{R34}]^{3+}$. The quenching mechanism involves a PET step from the electron-rich carbazole panels to the electron-poor PA, facilitated by $\pi$–$\pi$ stacking within the cage cavity.

Zhang and co-workers reported two hexanuclear heterometallic cages, $[Co_4Ln_2(LH_{2\text{-}5})_2(H_2O)_4]\cdot(ClO_4)_6\cdot NO_3\cdot nH_2O$ (Ln = Dy or Yb, **R35**), assembled solvothermally from a carboxylate-functionalized tris-triazamacrocyclic ligand ($H_6L$) with $Co^{2+}$ and $Ln^{3+}$ ions (Figure 39) [275]. The resulting nitrate-encapsulated cages were structurally robust in solution and in suspension. In DMSO, both complexes display ligand-centered luminescence that is strongly quenched by nitroaromatic analytes, with PA inducing near-complete quenching and affording nM LoD-levels. Control experiments confirmed that the cages remain structurally intact in the presence of PA, excluding decomposition as the origin of quenching. Mechanistic studies pointed to the involvement of both PET and Förster resonance energy transfer (FRET), supported by significant spectral overlap between the cage emission and PA absorption.

Reversal of AIE in the presence of PA for its detection was also exploited by Mukherjee and co-workers, who developed a tetraphenylpyrazine-based tetraimidazole ligand that self-assembled with Pt(II) to form a tetrafacial barrel, $Pt_8L_4(PEt_3)_{16}$ (**R36**, Figure 40) [276]. In acetone/$H_2O$ (80:20 *v*/*v*), where **R36** is less soluble due to the presence of water, it shows a nine-fold luminescence enhancement when compared to pure acetone, where it is soluble. Interestingly, the $Pd^{2+}$ analogue displays aggregation-induced quenching. **R36** functions as a highly selective luminescent sensor for PA. Indeed, titration studies showed a 98% quenching with PA, 40% with 4-nitrophenol, and a negligible response to other nitroaromatics. Mechanistic studies indicated that sensing arises from a combination of hydrogen bonding, $\pi$–$\pi$ stacking with the pyrazine core, and FRET enabled by strong overlap between PA absorption and cage emission.

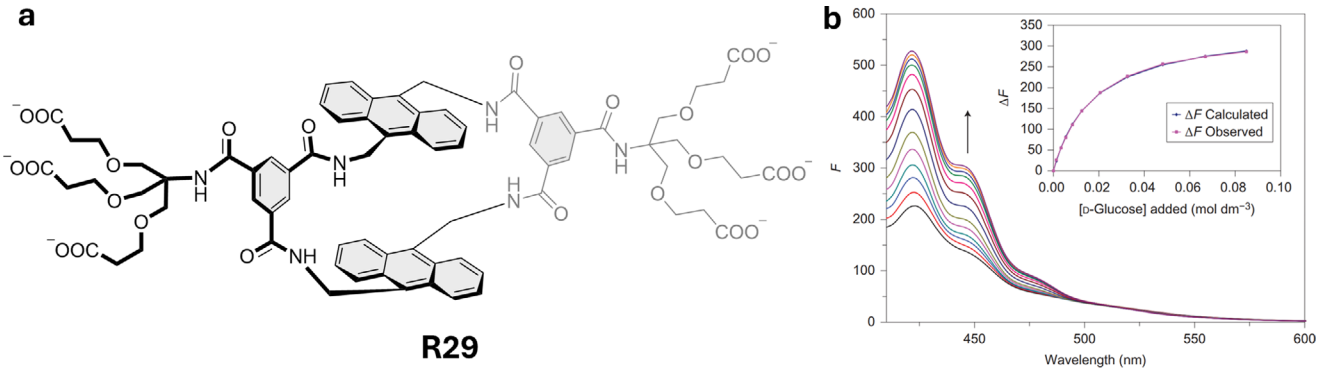


**FIGURE 34** | (a) Chemical structure of the bisanthracenyl-based cage-receptor R29 developed by Davis and coworkers, and (b) fluorescence-based detection of $\beta$glucose at millimolar concentrations in phosphate buffer. Adapted with permission. [269] Copyright 2012, Nature Springer.

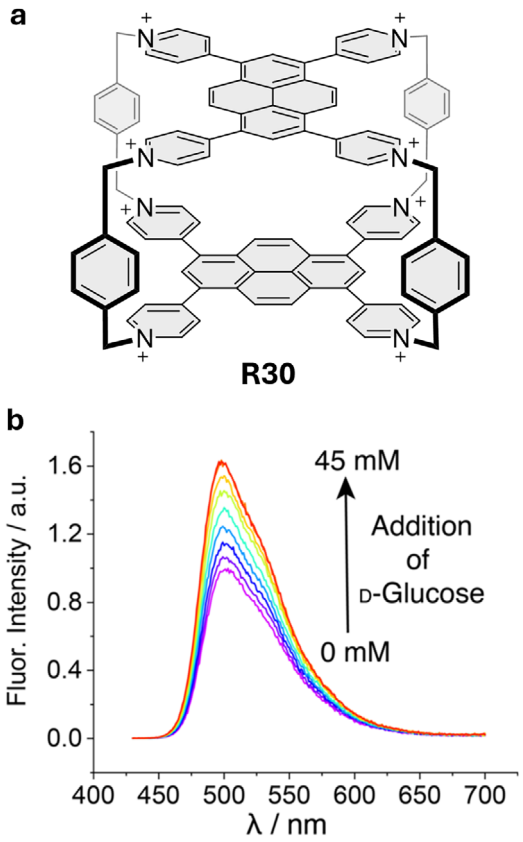


**FIGURE 35** | (a) Chemical structure of R30, and (b) its luminescence response to glucose binding in water. Adapted with permission. [270] Copyright 2021, American Chemical Society.

He and co-workers reported a phenoxazine-based supramolecular $Zn_2L_3$ cage (**R37**) constructed from V-shaped dipyridylphenoxazine ligands and $Zn(BF_4)_2$ by coordination-driven self-assembly (Figure 41) [277]. The resulting cage-receptor **R37** shows strong phenoxazine-centered emission in ACN. Luminescence titrations revealed highly selective quenching by PA, with the addition of one equivalent causing a pronounced decrease in emission, whereas other nitroaromatic analytes induced only minor effects. Mechanistic investigations confirmed the encapsulation of a single PA molecule within the cavity, and the sensing response was attributed to photoinduced electron transfer from the electron-rich phenoxazine core to the electron-deficient PA, further reinforced by $\pi$–$\pi$ stacking interactions and tight confinement within the host cavity.

Luminescence-based detection of monofluorinated compounds has become increasingly important because many are toxic and highly persistent. Furthermore, there is growing concern that, when used as replacements for classic per- and polyfluoroalkyl substances (PFAS), they might eventually be subject to a comparable regulatory framework [278]. Besides, traditional detection methods for such compounds rely on laborious and cost-intensive chromatography-based techniques [279]. In this respect, Nitschke and co-workers expanded the functional scope of $Cu^+$ coordination cages with a $Cu_6L_4$ pseudo-octahedral assembly (**R38**) that undergoes dynamic stereochemical reconfiguration while displaying highly selective guest recognition (Figure 42) [280]. The cage-receptor, formed by condensing trianiline with 6-methyl-2-formylpyridine and coordinating the ligand to $Cu(MeCN)_4BF_4$, encapsulates tetrahedral guests with extended arms to yield unprecedented 3D suitanes via mechanically interlocked host–guest architectures. It shows good selectivity for fluorinated corticosteroids, with NMR data indicating exo-binding on the host's closed faces. Future studies could explore the detection of such analytes via indicator displacement or luminescence methods, for which this cage is a promising receptor.

As mentioned, the detection of PFAS has become increasingly important due to their toxic nature, which has stimulated the development of rapid luminescent sensors. However, efficient luminescent sensing systems remain scarce. Notably, Severin and co-workers have reported a heteroleptic $Pd_2L_2L'_2$ cage (**R39**, Figure 43) specifically engineered for the selective recognition and extraction of short-chain perfluoroalkyl carboxylates [281]. The tetracationic cage, formed from diimidazolyl and dipyridyl ligands, presents polarized CH donors that are preorganized for carboxylate binding. In $CD_3CN$, **R39** binds trifluoroacetate ($TFA^-$) with medium affinity and encapsulated longer perfluorocarboxylates ($C_2F_5COO^-$ to $C_4F_9COO^-$) with slightly lower affinities. $TFA^-$ binding occurs through a dense network of CH···O and CH···F interactions. A key feature of **R39** is its ability to extract PFAS directly from buffered aqueous solution (50 mM HEPES, pH 7.5) into $CD_3NO_2$ with high efficiency, while common inorganic anions ($F^-$, $Cl^-$, $NO_3^-$, $AcO^-$, $CO_3^{2-}$, $HPO_4^{2-}$) are not extracted. Control experiments with related Pd complexes

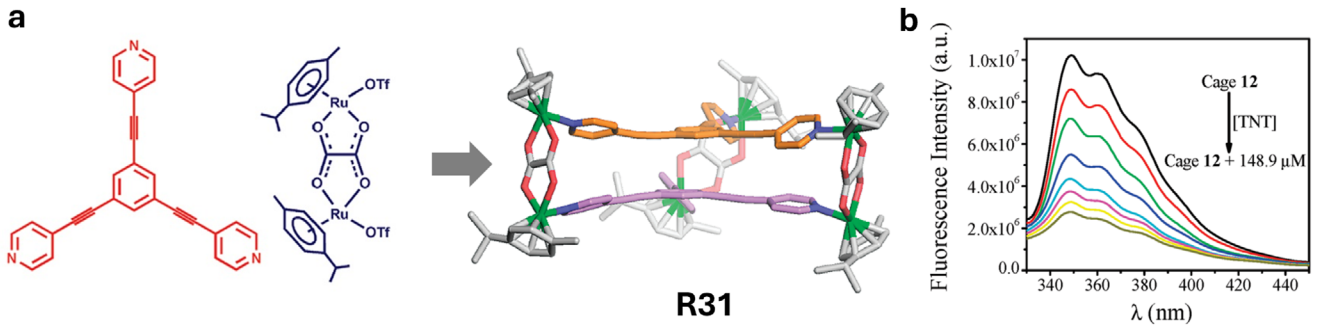


**FIGURE 36** | (a) Chemical structure of the building blocks of R31 and its X-ray derived molecular structure. (b) Fluorescence spectra of R31 (1.0 μM in methanol) in the presence of TNT (0–175 μM). Adapted with permission. [271] Copyright 2011, American Chemical Society.

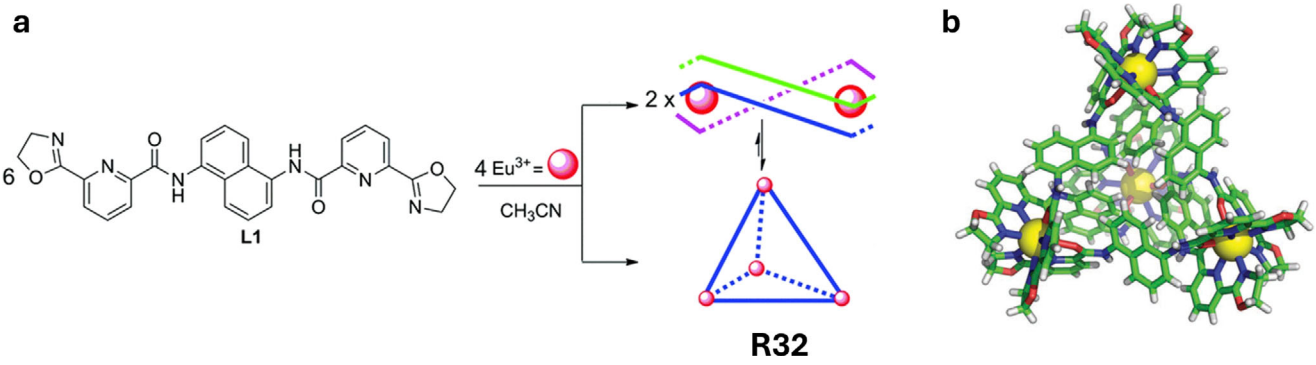


**FIGURE 37** | (a) Concentration-triggered self-assembly of either an $Eu_2(L1)_3$ helicate or an $Eu_4(L1)_6$ tetrahedron R32 from ligand L1. (b) X-ray-derived molecular structure of R32. Adapted with permission. [272] Copyright 2017, The Royal Society of Chemistry.

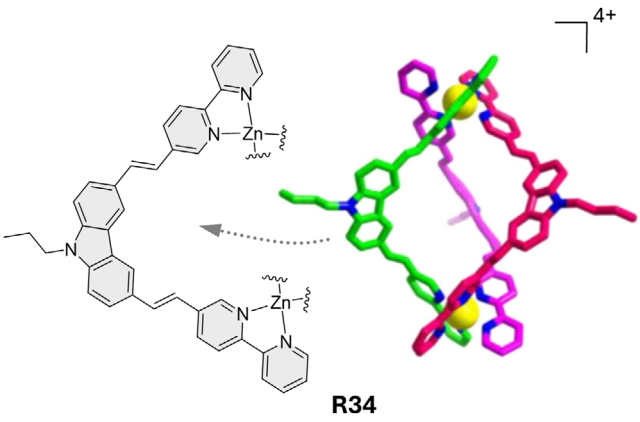


**FIGURE 38** | Truncated chemical structure and energy-optimized theoretical model of R34 used for the luminescence-based detection of nitroaromatic compounds, such as picric acid. Adapted with permission. [274] Copyright 2020, Elsevier.

or tetraalkylammonium salts showed markedly lower extraction (12%–27%), underscoring the essential role of the imidazole-based binding pocket and preorganized CH donors in enabling selective PFAS recognition.

Another significant form of environmental contamination can be further constituted by the employed dye molecules themselves, in the case in which they are not adequately removed from wastewater and subsequently able to enter drinking water

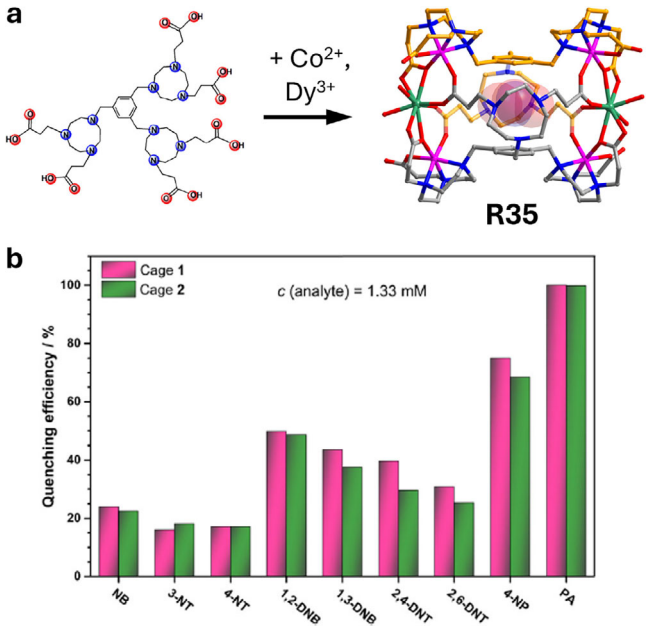


**FIGURE 39** | (a) Structure of the carboxylic acid functionalized tristriazamacrocyclic ligand $H_6L$. Mixing of $H_6L$ with $Co(ClO_4)_2{\cdot}6H_2O$ and $Dy(NO_3)_3{\cdot}6H_2O$ leads to the formation of R35. (b) Percentages of fluorescence quenching of R35 in DMSO obtained for various nitroaromatic analytes. Adapted with permission. [275] Copyright 2019, Wiley-VCH.

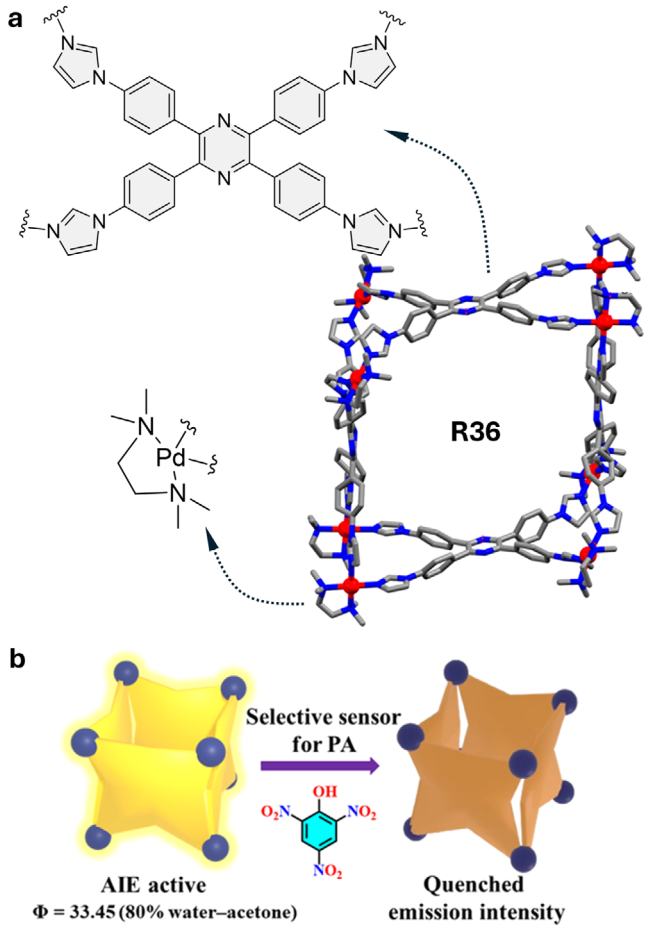


**FIGURE 40** | (a) Truncated chemical structures and molecular structure from X-ray diffraction experiments of R36 used for the luminescence-based detection of nitroaromatics, such as picric acid. (b) Sensing mechanism for the detection of PA by R36. Adapted with permission. [276] Copyright 2024, American Chemical Society.

sources. Hence, the monitoring of freshwater for organic dyes has become an increasingly important task. To this aim, Yoshizawa and co-workers reported a $Pt^{2+}$-linked $M_2L_4$ coordination capsule (**R40**) featuring an accessible hydrophobic cavity formed by bent bispyridine ligands and square-planar Pt(II) hinges, a design that stabilizes encapsulated $\pi$-chromophores by shielding them from solvent and suppressing nonradiative decay (Figure 44) [282]. Within this confined environment, dyes such as BODIPY, coumarin 153, and Nile red are quantitatively encapsulated in water and retain ≥60% of their intrinsic fluorescence efficiency, producing strongly emissive complexes (e.g., **R40**⊃BODIPY. Co-encapsulation with planar aromatics (anthracenes, phenanthrene, pyrenes) further modulated the emission wavelength and quantum yield via $\pi$–$\pi$ stacking and excimer-like interactions, yielding ternary complexes with color-tunable fluorescence from green to orange. Time-resolved spectroscopy confirmed long-lived excited states (**R40**⊃BODIPY), evidence that the capsule's rigid, metal-linked scaffold stabilizes emissive states far more effectively than $Pd^{2+}$ analogues. Together, these results demonstrate how the capsule's cavity geometry, $\pi$-acidic interior, and rigid $Pt^{2+}$ framework cooperate to enhance dye emission and enable fine control over photophysical properties, an approach with conceptual relevance for sensing emissive pollutants and designing aqueous photofunctional materials.

Fujita and co-workers showed that confinement within coordination cages can invert conventional guest photophysics, exemplified by tetraazaporphine (TAP) encapsulated in a $Pt^{2+}$-linked $M_6L_4$ cage (**R41**) in water (Figure 45) [283]. Within **R41**, TAP is stabilized through hydrophobic confinement and -surface interactions that suppress aggregation and, owing to the electron-deficient character of the cage, limit charge-transfer quenching, thereby preserving strong emission in water. The highly cationic host further influences the protonation state of TAP and shields its excited state from external quenchers, enabling reversible ON/OFF luminescence switching. Encapsulation of TAP in water, achieved upon heating, affords the **R41**⊃TAP inclusion complex, in which aggregation is effectively prevented, resulting in bright red luminescence arising from confinement within the cage-receptor. Notably, the emission is reversibly regulated by pH, with the addition of triethylamine under basic conditions inducing deprotonation of the encapsulated TAP and consequent luminescence quenching, whereas subsequent addition of $HNO_3$ restores the protonated, emissive state. In addition, the cage protects TAP from external quenchers such as dimethylformamide (DMF) and DMSO, reducing bimolecular quenching constants by nearly an order of magnitude.

Duan and co-workers reported the first amide-functionalized Ce(IV) tetrahedral cage (**R42**) for NO detection(Figure 46) [284]. The neutral $Ce_4(H_2TTS)_4$ cage features twelve inward-facing amide groups that create a hydrophilic–lipophilic cavity well suited to biological environments. In DMF/$H_2O$ (9:1, *v*/*v*), the cage exhibits weak blue emission that is almost completely quenched upon binding the nitronyl nitroxide 2-phenyl-4,4,5,5-tetra-methylimidazolineyloxyl-3-oxide (PTIO). Subsequent addition of NO to the **R42**⊃PTIO complex restores the emission within 5 min, producing up to a 12-fold turn-on and a detection limit of 5 nM. The response is highly selective for NO over other reactive oxygen and nitrogen species and remains stable across pH 5–9. Mechanistically, confinement of PTIO and NO within the cage brings the reactants into close proximity, accelerating the spin-trapping reaction in an enzyme-like fashion. Confocal microscopy in MCF-7 cells further demonstrated that intracellular fluorescence of **R42** is quenched by PTIO and recovered upon NO release from sodium nitroprusside, confirming its applicability for live-cell NO imaging.

While the use of pesticides has undoubtedly advanced agricultural practices and increased crop yields, their overuse and improper disposal have led to severe environmental contamination that threatens both ecosystems and human health. Prolonged exposure to certain pesticides, in particular, has been associated with a higher incidence of neurodegenerative diseases such as Parkinson's disease [285]. A recent study introduced a luminescent Ag(I)–carbene metallacage, $Ag_4(L)_{24}$, (L = tetraimidazolium ligand) formed through coordination-driven self-assembly of an AIE ligand [286]. This cage receptor **R43** (Figure 47) exhibits a 36-fold increase in fluorescence relative to the free ligand, owing to restricted intramolecular motion upon metal coordination. This strong emission enables sensitive detection of the pesticide 2,6-dichloro-nitroaniline (DCN) via fluorescence quenching, with a detection limit of 1.64 ppm arising from combined static and

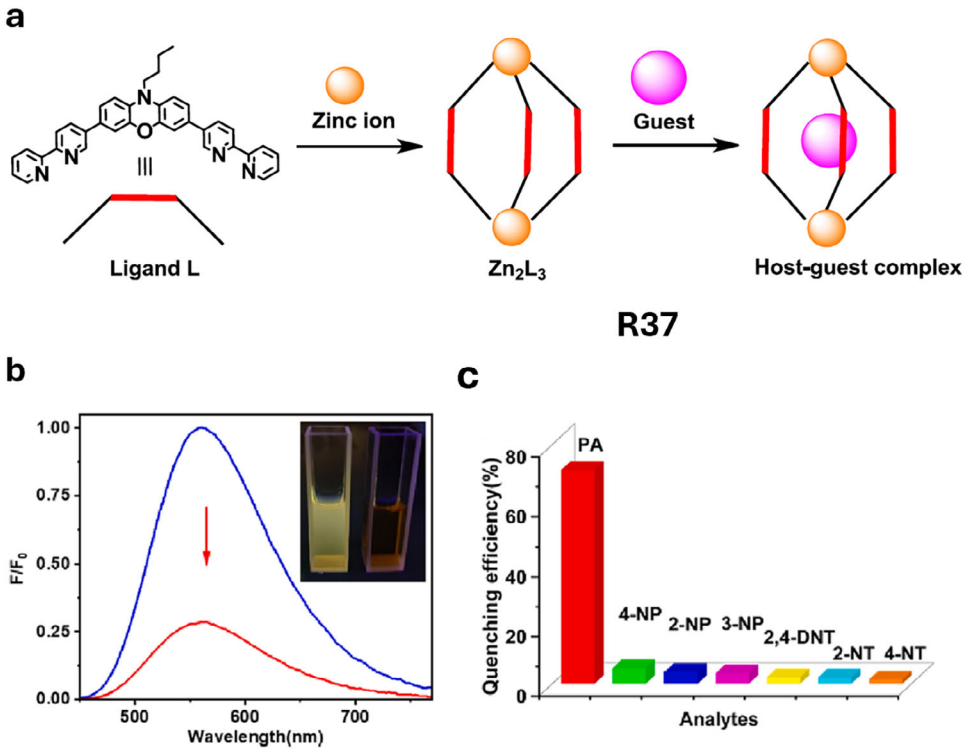


**FIGURE 41** | (a) Scheme for the synthesis of R37 and its formation of a host-guest complex with nitroaromatics, such as PA. (b) Fluorescent spectra of R37 upon the addition of PA (1.0 eq). (c) The quenching efficiencies of different nitroaromatic analytes. Adapted with permission. [277] Copyright 2023, Elsevier.

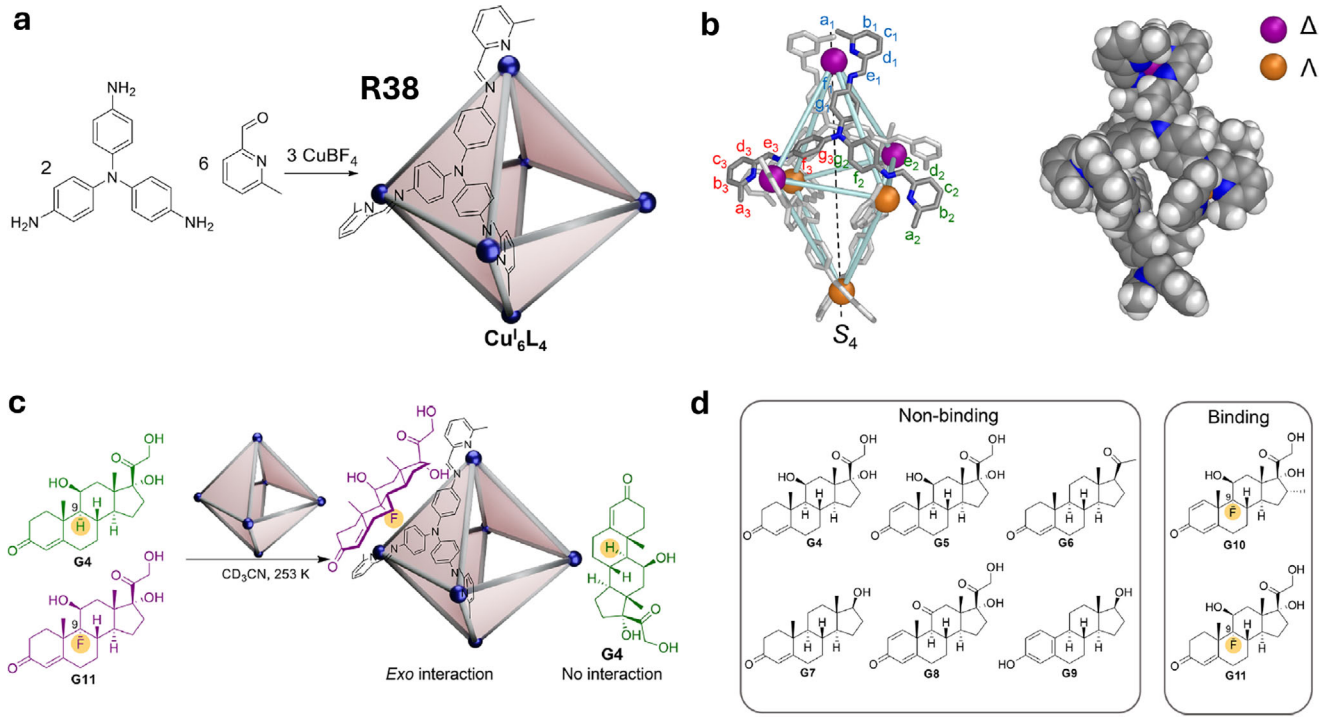


**FIGURE 42** | (a) Preparation and characterization of $CuI_6L_4$ cage R38. (b) Single-crystal X-ray structure of R38 and the pace-filling representation of R38. (c) Cartoon showing the putative *exo* binding mode of the fluorinated steroid G11 by R38 over its non-fluorinated steroid analogue. (d) The corticosteroids screened, showing those observed to bind and those that did not. Adapted with permission. [280] Copyright 2024, American Chemical Society.

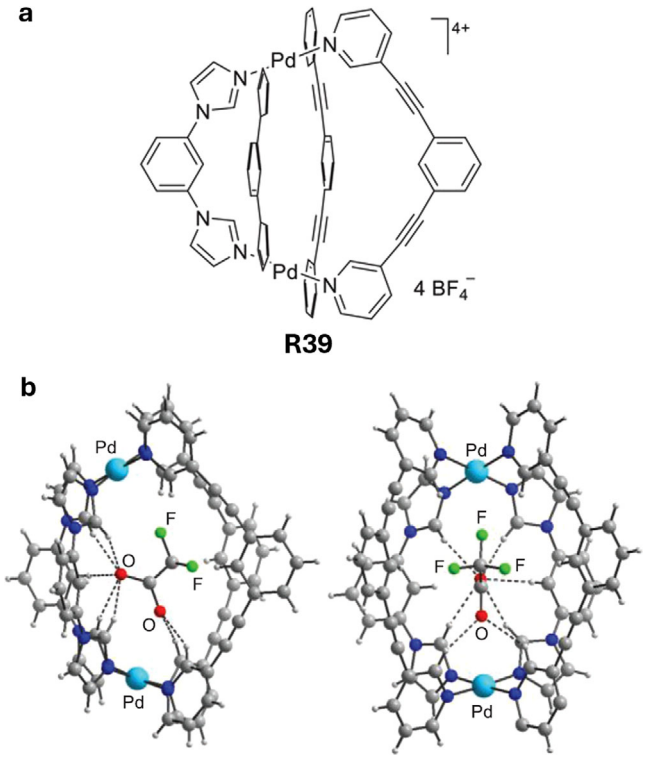


**FIGURE 43** | (a) Chemical structure of R39 used for the selective recognition and extraction PFAS. (b) Two different views of the molecular structure of R39⊃TFA as determined by single-crystal X-ray analysis. Adapted with permission. [281] Copyright 2024, Wiley-VCH.

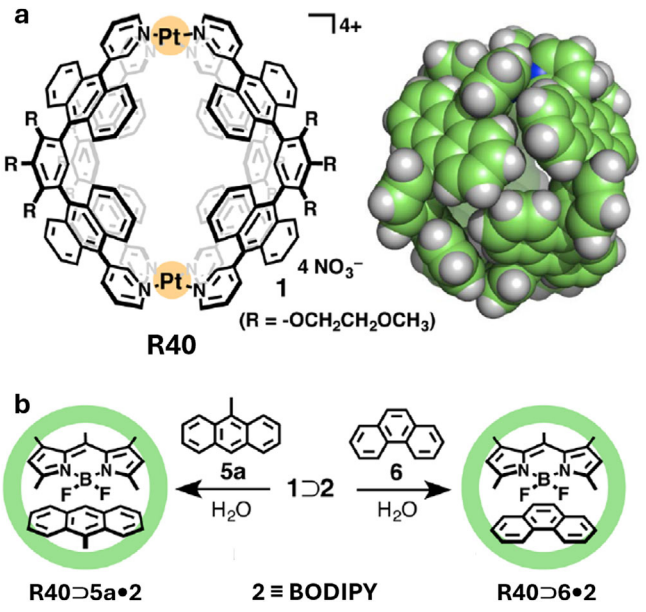


**FIGURE 44** | (a) Chemical structure of cage-receptor R40 and space-filling representation of its crystal structure (substituents and counterions omitted for clarity) used for the luminescence-based detection of aromatic compounds in water. (b) Schematic representation of the formation of R40⊃2·5a and R40⊃2·6 (2 ≡ BODIPY indicator dye). Adapted with permission. [282] Copyright 2015, American Chemical Society.

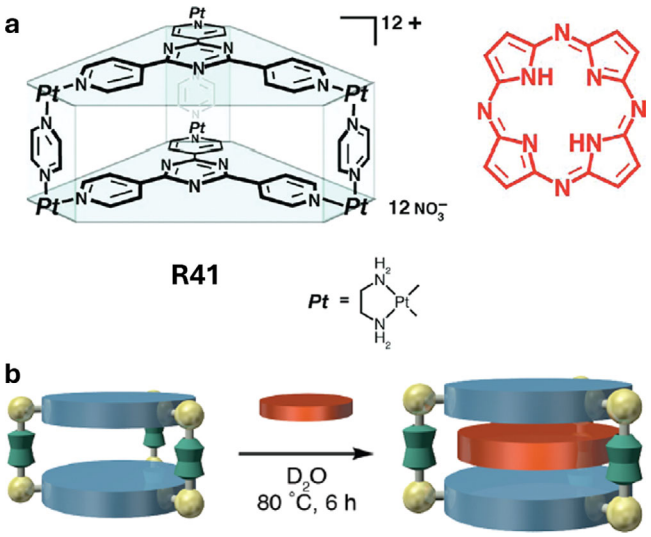


**FIGURE 45** | (a) Chemical structure of R41 and tetraazaporphine (TAP). (b) Schematic illustration of the host–guest complex formation between R41 and TAP (R41⊃TAP). Adapted with permission. [283] Copyright 2009, American Chemical Society.

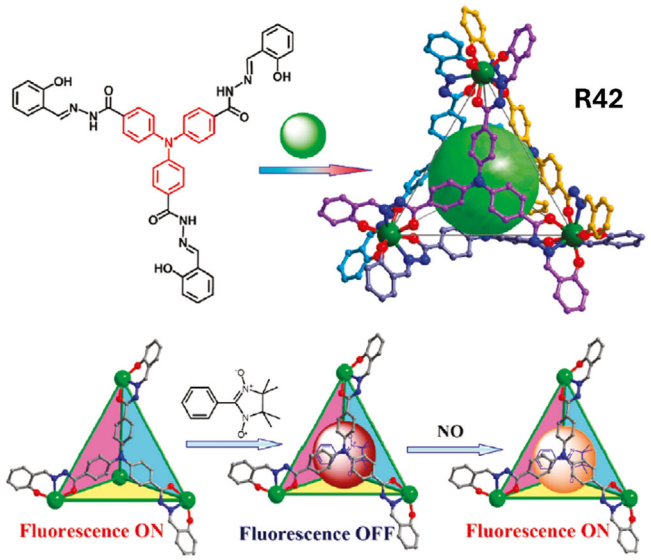


**FIGURE 46** | Chemical structure of **R42** and fragments of the functional tetrahedron showing the principle of fluorescent variation upon the addition of PTIO and NO. Adapted with permission. [284] Copyright 2011, American Chemical Society.

dynamic quenching. The study showcases silver–carbene coordination as a promising strategy for designing highly emissive supramolecular sensors for environmental monitoring. It will be interesting to explore whether analogous sensors can be developed for DCN detection in aqueous media.

## 5 | Biological Applications and Imaging

Imaging and tracking of diseases, drugs, and molecular signals in living systems, particularly in cells, rapidly and straightforwardly, is an important task for elucidating metabolic pathways and monitoring drug distribution, intending to improve therapeutic

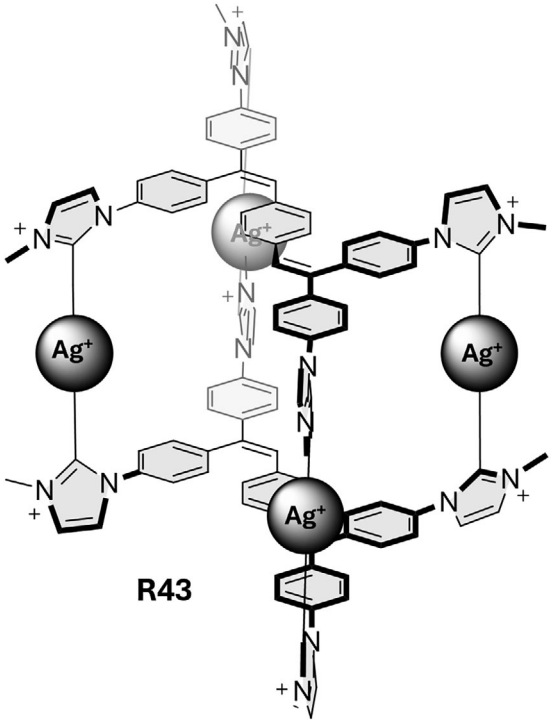


**FIGURE 47** | Chemical structure of R43 used for the luminescence-based detection of the pesticide 2,6-dichloro-nitroaniline in ACN.

efficiency and clarify underlying mechanisms. Among the available techniques, fluorescence-based detection methods remain particularly powerful, as they can be directly implemented in advanced microscopy platforms such as confocal, two-photon, or super-resolution microscopy, enabling spatially and temporally resolved studies within live cells. The continuous progress in luminescence spectroscopy has further enhanced the utility of these approaches: fluorescent and phosphorescent chemosensors or receptors now provide higher brightness, longer lifetimes, and improved photostability, allowing precise visualization even in complex biological environments [287–290]. Deoxyribonucleic acid (DNA) sensing and imaging play crucial roles in understanding cellular metabolism and disease detection. Beyond conventional DNA or ribonucleic acid (RNA) targets, DNA junctions [291] and G4s [292–294] have emerged as important DNA-based structures for sensing applications. G4s participate in gene regulation, replication, telomere maintenance, and genome stability, functioning both as beneficial regulators and potential genomic threats, thereby making them attractive targets for cancer therapy [295]. However, their selective detection and imaging remain challenging, because conventional DNA-binding dyes [45, 296] often fail to distinguish G4s from other nucleic acid structures, and cost-effective alternatives to antibody-based imaging protocols [297] are highly desired. Supramolecular chemistry has gained momentum as a strategy for G4 detection. In particular, host–guest-based transducer elements have been used in array formats to enable differential sensing and topology classification without the need for G4-selective ligands for each target [298]. After metal-based supramolecular squares and cylinder-like structures were shown to bind and stabilize DNA junctions [299, 300] and G4 structures [301–305], more recent studies have demonstrated that metallacages can also selectively recognize and stabilize these secondary structures [306, 307],

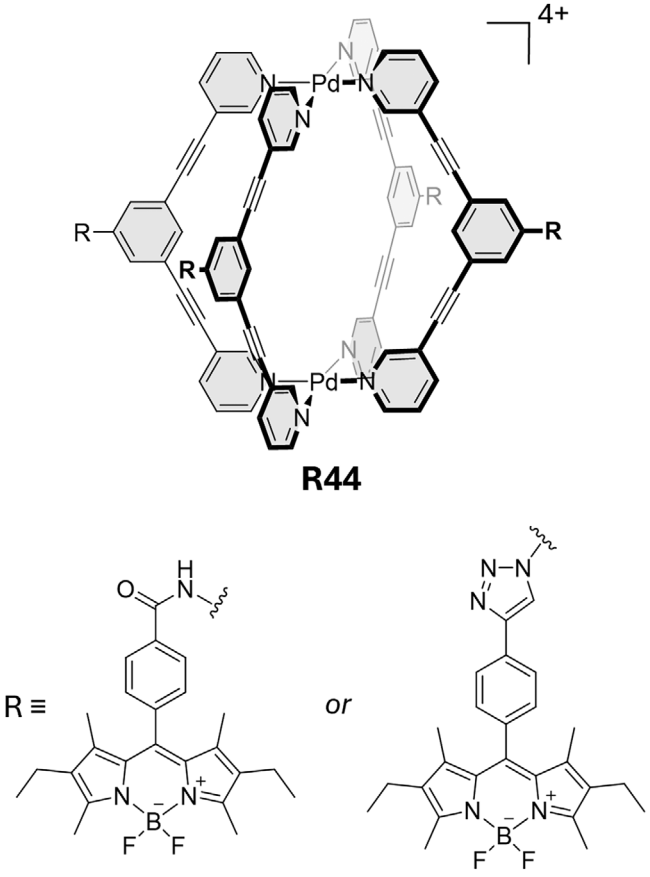


**FIGURE 48** | Synthesis of the $Pd_2L_4$ metallacages R44 *exo*-functionalized with BODIPY fluorophores.

thereby providing new opportunities to investigate G4 biology in living systems.

Casini and co-workers reported a family of BODIPY-functionalized $Pd_2L_4$ metallacages (**R44**) designed for fluorescence imaging and drug delivery in cancer cells (Figure 48) [308]. The cages were synthesized by self-assembly of bispyridyl ligands tethered to BODIPY dyes via amide or triazole linkages, yielding highly emissive complexes that remain stable for several hours in aqueous and PBS buffer. Noteworthy, the authors showed that glutathione promotes cage disassembly, where only part of the assembly remains intact (ca. 30%). Cytotoxicity assays in human melanoma A375 cells showed that the empty cages were non-toxic at concentrations up to 50 μM. In contrast, cisplatin-loaded cages retained anticancer activity comparable to free cisplatin, with $EC_{50}$ values of approximately 30 μM. Fluorescence microscopy showed efficient cellular uptake via endocytosis, with accumulation in cytoplasmic vesicles rather than in the nucleus, independent of counterion ($BF_4^-$ or $NO_3^-$). This work demonstrates how exo-functionalization with BODIPY enables bright luminescent metallacages for intracellular imaging, while preserving host–guest properties relevant to cisplatin encapsulation and delivery.

As noted above, G4s have emerged as important targets for imaging and sensing applications. However, despite the ability of metallacages to bind and stabilize these structures, a luminescence-based detection strategy has yet to be reported.

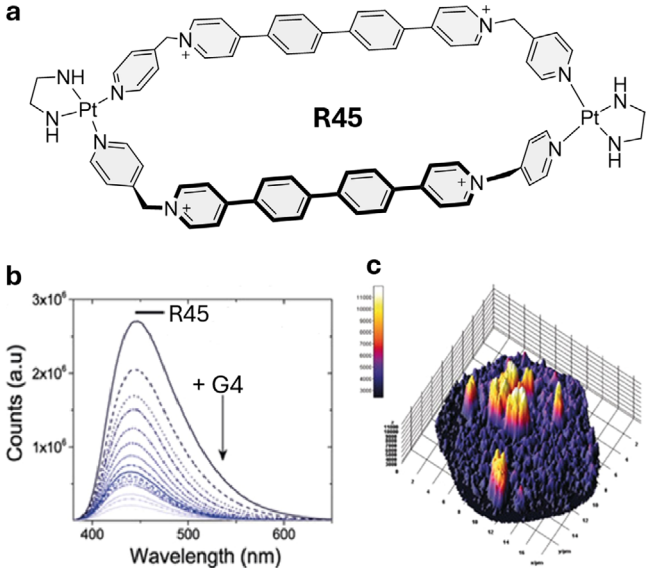


**FIGURE 49** | (a) Chemical structure of R45 used for G4 imaging in cells. (b) Luminescence response of R45 in the presence of G4s, showing increasing fluorescence quenching. (c) Subnuclear regions of a representative R45-treated nucleus visualized by three-dimensional surface plotting of single-pixel luminescence intensities (yellow: higher luminescence intensity due to G4-bound R45). Adapted with permission. [309] Copyright 2019, Wiley-VCH.

We nonetheless highlight here a system that, while not strictly a classical metallacage, is structurally closely related and has already been successfully applied to G4 imaging, and we anticipate that fully cage-like architectures for G4 sensing will follow in the near future. Subcellular duplex DNA and G-quadruplex interaction profiling of a hexagonal $Pt^{2+}$ metallacage was reported in cells by Peinador, Berger, Terenzi, and co-workers [309]. The metallacage-like receptor **R45** (Figure 49) is obtained by self-assembly of the 4,4′-([1,1′-biphenyl]-4,4′-diyl)bis(1-(pyridin-4-ylmethyl)pyridin-1-ium) ligand with $Pt^{2+}$ ethylenediamine dinitrate and targets G4-regulated genes in vivo, as it binds G4 structures and is readily visualized by luminescence microscopy due to its intrinsic emission. Notably, **R45** displays distinct photophysical behavior upon binding duplex DNA versus G4s. Indeed, G4 binding leads to decreased fluorescence and a concomitant spectral shift. In cells, **R45** produces intense, punctate nuclear and nucleolar signals that co-localize with G4-enriched regions, showing preferential engagement with G4 structures. The G4-binding nature can be attributed to the cage's tendency to interact with G4s through $\pi$–$\pi$ stacking on the terminal guanine quartets.

A tetragonal-prism Pt(II) metallacage (**R46**, Figure 50) incorporating a tetraphenylethene (TPE) ligand was developed by the Stang group as a prototypical theranostic scaffold [310], self-assembled from TPE-based donors and cis-$(PEt_3)_2Pt(OTf)_2$ acceptors into a discrete, cationic cage. Coordination to the Pt(II) nodes restricts intramolecular rotation of the TPE core and triggers AIE, rendering the metallacage weakly emissive in dilute solution but highly fluorescent when formulated as nanoparticles. Encapsulation into liposomes yields stable, biotin-targeted supramolecular nanoparticles that accumulate selectively in cancer cells overexpressing biotin receptors. Within cells, the $Pt^{2+}$ centers engage nuclear DNA in a manner analogous to classical platinum drugs, while the bright AIE fluorescence enables real-time visualization of uptake, tumor localization, and treatment response. This system exemplifies how TPE-based metallacages can integrate defined composition, robust luminescence, and Pt–DNA binding into a single, modular theranostic platform.

In brief, organic cages and metallacages employ largely similar signal-transduction strategies, with only nuanced differences in the dominant photophysical regimes they access. Both architectures predominantly rely on luminescent readout, as emissive ligands can be embedded directly into their scaffolds, enabling the use of diverse chromophores spanning UV–vis to near-infrared excitation and emission windows. Metallacages are particularly attractive in this regard, because metal-centered and charge-transfer excited states provide access to long-lived phosphorescence, large Stokes shifts, and environment-sensitive emission, features that are advantageous for time-gated detection and imaging but can also render the signal more susceptible to coordination-sphere perturbations and matrix-induced quenching. Organic cages, which more commonly exploit purely fluorescent states, typically offer simpler photophysics and straightforward spectral tuning, yet shorter lifetimes and smaller Stokes shifts can limit their suitability for time-resolved measurements in turbid or strongly autofluorescent media. The systems collected in Table 1 illustrate these design trends at the level of analyte scope and general photophysical response, while Table 2 specifically highlights the diversity and performance of luminescence-based readouts implemented in cage-based sensors.

With respect to robustness, both classes are still evolving toward improved stability in aqueous environments and complex matrices such as biofluids. For organic cages, moving beyond classical imine condensation toward more hydrolytically robust backbones, together with the emergence of peptide-based and related frameworks, has markedly enhanced chemical stability and water solubility. Metallacages, by contrast, remain to a significant extent prone to ligand-exchange reactions in the presence of competing nucleophiles and biomolecular ligands, which can compromise long-term sensing performance in realistic samples. A rigorous comparison of sensing performance across these platforms is further hampered by the limited number of studies in biologically or environmentally relevant samples and by the frequent absence of key analytical figures of merit, such as recoveries, validation against established methods, and standardized benchmarking protocols. Consequently, the field is still in a phase where establishing robust architectures and proof-of-concept demonstrations generally takes precedence over systematic, cross-platform performance comparisons.

## 6 | Hybrid Materials

Many metallic and organic cages still suffer from limited chemical stability in water and, in particular, in biological media. In real aqueous samples and biofluids, receptor performance is further compromised by deactivating species such as proteins, cell debris, and inorganic or organic particulates, which can bind to receptors, block their cavities, or induce aggregation, thereby impairing host–guest recognition. A promising strategy to address these limitations is the incorporation of these

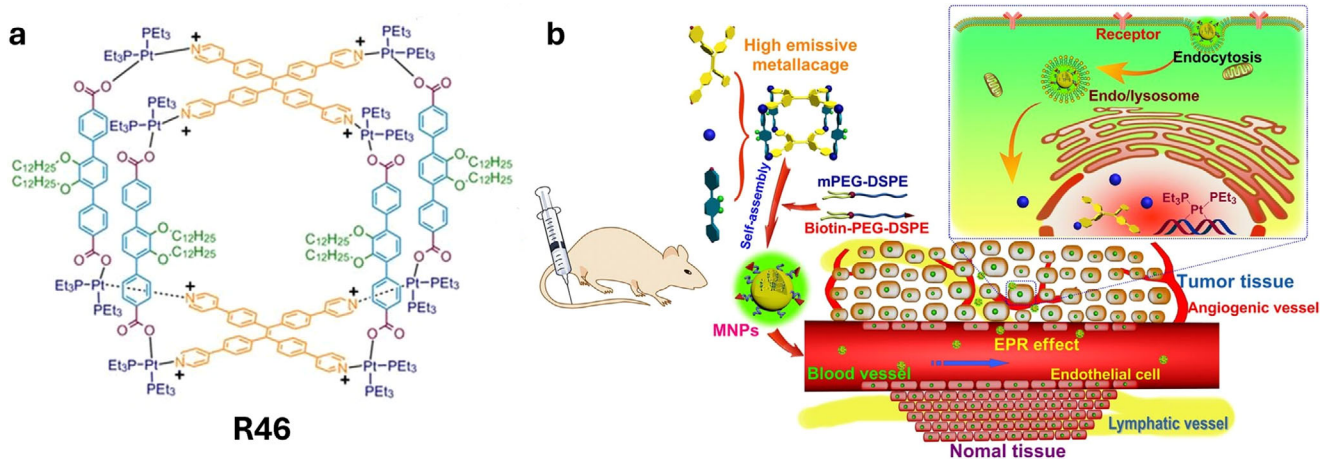


**FIGURE 50** | (a) Chemical structure of R46, which aggregates in aqueous media to form luminescent nanoparticles for theranostic applications. (b) Schematic representation of R46 nanoparticle transport within blood vessels, accumulation in tumor tissue, and subsequent uptake via receptor-mediated endocytosis. Adapted with permission. [310] Copyright 2016, National Academy of Sciences.

receptors into porous polymeric matrices [312]. These materials can function as size-selective sieves, offering protection from large macromolecules while allowing access to small analytes. In addition, immobilization often enhances receptor stability and enables the fabrication of hybrid materials suitable for device-oriented sensing applications.

Beyond environmental monitoring of wastewater or biological samples, this approach aligns well with the needs of personalized medicine, which increasingly requires continuous and minimally invasive analysis methods. In this context, immobilized receptors could, in principle, be integrated into wearable patches or subcutaneous sensors for the real-time detection of metabolites, disease biomarkers or toxins.

Hydrogels, owing to their high-water content, soft mechanics, and tunable structure, are widely used in biomedical contexts, including drug delivery, wound healing, biosensing, and tissue engineering. Their ability to mimic the native extracellular matrix makes them particularly attractive as scaffolds for cell growth and tissue regeneration [313]. However, conventional hydrogels often suffer from limitations in functionality, including poor mechanical strength, limited responsiveness to external stimuli, and insufficient dynamic behavior for complex biomedical environments [314, 315]. Here, supramolecular coordination cages offer several unique properties that can complement and enhance the performance of hydrogel materials. Their modular nature and structural tunability allow for precise control over size, shape, and functionality. Furthermore, their dynamic and reversible metal–ligand interactions make them inherently responsive to external stimuli such as pH, temperature, light or mechanical force, features that are increasingly desirable for biomedical materials operating in variable physiological conditions [157, 316].

In this chapter, we will discuss the immobilization of receptor-cage compounds for the preparation of hybrid materials and their key implementations, ranging from improved sensing and adsorption to enhanced mechanical properties, stimuli-responsive material design, and controlled release systems, areas where cage compounds play an essential role.

Maspoch and co-workers covalently integrated a $Rh^{2+}$ cuboctahedral cage-receptor, $[Rh_2(COOH\text{-}bdc)_2]_{12}$, onto a bimodal waveguide silicon interferometer for real-time sensing of nitrogenous organic pollutants in water (Figure 51) [317]. The 24 peripheral carboxylates were coupled to an APTES-modified surface, preserving the 12 open $Rh^{2+}$ axial sites for guest coordination. The resulting sensor enabled rapid (<15 min), label-free detection of benzotriazole with limits of detection of 0.064 μg $mL^{-1}$ in Milli-Q water and 0.068 μg·$mL^{-1}$ in tap water, and imidacloprid with 0.234 and 0.107 μg·$mL^{-1}$ in Milli-Q and tap water, respectively, all below their $EC_{50}$ toxicity thresholds. Control experiments showed that this polyhedral $Rh^{2+}$ arrangement significantly outperforms discrete $Rh_2(bdc)_4$ paddlewheel complexes (LoD ≈ 0.352 μg·$mL^{-1}$), while maintaining reproducibility and 80%–120% accuracy in line with FDA guidelines.

Network topology control and mechanical tunability are among the most impactful ways SMBAs enhance hydrogels. In a key study, Johnson and coworkers linked star-shaped polymers with preassembled $M_{12}L_{24}$ Fujita-type cages (12 $Pd^{2+}$, 24 bis(pyridyl) ligands), where each cage presents 24 outward-directed polyethylene glycol (PEG) arms that act as high-functionality junctions, enabling precise control over loop defects and connectivity beyond traditional covalent gels (Figure 52a) [318]. Such topology control directly impacts diffusion, viscoelasticity, and cell–matrix interactions in biomedical settings. Building on this concept, Johnson's star poly metal–organic cages (PolyMOCs) used multifunctional polymer arms coordinated around $M_{12}L_{24}$ cages to generate star-like architectures with tunable rheology and relaxation dynamics, allowing the design of injectable hydrogels or cell-instructive scaffolds with tailored mechanical lifetimes (Figure 52b) [319].

Nitschke and co-workers further expanded metallacage–hydrogel complexity using $Fe_4L_6$ cage-crosslinked polymer gels featuring differentially addressable cavities [320]. These $Fe^{2+}$–imine $M_4L_6$ tetrahedral cages, assembled from $Fe^{2+}$, 2-formylpyridines, and aromatic diamines, are integrated via PEG-aldehyde ligands as dynamic cross-linking nodes in water-based hydrogels (Figure 53), imparting coordination-

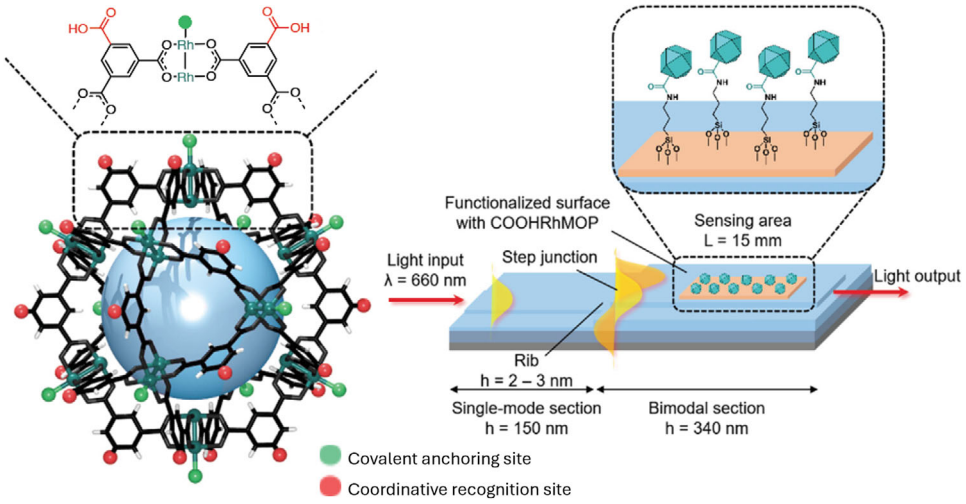


**FIGURE 51** | Integration of supramolecular cages into sensors and polymeric networks. (a) Structure of Rh(II)-metallacage, showing covalent anchoring (red) and coordination sites (green), and schematic of the cage-receptor-BiMW sensor for label-free detection of nitrogenous pollutants. Adapted with permission. [317] Copyright 2023, American Chemical Society.

driven stimuli-responsiveness. Orthogonal guest binding (e.g., fluorobenzene, $K_a = 6.1 \cdot 10^2\ M^{-1}$) enables multiple functions to be independently activated within a single material, offering a promising platform for future multi-functional biomedical systems such as smart wound dressings or drug delivery gels with spatially and temporally controlled therapeutic responses.

An interesting example of mechanochemical responsiveness is presented by Göstl, Schmidt, and coworkers developed water-based hydrogels in which mechanical stress triggers (i.e., ultrasounds) the release of non-covalently bound guest molecules from polymer-decorated cages [321]. They reported a polymer-decorated $Pd^{2+}{}_6(TPT)_4$ (TPT = triazine) octahedral cage assembled from six PEG-functionalized bipyridyl–$Pd^{2+}$ corners and four TPT faces. The PEG chains ($M_w$ = 10–20 kDa) imparted high water solubility and enabled the hydrophobic cavity to encapsulate pharmaceutically active guests such as progesterone (1:1) and ibuprofen (2:1), as confirmed by NMR spectroscopy. Guest uptake was driven by the hydrophobic effect, while encapsulation was reversible. Remarkably, cargo release was achieved mechanochemically by ultrasonication (20 kHz, aqueous solution), which ruptured Pd–N coordination bonds and fragmented the cage, leading to complete release of the encapsulated drugs, i.e., progesterone or ibuprofen. Control experiments showed that a model cage lacking PEG chains did not undergo mechanochemical activation and retained its cargo under identical conditions, underscoring the role of polymer handles in force transduction. Release efficiency depended strongly on polymer length: longer PEG chains ($M_w$ = 20 kDa) doubled the release efficiency relative to shorter ones ($M_w$ = 10 kDa). While the intact cage is stable in aqueous solution and protects hydrophobic drugs from precipitation, sonication selectively activates disassembly, linking structural fragility to a useful stimulus-response mechanism. This work highlights how polymer-decorated cages can act as water-soluble drug carriers that release non-covalently bound cargo in response to mechanical force, opening opportunities for ultrasound-triggered delivery systems. Besides, unlike covalent mechanophores, this strategy enables non-destructive, force-triggered cargo release, which could be leveraged for motion-activated drug delivery or feedback-controlled therapeutics responsive to tissue strain.

Incorporating metallacages as dynamic crosslinkers in hydrogels imparts mechanoresponsive and stimuli-adaptable properties. The Schmidt group demonstrated this using palladium-based $M_6L_4$ metal–organic cages formed from bis(bipyridine)-terminated PEG ligands (1–6 kDa) and 2,4,6-tri(4-pyridyl)-1,3,5-triazine (TPT) panels as multifunctional, non-covalent crosslinkers (Figure 54) [322] Hydrogels prepared at 10–20 wt% in water were transparent, with tunable mesh sizes and swelling ratios. The intact $M_6L_4$ cavities encapsulated hydrophobic drugs such as ibuprofen, progesterone, and drospirenone, supported by upfield $^1H$ NMR shifts. Drug loadings reached up to 6.2 wt%, surpassing earlier star-polymer–cage systems (~0.7 wt%). Ultrasound irradiation (20 kHz, 3 h) induced Pd—N bond scission, triggering ibuprofen release (~66%) by the hydrogel. These cage-crosslinked hydrogels enable reversible, force-triggered release of unmodified molecules and self-rearrangement under stress, combining coordination-cage host—guest chemistry with polymer mechanochemistry, an attractive feature for resilient, soft-tissue materials.

Beyond mechanical stimuli, light-responsive control of metallacage-hydrogel systems has also emerged as a tool to enable spatiotemporal control over hydrogel properties. Johnson and coworkers designed light-responsive metallacage hydrogels by incorporating photoisomerizable dithienylethene (DTE) [323] ligands into Pd-based metallacage-crosslinked PEG networks (Figure 55). [324] PEG–DTE ligands (≈4.6 kDa) formed $Pd_3L_6$ rings in the open form and $Pd_{24}L_{48}$ cages in the closed form upon UV irradiation, shifting the hydrogel from a soft o-gel to a stiffer c-gel. Green light reversed the process, restoring the softer, dynamic state. Systems with excess free ligand showed a similar but amplified light-induced stiffening (≈ ten-fold). The closed-state cages displayed slower ligand exchange ($\tau \approx 1{,}085$ s *vs* 555 s), reducing self-healing ability. This reversible photo-switching between soft/healable and stiff/static states demonstrates precise light-controlled tuning of hydrogel mechanics and

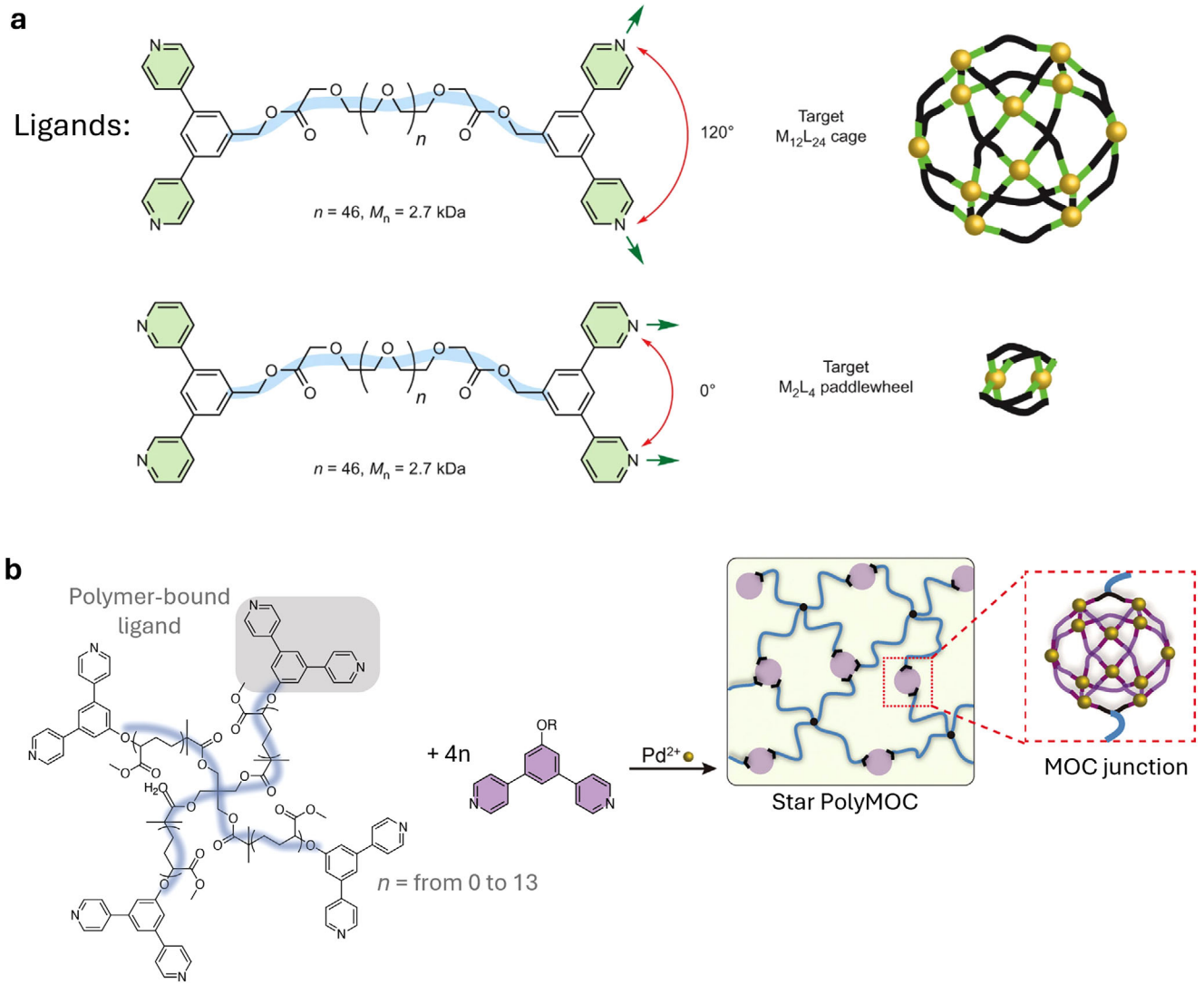


**FIGURE 52** | (a) Comparison between the traditional supramolecular metallogels and the polyMOCs with $M_2L_4$ and $M_{12}L_{24}$ junctions with chemical structure of polymeric ligands that target $M_{12}L_{24}$ and $M_2L_4$ cage junctions, respectively. Adapted with permission. [318] Copyright 2016, Nature Springer. (b) Synthesis of polyMOC by coordination of polymer-bound ligands and small molecule ligands (SMLs) with $Pd^{2+}$ to form metallacage junctions within star polymers. Adapted with permission. [319] Copyright 2017, Wiley-VCH.

functionality, enabling applications in cell culture, drug delivery, and photoresponsive biomaterials.

From a structural perspective, the polymer architecture used in metallacage–hydrogels significantly affects the hierarchical structure of the material and mechanical performance. For example Johnson and co-workers [325] showed that the polymer architecture in SMBA hydrogels strongly influences network hierarchy and mechanics. Linear and star-shaped PEG macromers (2.7–22 kDa) with $Pd(NO_3)_2$ form $M_{12}L_{24}$ or $M_2L_4$ cages, giving gels at only 5.4–5.9 wt% polymer and ≈240 μM $Pd^{2+}$. Scattering data shows intact MOCs, with $M_{12}L_{24}$ units clustering into cage-dense domains that introduce hierarchical structure. Rheology reveals high junction connectivity (branch functionality up to ~12, and ≈9–10 with star PEG) and outperforming typical metallogels with similar metal loading. Tuning polymer length and architecture thus enables polyMOCs that couple molecularly precise junctions with robust mechanics, relevant for load-bearing tissues such as cardiac and musculoskeletal systems.

Metallacages can direct cargo transport within soft matter, mimicking biological processes. Nitschke and co-workers advanced this concept with a thermoresponsive $Fe^{2+}{}_4L_4$ cage (present as triflimide salt functionalized with PEG1000$(mim)^+$ chains ($mim^+$ = 1-methylimidazolium), enabling reversible phase transfer between water and ethyl acetate (Figure 56). [326] At ≤10°C the cage is water-soluble, while at 70°C chain expansion drives solubility in ethyl acetate. UV–vis and DLS showed complete shuttling within 30 s, and stablility over 15 heating–cooling cycles. The cage encapsulates 1-fluoroadamantane, which transferred quantitatively between phases upon thermal cycling, with ≈71% retention after six phase-boundary crossings. This "heat engine" thus translates thermal gradients into directional chemical work, offering a generalizable route to stimuli-responsive transport and purification systems. Combined with the possibility of designing light-healable supramolecular polymers, demonstrated by Burnworth et al. [327], this non-equilibrium behavior suggests the potential for biomimetic drug carriers that move toward infection or inflammation sites guided by local thermal or chemical cues to

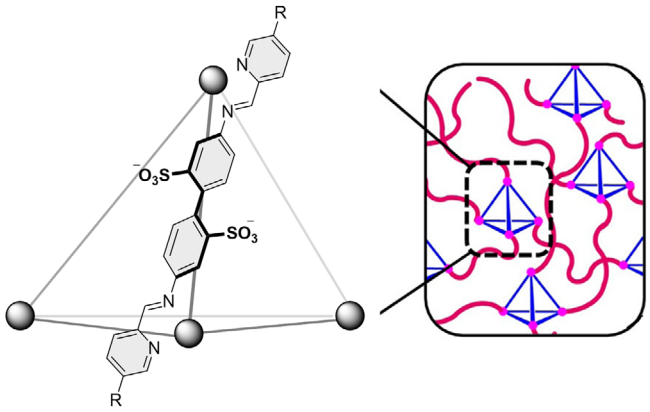

**FIGURE 53** | Chemical structure of $Fe^{2+}$–imine $M_4L_6$ tetrahedral cage used for preparing cage-crosslinked, stimuli-responsive hydrogels. Hydrogels are formed from polymers crosslinked by subcomponent metallacages, creating two internal phases that give distinct release profiles depending on guest encapsulation. Adapted with permission. [320] Copyright 2015, American Chemical Society.

then self assemble into biomimetic materials, suchs as hydrogels as a response to a secontary stimulus.

## 7 | Summary

Water-compatible cages are generally constructed either by covalent assembly of shape-persistent organic building blocks or by coordination-driven self-assembly of metal ions with preorganized ligands. For organic cages, dynamic covalent linkages such as imines enable error correction, followed by chemical "locking" (e.g., reduction of imines) to generate hydrolytically robust frameworks, while metallacages rely on metal centers and ligand sets that combine efficient self-assembly with high kinetic and thermodynamic stability in water. In both families, water solubility is usually achieved by decorating the cage exterior with polar or charged groups, and the interior cavity is tailored with specific functional motifs to control size, shape, polarity, and binding interactions. The water stability in metallacages has been significantly improved through strong Pd—N bonds, multidentate ligands, and stabilizing bimetallic $Pd^{2+}$ corners [234], however, stability in the presence of biologically relevant nucleophiles is still a challenge. Organic cages exploit charge-assisted hydrogen bonding using triply cationic, pyridinium-rich scaffolds bearing amide N—H and pyridinium C—H donors to bind strongly hydrated anions [237], with additional gains in apparent affinity achievable by combining cages with charged micelles that locally concentrate the host and enable anion transfer into hydrophobic environments [238]. Anion sensing is currently the most advanced application, with high affinities in water achieved by strategically placing positive charges and hydrogen-bond donors, and peptide-based macrocyclic and cage-like receptors offering multivalent N—H···anion interactions, hydrolytic robustness, intrinsic biocompatibility, and modular routes to incorporate luminescent or electrochemical reporters. Despite extensive structural and binding studies, signal transduction remains a bottleneck. Many cages lack suitable chromophores, prompting post-assembly functionalization, indicator displacement, or analyte-triggered disassembly, while emerging optical strategies such as reverse FRET (rFRET) [328], and chiral cages exhibiting CPL [329–333], open avenues for chiroptical sensing, including enantiomeric excess determination.

In terms of analyte scope, although anion sensing (such as for inorganic anions or carbohydrates) is relatively well established, cage-based sensing has seen substantial developement in the area of nitroaromatics, especially nitrobenzene derivatives and nitroaromatic pesticides [334, 335], while persistent pollutants such as PFAS [336, 285, 337–339] remain underexplored despite their health impact [340]. And for such targets sensing

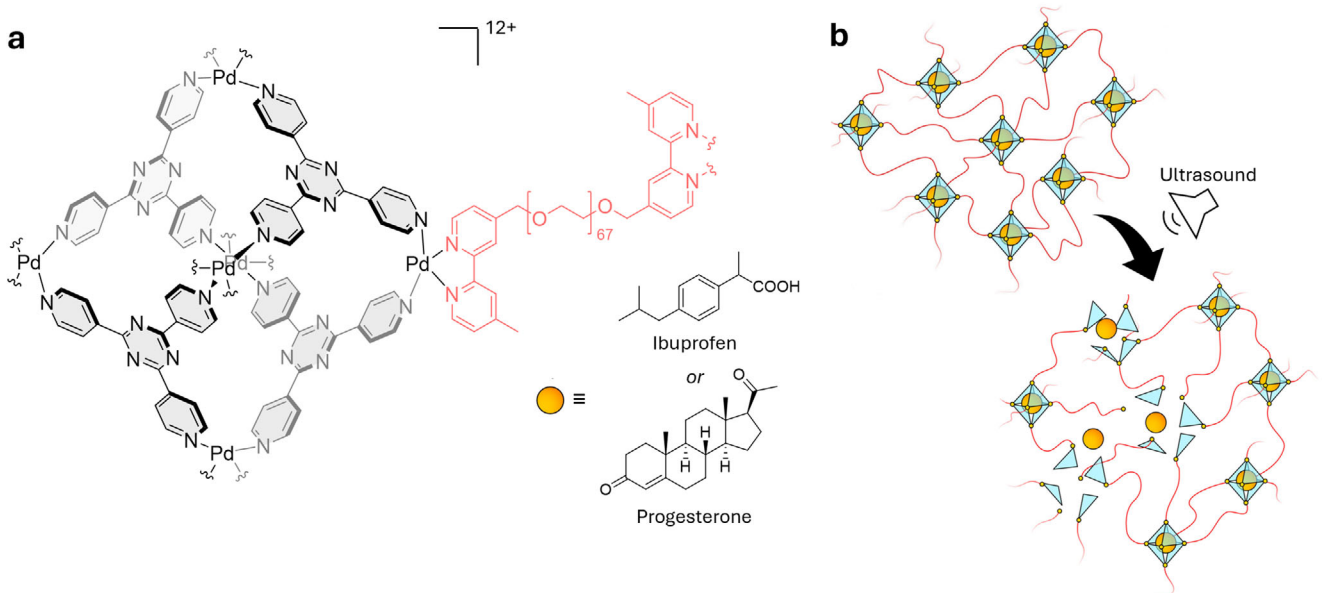


**FIGURE 54** | (a) Chemical structure of the $Pd^{2+}{}_6(TPT)_4$ octahedral cage assembled from six PEG-functionalized bipyridyl–$Pd^{2+}$ corners and four TPT faces, which can encapsulate drugs, and (b) its use in an ultrasound-responsive system enabling triggered drug release from the cage–polymer network. Adapted with permission. [322] Copyright 2023, Wiley-VCH.

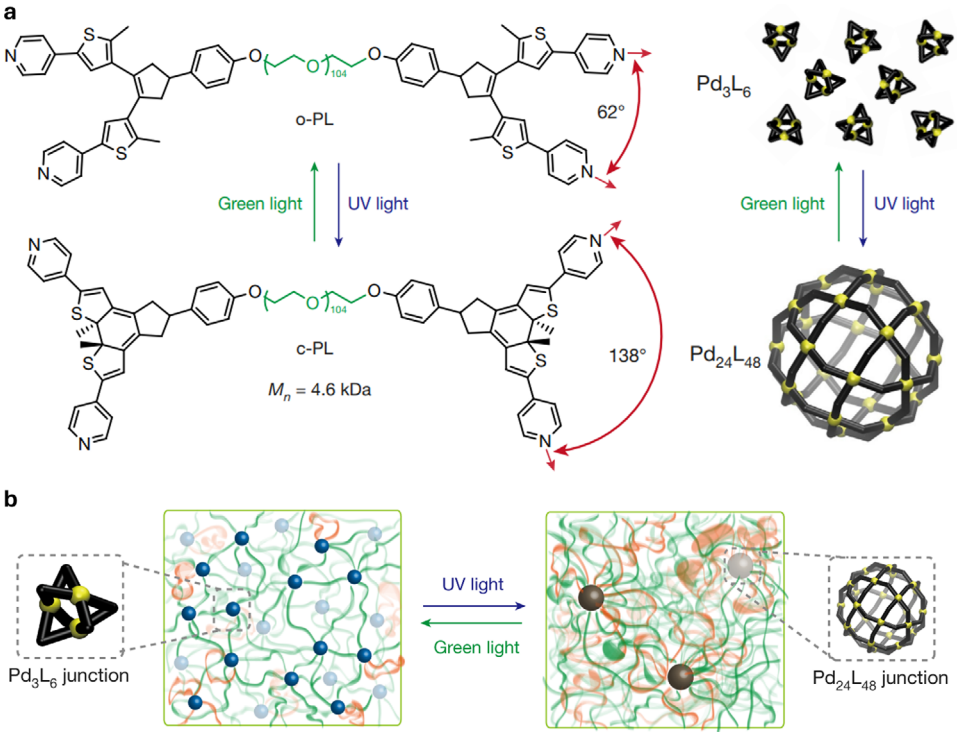


**FIGURE 55** | Chemical structure of the photoswitchable polyMOC. Photoresponsive Pd-based metal–organic cages act as reversible junctions in polymer networks, allowing light-gated switching between two topologies. UV irradiation drives DTE-based polymer ligands from an open to a closed form, changing their bite angle and converting small $Pd_3L_6$ rings into larger $Pd_{24}L_{48}$ cages, which alters branch functionality and defect structure. Subsequent green-light exposure reopens the DTE units, regenerating the original $Pd_3L_6$ network without inhibiting cage assembly despite multiple diastereomeric products. Adapted with permission. [324] Copyright 2018, Springer Nature.

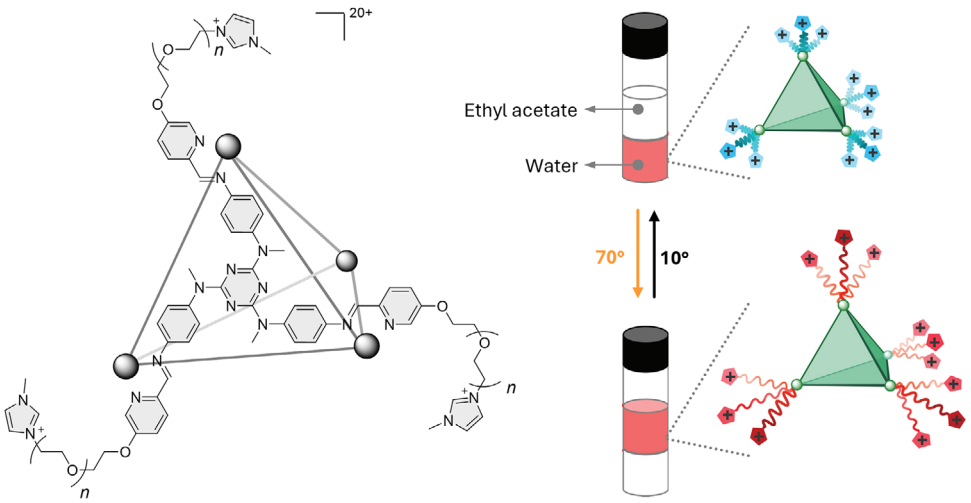


**FIGURE 56** | Chemical structure of the $Fe^{2+}{}_4L_4$ cage bearing twelve PEG1000(mim)$^+$ chains that can undergo thermally driven phase transfer between water and ethyl acetate. At 10°C, contracted PEG chains expose charged imidazolium and ether oxygens, making the cage water-soluble. At 70°C, expanded PEG chains expose hydrophobic ethylene segments, shifting solubility to ethyl acetate. Adapted with permission. [326] Copyright 2020, Wiley-VCH.

in organic phases may be acceptable or necessary, so current cage sensors are better suited for presumptive environmental monitoring than fully quantitative analysis. Biologically relevant analytes such as carbohydrates are relatively widely explored, [218, 222] whereas neurotransmitters and hormones remain challenging targets because of their low concentrations and close chemical similarity, and current cages lack sufficient sensitivity and selectivity. An interesting recent developement is that cages can stabilize DNA junctions and G4 structures and thus appear promising for targeting and imaging secondary DNA

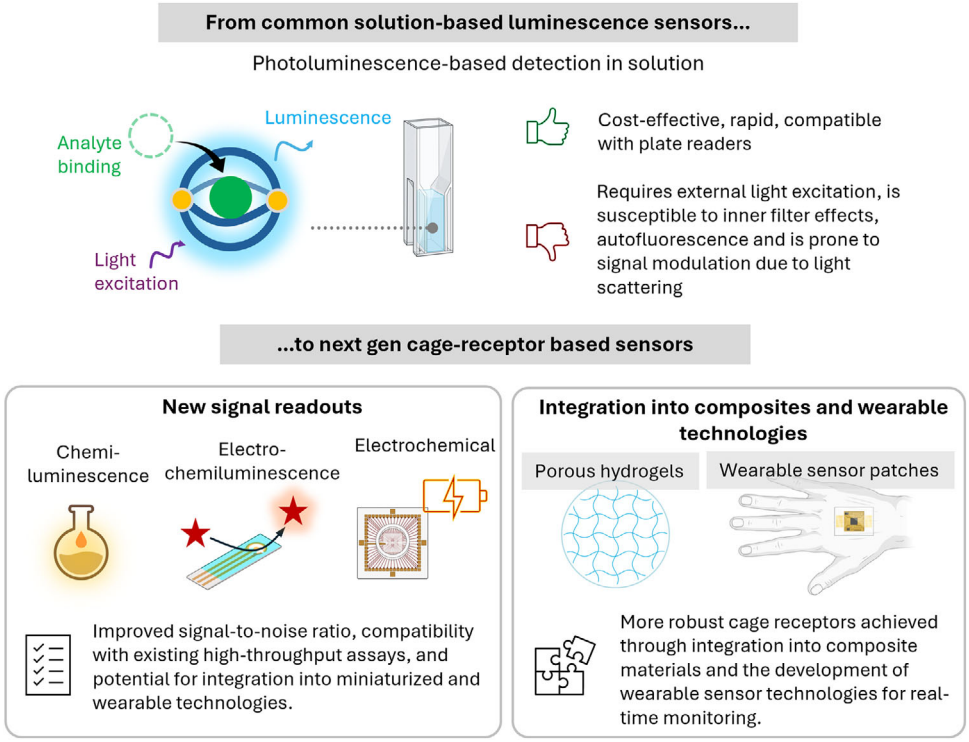


**FIGURE 57** | The future development of cage receptors should move beyond purely photoluminescence-based detection and exploit other established sensing modalities, such as chemiluminescence, electrochemiluminescence, and electrochemical readouts. Coupled with device miniaturization, the use of composite materials, and integration into wearable technologies, these advances are expected to significantly enhance the practical utility and real-world applicability of cage-receptor-based sensing systems.

structures, as well as for fundamental studies of nucleic-acid architecture.

Hybrid strategies, embedding cages into hydrogels or membranes for analyte preconcentration and matrix exclusion, or using sensor arrays with fingerprint analysis, provide routes to enhanced selectivity. Cage–hydrogel systems offer adaptive soft materials with structural crosslinking, stimuli-responsive cargo delivery, self-healing, multi-cargo encapsulation, and tissue-tuned mechanics. Overall, receptor cages are progressing toward more robust and deployable sensing systems but have not yet surpassed classical cryptands that underpin commercial blood-ion sensors [227], with notable alternatives such as cubane-like zinc phosphate architectures from Murugavel and co-workers that bind fluoride across multiple charge states with detection limits near 1 ppm [341], and intracellular sensing is still constrained by uptake, endosomal trapping, corona formation, instability, and toxicity, highlighting the need for improved water stability, ratiometric or lifetime-based readout, and targeted functionalization.

## 8 | Perspectives

Organo- and metallacages have emerged as powerful molecular receptors for sensing in aqueous environments, but future work must focus on real-world implementation, where the main challenges are stability, selectivity, advanced signal readouts, and device integration (Figure 57). Substantial progress in cavity design, signal modulation, and analyte scope has been achieved, and promisingstrategies are emerging. For example, crown-ether-based $Pd^{2+}$ metallacages assembled from flexible bidentate pyridyl ligands, as shown by Clever and co-workers [342], alkoxysilane- and orthoester-based hosts that mimick crown-ether complexationreported by von Delius and colleagues [343], and new quantitative imine-forming methodologies from Prins and co-workers that use auxiliary metal coordination to stabilize imine linkages in organic cages [344] all represent powerful structural motifs and design strategies. Nevertheless, cages containing hydrolysable groups or metal nodes prone to ligand exchange remain problematic for real-world applications, although the developments mentioned above and the use of covalently robust organic cages (e.g., peptide-based cages) are promising. For more robust cage-receptor based sensors, embedding them into composite materials will be crucial to protect them from chemical degradation and to enable practical devices such as continuousmonitoring platforms and wearable technologies [345], although in the near term their use will likely remain focused on presumptive detection rather than fully quantitative diagnostics. Embedding cagereceptors into suitable polymeric matrices can help mitigate surface fouling by physically separating the receptors from interfering species while still allowing target analytes to reach the sensing sites, which is crucial for real-world applications [346]. Once stability and selectivity are improved, cage-receptors will be well positioned for multiplexed and multimodal sensing, combining confined cavities with tunable readouts (ratiometric luminescence, electrochemical signals, circularly polarized emission) and integration into optical fibers, field-effect transistors, or wearable sensors, thereby uniting sensing, imaging, and therapy in biomedicine and enabling portable

environmental detectors. Future design principles should more fully exploit IDA [46] concepts and integrate them with "chemical nose"–type [347] sensing strategies. This approach will enable multiplexed detection [348], the tailoring of receptor derivatives with differential selectivity for biorelevant analytes, and the use of data-driven methods such as principal component analysis [349], to extract analyte-specific fingerprints. At the same time, efforts should extend beyond traditional luminescence toward electrochemical and electrochemiluminescent (ECL) readouts, [350–362] which remain largely unexplored.

From a production and real-world performance perspective the sensing examples herein discussed must be evaluated critically, as in many cases the synthetic yields remain moderate, if not low, and scale-up is rarely reported and frequently overlooked bottleneck. Finally, computational design, machine learning, and automated synthesis [363–369] are expected to accelerate the discovery of cages with optimized binding and signaling, and, when coupled with advanced device engineering, should help transition cage-based sensors from proof-of-concept studies to deployable technologies.

## 9 | Conclusions

Supramolecular cages have evolved from elegant self-assembled structures into versatile platforms for molecular recognition and sensing. The ability to tune their cavity physicochemical properties, externally functionalize their surfaces, and incorporate signal-transduction elements such as luminophores makes them uniquely powerful compared to classical macrocyclic receptors. In recent years, major advances in synthetic strategies aimed at increasing structural diversity, water compatibility, analyte scope, and functional outputs, including luminescence, electrochemistry, and even multimodal readouts, have further expanded their utility. Yet, one can say that the journey toward practical deployment has only begun. Challenges of stability in complex media, reliable quantitative sensing, and seamless integration into devices remain to be solved. Encouragingly, progress in robust cage scaffolds, hybrid materials such as hydrogels, and computationally guided design points to viable pathways forward. Looking ahead, supramolecular cages are poised to develop into multimodal chemosensing systems, for example by integrating electrochemical and luminescence readouts to afford user-friendly, cost-effective sensors for diagnostics, environmental monitoring, and biomedical applications. Over the next decade, they are expected to mature into multifunctional, multiplexed platforms that are increasingly robust, selective, and readily integrated, and that not only sense but also respond and adapt to their environment. Consequently, supramolecular cages are likely to transition from isolated receptors to active components within smart materials and devices, including wearable sensors designed to address pressing challenges in diagnostics, therapeutics, and environmental monitoring.


### Acknowledgments

R.Z. and P.P gratefully acknowledge the financial support provided by the Fonds der Chemischen Industrie (FCI, Liebig Fellowship). G. M. -A. acknowledges the Grant RYC2024-048755-I funded by MCIN/AEI/10.13039/501100011033 and by ESF+. This article is also based on work done in the framework of the COST Action CA22131, LUCES Supramolecular Luminescent Chemosensors for Environmental Security, supported by COST (European Cooperation in Science and Technology). The TOC image, as well as Figures 6 and 57 were created with the help of https://BioRender.com.

Open access funding enabled and organized by Projekt DEAL.


### Conflicts of Interest

The authors declare no conflicts of interest.

### Data Availability Statement

All data supporting the findings in this review are available from the referenced sources listed in the manuscript. A list of common abbreviations can be found in the ESI.

### References


1. E. Ortiz-Gómez, R. Martínez-Máñez, and V. Martí-Centelles, "Molecular Cages: Emerging Applications in Diverse Fields," *Trends in Chemistry* 7, no. 8 (2025): 429–443.

2. T. K. Piskorz, V. Marti-Centelles, R. L. Spicer, F. Duarte, and P. J. Lusby, "Picking the Lock of Coordination Cage Catalysis," *Chemical Science* 14, no. 41 (2023): 11300–11331.

3. M. D. Ward, "New Insights Into Coordination-Cage Based Catalysis," *Chemical Communications* 60, no. 76 (2024): 10464–10475.

4. P. Bhandari and P. S. Mukherjee, "Covalent Organic Cages in Catalysis," *ACS Catalysis* 13, no. 9 (2023): 6126–6143.

5. S. Zarra, D. M. Wood, D. A. Roberts, and J. R. Nitschke, "Molecular Containers in Complex Chemical Systems," *Chemical Society Reviews* 44, no. 2 (2015): 419–432.

6. A. B. Grommet, M. Feller, and R. Klajn, "Chemical Reactivity Under Nanoconfinement," *Nature Nanotechnology* 15, no. 4 (2020): 256–271.

7. Q. Zhang, L. Catti, and K. Tiefenbacher, "Catalysis inside the Hexameric Resorcinarene Capsule," *Accounts of Chemical Research* 51, no. 9 (2018): 2107–2114.

8. R. Ham, C. J. Nielsen, S. Pullen, and J. N. H. Reek, "Supramolecular Coordination Cages for Artificial Photosynthesis and Synthetic Photocatalysis," *Chemical Reviews* 123, no. 9 (2023): 5225–5261.

9. R. Ning and Q. Q. Wang, "Supramolecular Catalysis With Emerging, Functional Organic Macrocycles and Cages," *Chemical Society Reviews* 54, no. 23 (2025): 11105–11140.

10. L. Cognata and V. Amendola, "Recent Applications of Organic Cages in Sensing and Separation Processes in Solution," *Chemical Communications* 59, no. 92 (2023): 13668–13678.

11. D. Zhang, T. K. Ronson, Y. Q. Zou, and J. R. Nitschke, "Metal–Organic Cages for Molecular Separations," *Nature Reviews Chemistry* 5, no. 3 (2021): 168–182.

12. A. Ghosh and J. R. Nitschke, "Light-Controlled Functions With Metal–Organic Capsules: From Guest Release to Catalysis, Separation, and Molecular Transport," *Accounts of Chemical Research* 59 (2026): 372–381.

13. G. Moreno-Alcantar and A. Casini, "Bioinorganic Supramolecular Coordination Complexes and Their Biomedical Applications," *FEBS Letters* 597, no. 1 (2023): 191–202.

14. Y.-P. Wang, Y. Zhang, X.-H. Duan, et al., "Recent Progress in Metal-Organic Cages for Biomedical Application: Highlighted Research During 2018–2023," *Coordination Chemistry Reviews* 501 (2024): 215570.

15. L. Tapia, I. Alfonso, and J. Solà, "Molecular Cages for Biological Applications," *Organic & Biomolecular Chemistry* 19, no. 44 (2021): 9527–9540.

16. G. Moreno-Alcantár, M. Drexler, and A. Casini, "Assembling a New Generation of Radiopharmaceuticals With Supramolecular Theranostics," *Nature Reviews Chemistry* 8, no. 12 (2024): 893–914.

17. C. J. Pedersen, "Cyclic Polyethers and Their Complexes With Metal Salts," *Journal of the American Chemical Society* 89, no. 26 (1967): 7017–7036.

18. J. M. Lehn and M. E. Stubbs, "Cryptates. XIII. Intramolecular cation exchange in [3]cryptates of Alkaline Earth Cations," *Journal of the American Chemical Society* 96, no. 12 (1973): 4011–4012.

19. J.-M. Lehn and J. P. Sauvage, "Cryptates. XVI. [2]-Cryptates. Stability and Selectivity of Alkali and Alkaline-Earth Macrobicyclic Complexes," *Journal of the American Chemical Society* 97 (1975): 6700–6707.

20. J. M. Lehn, "Cryptates: The Chemistry of Macropolycyclic Inclusion Complexes," *Accounts of Chemical Research* 11, no. 2 (1978): 49–57.

21. J. S. Bradshaw and R. M. Izatt, "Crown Ethers: The Search for Selective Ion Ligating Agents," *Accounts of Chemical Research* 30, no. 8 (1997): 338–345.

22. J. R. Moran, S. Karbach, and D. J. Cram, "Cavitands: Synthetic Molecular Vessels," *Journal of the American Chemical Society* 104, no. 21 (1982): 5826–5828.

23. D. J. Cram, S. Karbach, H. E. Kim, et al., "Host-Guest Complexation. 46. Cavitands as Open Molecular Vessels Form Solvates," *Journal of the American Chemical Society* 110, no. 7 (1988): 2229–2237.

24. A. Bianchi, M. Micheloni, and P. Paoletti, "Supramolecular Interaction Between Adenosine 5′-Triphosphate (ATP) and Polycharged Tetraazamacrocycles. Thermodynamic and 31P NMR Studies," *Inorganica Chimica Acta* 151, no. 4 (1988): 269–272.

25. F. P. Schmidtchen and M. Berger, "Artificial Organic Host Molecules for Anions," *Chemical Reviews* 97, no. 5 (1997): 1609–1646.

26. C. Reyheller and S. Kubik, "Selective Sensing of Sulfate in Aqueous Solution Using a Fluorescent Bis(cyclopeptide)," *Organic Letters* 9, no. 25 (2007): 5271–5274.

27. S. Kubik, R. Goddard, R. Kirchner, D. Nolting, and J. Seidel, "A Cyclic Hexapeptide Containing L -Proline and 6-Aminopicolinic Acid Subunits Binds Anions in Water," *Angewandte Chemie International Edition* 40, no. 14 (2001): 2648–2651.

28. S. Kubik, "Anion Recognition in Aqueous Media by Cyclopeptides and Other Synthetic Receptors," *Accounts of Chemical Research* 50, no. 11 (2017): 2870–2878.

29. S. O. Kang, J. M. Llinares, V. W. Day, and K. Bowman-James, "Cryptand-Like Anion Receptors," *Chemical Society Reviews* 39, no. 10 (2010): 3980–4003.

30. K. Freudenberg and F. Cramer, "Notizen: Die Konstitution Der Schardinger-Dextrine $\alpha$, $\beta$ und $\gamma$," *Zeitschrift für Naturforschung B* 3 (1948): 464–466.

31. D. French and R. E. Rundle, "The Molecular Weights of the Schardinger Alpha and Beta Dextrins 1," *Journal of the American Chemical Society* 64, no. 7 (1942): 1651–1653.

32. H. Ikeda, M. Nakamura, N. Ise, et al., "Fluorescent Cyclodextrins for Molecule Sensing: Fluorescent Properties, NMR Characterization, and Inclusion Phenomena of N-Dansylleucine-Modified Cyclodextrins," *Journal of the American Chemical Society* 118, no. 45 (1996): 10980–10988.

33. W. A. Freeman, W. L. Mock, and N. Y. Shih, "Cucurbituril," *Journal of the American Chemical Society* 103, no. 24 (1981): 7367–7368.

34. K. I. Assaf and W. M. Nau, "Cucurbiturils: From Synthesis to High-Affinity Binding and Catalysis," *Chemical Society Reviews* 44, no. 2 (2015): 394–418.

35. A. Zinke and E. Ziegler, "Zur Kenntnis des Härtungsprozesses von Phenol-Formaldehyd-Harzen, X. Mitteilung," *Berichte Der Deutschen Chemischen Gesellschaft (A and B Series)* 77 (1944): 264–272.

36. C. D. Gutsche, "Calixarenes," *Accounts of Chemical Research* 16, no. 5 (1983): 161–170.

37. H. Ren, H. Wang, W. Wen, et al., "A Summary of Calixarene-Based Fluorescent Sensors Developed During the Past Five Years," *Chemical Communications* 59, no. 93 (2023): 13790–13799.

38. A. Lazaro, E. Valencia, P. Ballester, and L. Rodriguez, "Binding Studies of a Luminescent Pt(II) Organometallic Calix[4]Pyrrole With Halide Salts," *ACS Omega* 10, no. 8 (2025): 8665–8674.

39. T. Ogoshi, S. Kanai, S. Fujinami, T. Yamagishi, and Y. Nakamoto, "Para -Bridged Symmetrical Pillar[5]arenes: Their Lewis Acid Catalyzed Synthesis and Host–Guest Property," *Journal of the American Chemical Society* 130, no. 15 (2008): 5022–5023.

40. J. F. Chen, Q. Lin, Y. M. Zhang, H. Yao, and T. B. Wei, "Pillararene-Based Fluorescent Chemosensors: Recent Advances and Perspectives," *Chemical Communications* 53, no. 100 (2017): 13296–13311.

41. P. Soncini, S. Bonsignore, E. Dalcanale, and F. Ugozzoli, "Cavitands as Versatile Molecular Receptors," *The Journal of Organic Chemistry* 57, no. 17 (1992): 4608–4612.

42. R. Pinalli, M. Suman, and E. Dalcanale, "Cavitands at Work: From Molecular Recognition to Supramolecular Sensors," *European Journal of Organic Chemistry* 2004, no. 3 (2004): 451–462.

43. H. Xi, C. L. D. Gibb, and B. C. Gibb, "Functionalized Deep-Cavity Cavitands," *The Journal of Organic Chemistry* 64, no. 25 (1999): 9286–9288.

44. E. Biavardi, S. Federici, C. Tudisco, et al., "Cavitand-Grafted Silicon Microcantilevers as a Universal Probe for Illicit and Designer Drugs in Water," *Angewandte Chemie International Edition* 53, no. 35 (2014): 9183–9188.

45. J. Krämer, R. Kang, L. M. Grimm, L. De Cola, P. Picchetti, and F. Biedermann, "Molecular Probes, Chemosensors, and Nanosensors for Optical Detection of Biorelevant Molecules and Ions in Aqueous Media and Biofluids," *Chemical Reviews* 122, no. 3 (2022): 3459–3636.

46. A. C. Sedgwick, J. T. Brewster, T. Wu, et al., "Indicator Displacement Assays (IDAs): The Past, Present and Future," *Chemical Society Reviews* 50, no. 1 (2021): 9–38.

47. K. Kikuchi, "Design, Synthesis and Biological Application of Chemical Probes for Bio-Imaging," *Chemical Society Reviews* 39, no. 6 (2010): 2048–2053.

48. A. Lázaro, A. Pinto, and L. Rodríguez, "Supramolecular Sensing With Luminescent Gold(I) and Platinum(II) Organometallics," *Coordination Chemistry Reviews* 550 (2026): 217411.

49. L. Prodi, F. Bolletta, M. Montalti, and N. Zaccheroni, "Luminescent Chemosensors for Transition Metal Ions," *Coordination Chemistry Reviews* 205 (2000): 59–83.

50. J. C. Sherman and D. J. Cram, "Carcerand Interiors Provide a New Phase of Matter," *Journal of the American Chemical Society* 111 (1989): 4527–4528.

51. C. J. T. Cox, J. Hale, P. Molinska, and J. E. M. Lewis, "Supramolecular and Molecular Capsules, Cages and Containers," *Chemical Society Reviews* 53, no. 21 (2024): 10380–10408.

52. P. Ballester, "Anion Binding in Covalent and Self-Assembled Molecular Capsules," *Chemical Society Reviews* 39, no. 10 (2010): 3810–3830.

53. J. M. Rivera, T. Martín, and J. Rebek Jr., "Chiral Spaces: Dissymmetric Capsules Through Self-Assembly," *Science* 279 (1998): 1021–1023.

54. D. J. Cram, "Molecular Container Compounds," *Nature* 356 (1992): 29–36.

55. D. J. Cram, "Preorganization—From Solvents to Spherands," *Angewandte Chemie International Edition in English* 25, no. 12 (1986): 1039–1057.

56. L. Fabbrizzi, I. Faravelli, G. Francese, M. Licchelli, A. Perotti, and A. Taglietti, "A Fluorescent Cage for Anion Sensing in Aqueous Solution," *Chemical Communications* (1998): 971–972.

57. F. J. Rizzuto, L. K. S. von Krbek, and J. R. Nitschke, "Strategies for Binding Multiple Guests in Metal–Organic Cages," *Nature Reviews Chemistry* 3, no. 4 (2019): 204–222.

58. F. Beuerle and B. Gole, "Covalent Organic Frameworks and Cage Compounds: Design and Applications of Polymeric and Discrete Organic Scaffolds," *Angewandte Chemie International Edition* 57, no. 18 (2018): 4850–4878.

59. S. Leininger, B. Olenyuk, and P. J. Stang, "Self-Assembly of Discrete Cyclic Nanostructures Mediated by Transition Metals," *Chemical Reviews* 100, no. 3 (2000): 853–908.

60. S. R. Thomas, N. Willnhammer, A. Casini, and G. Moreno-Alcántar, "Gold Metallacages: Design Principles and Applications," *Chemistry* 11, no. 6 (2025): 102502.

61. G. Wu, Y. Chen, S. Fang, et al., "A Self-Assembled Cage for Wide-Scope Chiral Recognition in Water," *Angewandte Chemie International Edition* 60, no. 30 (2021): 16594–16599.

62. M. Pan, K. Wu, J.-H. Zhang, and C.-Y. Su, "Chiral Metal–Organic Cages/Containers (MOCs): From Structural and Stereochemical Design to Applications," *Coordination Chemistry Reviews* 378 (2019): 333–349.

63. S. Míguez-Lago, B. D. Gliemann, M. Kivala, and M. M. Cid, "A Chiral Molecular Cage Comprising Diethynylallenes and N -Heterotriangulenes for Enantioselective Recognition," *Chemistry – A European Journal* 27, no. 53 (2021): 13352–13357.

64. S. Shanmugaraju and P. S. Mukherjee, "Self-Assembled Discrete Molecules for Sensing Nitroaromatics," *Chemistry – A European Journal* 21, no. 18 (2015): 6656–6666.

65. Y. M. Guan, H. Gao, W. B. Xu, et al., "Nanoarchitectonics of a Covalent Organic Supramolecular Cage (COSC) for Fluorescent Visual Detection of Macrolides," *RSC Advances* 15, no. 20 (2025): 15476–15479.

66. M.-J. Li, J. Liu, Z.-Q. Wang, et al., "A Fluorescent Organic Cage for Tetracyclines Detection," *Crystal Growth & Design* 25, no. 16 (2025): 6492–6496.

67. G. Li, T. K. Ronson, R. Lavendomme, et al., "Enantiopure $Fe^{II}_4L_4$ Cages Bind Steroids Stereoselectively," *Chemistry* 9, no. 6 (2023): 1549–1561.

68. T. K. Ronson, A. B. League, L. Gagliardi, C. J. Cramer, and J. R. Nitschke, "Pyrene-Edged $Fe^{II}_4$ $L_6$ Cages Adaptively Reconfigure During Guest Binding," *Journal of the American Chemical Society* 136, no. 44 (2014): 15615–15624.

69. T. K. Ronson, W. Meng, and J. R. Nitschke, "Design Principles for the Optimization of Guest Binding in Aromatic-Paneled $Fe^{II}_4L_6$ Cages," *Journal of the American Chemical Society* 139, no. 28 (2017): 9698–9707.

70. T. Liu, H. Qu, S. D. Harding, et al., "Bottom-Up Computational Design of Shape-Selective Organic Macrocycles for Humid $CO_2$ Capture," *Nature Chemistry* 17 (2025): 1696–1704, https://doi.org/10.1038/s41557-025-01873-1.

71. W.-T. Dou, C.-Y. Yang, L.-R. Hu, et al., "Metallacages and Covalent Cages for Biological Imaging and Therapeutics," *ACS Materials Letters* 5, no. 4 (2023): 1061–1082.

72. N. Ahmad, H. A. Younus, A. H. Chughtai, and F. Verpoort, "Metal–Organic Molecular Cages: Applications of Biochemical Implications," *Chemical Society Reviews* 44, no. 1 (2015): 9–25.

73. A. Credi and L. Prodi, "Inner Filter Effects and Other Traps in Quantitative Spectrofluorimetric Measurements: Origins and Methods of Correction," *Journal of Molecular Structure* 1077 (2014): 30–39.

74. M. Montalti, A. Credi, L. Prodi, and M. Teresa Gandolfi, *Handbook of Photochemistry*., 3rd ed. (Taylor&Francis Group, 2006).

75. M. van de Weert and L. Stella, "Fluorescence Quenching and Ligand Binding: A Critical Discussion of a Popular Methodology," *Journal of Molecular Structure* 998, no. 1-3 (2011): 144–150.

76. T. Weitner, T. Friganović, and D. Šakić, "Inner Filter Effect Correction for Fluorescence Measurements in Microplates Using Variable Vertical Axis Focus," *Analytical Chemistry* 94, no. 19 (2022): 7107–7114.

77. Y. Wang and P. D. Townsend, "Common Mistakes in Luminescence Analysis," *Journal of Physics: Conference Series* 398 (2012): 012003.

78. E. G. Percastegui, T. K. Ronson, and J. R. Nitschke, "Design and Applications of Water-Soluble Coordination Cages," *Chemical Reviews* 120, no. 24 (2020): 13480–13544.

79. D. Fujita, Y. Ueda, S. Sato, N. Mizuno, T. Kumasaka, and M. Fujita, "Self-Assembly of Tetravalent Goldberg Polyhedra From 144 Small Components," *Nature* 540, no. 7634 (2016): 563–566.

80. C. S. Diercks and O. M. Yaghi, "The Atom, the Molecule, and the Covalent Organic Framework," *Science* 355, no. 6328 (2017): eaal1585.

81. A. P. Côté, A. I. Benin, N. W. Ockwig, M. O'Keeffe, A. J. Matzger, and O. M. Yaghi, "Porous, Crystalline, Covalent Organic Frameworks," *Science* 310, no. 5751 (2005): 1166–1170.

82. T. Kitazawa, S. Nishikiori, R. Kuroda, and T. Iwamoto, "Novel Clathrate Compound of Cadmium Cyanide Host With an Adamantane-Like Cavity. Cadmium Cyanide-Carbon Tetrachloride(1/1)," *Chemistry Letters* 17 (1988): 1729–1732.

83. Y. Kinoshita, I. Matsubara, T. Higuchi, and Y. Saito, "The Crystal Structure of Bis(Adiponitrilo)Copper (I) Nitrate," *Bulletin of the Chemical Society of Japan* 32 (1959): 1221–1226.

84. B. F. Hoskins and R. Robson, "Infinite Polymeric Frameworks Consisting of Three Dimensionally Linked Rod-Like Segments," *Journal of the American Chemical Society* 111, no. 15 (1989): 5962–5964.

85. B. F. Hoskins and R. Robson, "Design and Construction of a New Class of Scaffolding-Like Materials Comprising Infinite Polymeric Frameworks of 3D-linked Molecular Rods. A Reappraisal of the Zinc Cyanide and Cadmium Cyanide Structures and the Synthesis and Structure of the Diamond-related Frameworks [N(CH3)4][CuIZnII(CN)4] and CuI[4,4′,4″,4‴-tetracyanotetraphenylmethane]BF4.XC6H5NO2," *Journal of the American Chemical Society* 112, no. 4 (1990): 1546–1554.

86. S. Kitagawa, M. Munakata, and T. Tanimura, "Synthesis of the Novel Infinite-Sheet and -Chain Copper(I) Complex Polymers {[Cu(C4H4N2)3/2(CH3CN)](PF)6}.cntdot.0.5C3H6O}.infin. and {[Cu2(C8H12N2)3](ClO4)2}.infin. and Their X-Ray Crystal Structures," *Inorganic Chemistry* 31, no. 9 (1992): 1714–1717.

87. O. M. Yaghi, G. Li, and H. Li, "Selective Binding and Removal of Guests in a Microporous Metal–Organic Framework," *Nature* 378 (1995): 703–706.

88. H. Li, M. Eddaoudi, M. O'Keeffe, and O. M. Yaghi, "Design and Synthesis of an Exceptionally Stable and Highly Porous Metal-Organic Framework," *Nature* 402 (1999): 276–279.

89. M. Kondo, T. Yoshitomi, H. Matsuzaka, S. Kitagawa, and K. Seki, "Three-Dimensional Framework with Channeling Cavities for Small Molecules: {$[M_2(4, 4'\text{-bpy})_3\ (NO_3)_4\ ]\cdot xH_2O$} n (M═Co, Ni, Zn)," *Angewandte Chemie International Edition in English* 36, no. 16 (2003): 1725–1727.

90. H. Furukawa, K. E. Cordova, M. O'Keeffe, and O. M. Yaghi, "The Chemistry and Applications of Metal-Organic Frameworks," *Science* 341, no. 6149 (2013): 1230444.

91. M. D. Ward, "Polynuclear Coordination Cages," *Chemical Communications* (2009): 4487–4499.

92. R. M. Yeh, J. Xu, G. Seeber, and K. N. Raymond, "Large $M_4L_4$ (M=Al(III), Ga(III), In(III), Ti(IV)) Tetrahedral Coordination Cages: An Extension of Symmetry-Based Design," *Inorganic Chemistry* 44, no. 18 (2005): 6228–6239.

93. A. Mishra, S. C. Kang, and K. W. Chi, "Coordination-Driven Self-Assembly of Arene–Ruthenium Compounds," *European Journal of Inorganic Chemistry* 2013, no. 30 (2013): 5222–5232.

94. X. Yang, Z. Ullah, J. F. Stoddart, and C. T. Yavuz, "Porous Organic Cages," *Chemical Reviews* 123, no. 8 (2023): 4602–4634.

95. G. Montà-González, F. Sancenón, R. Martínez-Máñez, and V. Martí-Centelles, "Purely Covalent Molecular Cages and Containers for Guest Encapsulation," *Chemical Reviews* 122, no. 16 (2022): 13636–13708.

96. I. A. Rather, F. Wang, R. Siddiqui, et al., "Covalent Organic Cages in Supramolecular Separation," *Coordination Chemistry Reviews* 535 (2025): 216648.

97. S. Pullen, J. Tessarolo, and G. H. Clever, "Increasing Structural and Functional Complexity in Self-Assembled Coordination Cages," *Chemical Science* 12, no. 21 (2021): 7269–7293.

98. A. J. McConnell, "Metallosupramolecular Cages: From Design Principles and Characterisation Techniques to Applications," *Chemical Society Reviews* 51, no. 8 (2022): 2957–2971.

99. T. Tateishi, M. Yoshimura, S. Tokuda, F. Matsuda, D. Fujita, and S. Furukawa, "Coordination/Metal–Organic Cages Inside Out," *Coordination Chemistry Reviews* 467 (2022): 214612.

100. M. Rondelli, A. H. Daranas, and T. Martin, "Importance of Precursor Adaptability in the Assembly of Molecular Organic Cages," *The Journal of Organic Chemistry* 88, no. 4 (2023): 2113–2121.

101. S. Ivanova and F. Beuerle, "Porous Crystalline Organic Cages Made by Design," *Israel Journal of Chemistry* 64, no. 6-7 (2024): e202400025.

102. D. A. Poole Iii, E. O. Bobylev, S. Mathew, and J. N. H. Reek, "Entropy Directs the Self-Assembly of Supramolecular Palladium Coordination Macrocycles and Cages," *Chemical Science* 13, no. 34 (2022): 10141–10148.

103. S. Fisher, H. H. Huang, L. Sokoliuk, A. Prescimone, O. Fuhr, and T. Solomek, "Kinetic Trapping of Rylene Diimide Covalent Organic Cages," *The Journal of Organic Chemistry* 90, no. 12 (2025): 4158–4166.

104. S. Maji, J. Samanta, K. Samanta, and R. Natarajan, "Emissive Click Cages," *Chemistry – A European Journal* 29, no. 56 (2023): e202301985.

105. E. J. Dale, N. A. Vermeulen, A. A. Thomas, et al., "ExCage," *Journal of the American Chemical Society* 136, no. 30 (2014): 10669–10682.

106. P. Bolgar, M. Dhiman, D. Núñez-Villanueva, and C. A. Hunter, "Covalent Template-Directed Synthesis: A Powerful Tool for the Construction of Complex Molecules," *Chemical Reviews* 125, no. 3 (2025): 1629–1657.

107. T. J. McMurry, S. J. Rodgers, and K. N. Raymond, "Ferric Ion Sequestering Agents. 16. Template and Stepwise Syntheses of a Macrobicyclic Catechoylamide Ferric Ion Sequestering Agent," *Journal of the American Chemical Society* 109, no. 11 (1987): 3451–3453.

108. L. Schoepff, L. Kocher, S. Durot, and V. Heitz, "Chemically Induced Breathing of Flexible Porphyrinic Covalent Cages," *The Journal of Organic Chemistry* 82, no. 11 (2017): 5845–5851.

109. S. I. Swamy, J. Bacsa, J. T. A. Jones, et al., "A Metal−Organic Framework With a Covalently Prefabricated Porous Organic Linker," *Journal of the American Chemical Society* 132, no. 37: 12773–12775.

110. C. F. Macrae, I. Sovago, S. J. Cottrell, et al., "Mercury 4.0: From Visualization to Analysis, Design and Prediction," *Journal of Applied Crystallography* 53 (2020): 226–235.

111. Z. Yang, F. Esteve, C. Antheaume, and J. M. Lehn, "Dynamic Covalent Self-Assembly and Self-Sorting Processes in the Formation of Imine-Based Macrocycles and Macrobicyclic Cages," *Chemical Science* 14, no. 24 (2023): 6631–6642.

112. M. Liu, M. A. Little, K. E. Jelfs, et al., "Acid- and Base-Stable Porous Organic Cages: Shape Persistence and pH Stability via Post-Synthetic "Tying" of a Flexible Amine Cage," *Journal of the American Chemical Society* 136, no. 21 (2014): 7583–7586.

113. A. S. Bhat, S. M. Elbert, W. S. Zhang, et al., "Transformation of a [4+6] Salicylbisimine Cage to Chemically Robust Amide Cages," *Angewandte Chemie International Edition* 58, no. 26 (2019): 8819–8823.

114. H. Wang, Y. Jin, N. Sun, W. Zhang, and J. Jiang, "Post-Synthetic Modification of Porous Organic Cages," *Chemical Society Reviews* 50 (2021): 8874–8886.

115. R. Wyler, J. de Mendoza, and J. Rebek, "A Synthetic Cavity Assembles Through Self-Complementary Hydrogen Bonds," *Angewandte Chemie International Edition in English* 32, no. 12 (2003): 1699–1701.

116. M. R. Ghadiri, K. Kobayashi, J. R. Granja, R. K. Chadha, and D. E. McRee, "The Structural and Thermodynamic Basis for the Formation of Self-Assembled Peptide Nanotubes," *Angewandte Chemie International Edition in English* 34, no. 1 (2003): 93–95.

117. M. Alajarín, A. López-Lázaro, A. Pastor, P. D. Prince, J. W. Steed, and R. Arakawa, "Dimerization of Tris(o-ureidobenzyl)Amines: A Novel Class of Aggregates," *Chemical Communications* (2001): 169–170.

118. A. Shivanyuk, E. F. Paulus, and V. Böhmer, "Guest-Controlled Formation of a Hydrogen-Bonded Molecular Capsule," *Angewandte Chemie International Edition* 38, no. 19 (1999): 2906–2909.

119. R. Zadmard, T. Schrader, T. Grawe, and A. Kraft, "Self-Assembly of Molecular Capsules in Polar Solvents," *Organic Letters* 4, no. 10 (2002): 1687–1690.

120. J. S. Sasine, R. E. Breester, and K. L. Caran, "Heterodimerization Studies of Calix[4]Arene Derivatives in Polar Solvents," *Organic Letters* 8, no. 14 (2006): 2913–2915.

121. F. Corbellini, L. Di Costanzo, M. Crego-Calama, S. Geremia, and D. N. Reinhoudt, "Guest Encapsulation in a Water-Soluble Molecular Capsule Based on Ionic Interactions," *Journal of the American Chemical Society* 125, no. 33 (2003): 9946–9947.

122. K. D. Zhang, D. Ajami, and J. Rebek, "Hydrogen-Bonded Capsules in Water," *Journal of the American Chemical Society* 135, no. 48 (2013): 18064–18066.

123. F. U. Rahman, D. Tzeli, I. D. Petsalakis, et al., "Chalcogen Bonding and Hydrophobic Effects Force Molecules Into Small Spaces," *Journal of the American Chemical Society* 142, no. 12 (2020): 5876–5883.

124. J. Zhao, D. Yang, X.-J. Yang, and B. Wu, "Anion Coordination Chemistry: From Recognition to Supramolecular Assembly," *Coordination Chemistry Reviews* 378 (2019): 415–444.

125. H. Irving and R. J. P. Williams, "Order of Stability of Metal Complexes," *Nature* 162 (1948): 746–747.

126. D. L. Caulder, R. E. Powers, T. N. Parac, and K. N. Raymond, "The Self-Assembly of a Predesigned Tetrahedral $M_4L_6$ Supramolecular Cluster," *Angewandte Chemie International Edition* 37, no. 13-14 (1998): 1840–1843.

127. A. J. Metherell and M. D. Ward, "Geometric Isomerism in Coordination Cages Based on Tris-Chelate Vertices: A Tool to Control Both Assembly and Host/Guest Chemistry," *Dalton Transactions* 45, no. 41 (2016): 16096–16111.

128. B. E. Barber, E. M. G. Jamieson, L. E. M. White, and C. T. McTernan, "Metal-Peptidic Cages—Helical Oligoprolines Generate Highly Anisotropic Nanospaces With Emergent Isomer Control," *Chemistry* 10, no. 9 (2024): 2792–2806.

129. W. M. Bloch and G. H. Clever, "Integrative Self-Sorting of Coordination Cages Based on 'Naked' metal Ions," *Chemical Communications* 53, no. 61 (2017): 8506–8516.

130. D. F. Brightwell, K. Samanta, J. Muldoon, et al., "Applying Metallo-Organic Ligand Design Principles to the Stereoselective Synthesis of a Peptide-Based $Pd_2L_4X_4$ Cage," *ChemistryEurope* 3, no. 1 (2024): e202400050.

131. N. Willnhammer, F. Böhm, L. Rieder, et al., "Post-Assembly Modification of Pt(II) Metallacages: An Open Door to Medicinal Applications," *ChemRxiv* V1 (2025): 1–14.

132. Z. T. Avery, M. G. Gardiner, and D. Preston, "Using a New Pt(II) Source to Make Pt(II) Lantern-Shaped Cages, Including Low-Symmetry, Heteroleptic, and Multicavity Examples," *Angewandte Chemie International Edition* 64, no. 6 (2025): e202418079.

133. C. Xiao, J. Tian, Q. Chen, and M. Hong, "Water-Stable Metal–Organic Frameworks (MOFs): Rational Construction and Carbon Dioxide Capture," *Chemical Science* 15, no. 5 (2024): 1570–1610.

134. X. Liu, X. Wang, and F. Kapteijn, "Water and Metal–Organic Frameworks: From Interaction Toward Utilization," *Chemical Reviews* 120, no. 16 (2020): 8303–8377.

135. E. M. El-Sayed, Y. D. Yuan, D. Zhao, and D. Yuan, "Zirconium Metal–Organic Cages: Synthesis and Applications," *Accounts of Chemical Research* 55, no. 11 (2022): 1546–1560.

136. Y. Zhang, R. Q. Chen, S. T. Wang, Y. J. Liu, W. H. Fang, and J. Zhang, "From an Aluminum Oxo Cluster to an Aluminum Oxo Cluster Organic Cage," *Chemical Communications* 59, no. 23 (2023): 3411–3414.

137. B. Therrien, "Arene Ruthenium Cages: Boxes Full of Surprises," *European Journal of Inorganic Chemistry* 2009, no. 17 (2009): 2445–2453.

138. B. H. Northrop, Y. R. Zheng, K. W. Chi, and P. J. Stang, "Self-Organization in Coordination-Driven Self-Assembly," *Accounts of Chemical Research* 42, no. 10: 1554–1563.

139. A. Pöthig and A. Casini, "Recent Developments of Supramolecular Metal-Based Structures for Applications in Cancer Therapy and Imaging," *Theranostics* 9, no. 11 (2019): 3150–3169.

140. P. Mal, D. Schultz, K. Beyeh, K. Rissanen, and J. R. Nitschke, "An Unlockable–Relockable Iron Cage by Subcomponent Self-Assembly," *Angewandte Chemie International Edition* 47, no. 43 (2008): 8297–8301.

141. J. L. Bolliger, A. M. Belenguer, and J. R. Nitschke, "Enantiopure Water-Soluble [$Fe_4L_6$] Cages: Host–Guest Chemistry and Catalytic Activity," *Angewandte Chemie International Edition* 52, no. 31 (2013): 7958–7962.

142. M. Whitehead, S. Turega, A. Stephenson, C. A. Hunter, and M. D. Ward, "Quantification of Solvent Effects on Molecular Recognition in Polyhedral Coordination Cage Hosts," *Chemical Science* 4, no. 7 (2013): 2744–2751.

143. B. Woods, M. N. Wenzel, T. Williams, S. R. Thomas, R. L. Jenkins, and A. Casini, "Exo-Functionalized Metallacages as Host-Guest Systems for the Anticancer Drug Cisplatin," *Frontiers in Chemistry* 7 (2019): 68.

144. J. Han, A. Schmidt, T. Zhang, et al., "Bioconjugation Strategies to Couple Supramolecular Exo-Functionalized Palladium Cages to Peptides for Biomedical Applications," *Chemical Communications* 53, no. 8 (2017): 1405–1408.

145. C. Pritchard, M. Ligorio, G. D. Jackson, M. I. Gibson, and M. D. Ward, "Programmable Monodisperse Glyco-Multivalency Using Self-Assembled Coordination Cages as Scaffolds," *ACS Applied Materials & Interfaces* 15, no. 30 (2023): 36052–36060.

146. J. E. M. Lewis, "Developing Sophisticated Microenvironments in Metal-Organic Cages," *Trends in Chemistry* 5, no. 10 (2023): 717–719.

147. J.-W. Cui, S.-H. Liu, L.-X. Tan, and J.-K. Sun, "Engineering Hierarchy to Porous Organic Cages for Biomimetic Catalytic Applications," *Accounts of Chemical Research* 6, no. 4 (2025): 484–498.

148. J. E. M. Lewis, "Pseudo-Heterolepticity in Low-Symmetry Metal-Organic Cages," *Angewandte Chemie International Edition* 61, no. 44 (2022): e202212392.

149. K. G. Andrews, P. N. Horton, and S. J. Coles, "Programmable Synthesis of Organic Cages With Reduced Symmetry," *Chemical Science* 15, no. 17 (2024): 6536–6543.

150. K. Wu, E. Benchimol, A. Baksi, and G. H. Clever, "Non-Statistical Assembly of Multicomponent [$Pd_2$ABCD] Cages," *Nature Chemistry* 16, no. 4 (2024): 584–591.

151. E. Benchimol, I. Regeni, B. Zhang, M. Kabiri, J. J. Holstein, and G. H. Clever, "Heteromeric Completive Self-Sorting in Coordination Cage Systems," *Journal of the American Chemical Society* 146, no. 10 (2024): 6905–6911.

152. H. Yu, Z. Guo, J. Tang, et al., "Configurational Control of Low-Symmetry Heteroleptic Metal–Organic Cages With Asymmetric Ligands," *Chemical Science* 16, no. 14 (2025): 6114–6120.

153. E. Benchimol, A. Rivoli, M. Kabiri, et al., "Guest Segregation in Heteromeric Multicage Systems," *Journal of the American Chemical Society* 147, no. 4 (2025): 3823–3829.

154. L. K. Moree, L. A. V. Faulkner, and J. D. Crowley, "Heterometallic Cages: Synthesis and Applications," *Chemical Society Reviews* 53, no. 1 (2024): 25–46.

155. T. Sawada, Y. Inomata, K. Shimokawa, and M. Fujita, "A Metal–Peptide Capsule by Multiple Ring Threading," *Nature Communications* 10, no. 1 (2019): 5687.

156. B. E. Barber, E. M. G. Jamieson, L. E. M. White, and C. T. McTernan, "Embracing Complexity: Peptides as Tunable Scaffolds in the Construction of Discrete Supramolecular Systems," *Angewandte Chemie International Edition* 64, no. 34 (2025): e202512014.

157. J. Liu, Z. Wang, P. Cheng, M. J. Zaworotko, Y. Chen, and Z. Zhang, "Post-Synthetic Modifications of Metal–Organic Cages," *Nature Reviews Chemistry* 6, no. 5 (2022): 339–356.

158. D. A. Roberts, B. S. Pilgrim, and J. R. Nitschke, "Covalent Post-Assembly Modification in Metallosupramolecular Chemistry," *Chemical Society Reviews* 47, no. 2 (2018): 626–644.

159. D. Luo, X. W. Zhu, X. P. Zhou, and D. Li, "Covalent Post-Synthetic Modification of Metal-Organic Cages: Concepts and Recent Progress," *Chemistry – A European Journal* 30, no. 24 (2024): e202400020.

160. M. Otte, "Reactions in Endohedral Functionalized Cages," *European Journal of Organic Chemistry* 26, no. 18 (2023): e202300012.

161. B. Hribar, N. T. Southall, V. Vlachy, and K. A. Dill, "How Ions Affect the Structure of Water," *Journal of the American Chemical Society* 124, no. 41 (2002): 12302–12311.

162. T. Nevolianis, J. W. Zheng, S. Muller, et al., "Solvation Free Energies of Anions: From Curated Reference Data to Predictive Models," *Journal of the American Chemical Society* 147, no. 34 (2025): 30626–30646.

163. S. Bhattacharyya, M. R. Black, and B. S. Pilgrim, "Encapsulation of Reactive Species Within Metal–Organic Cages," *Chemical Science* 16 (2025): 21238–21258.

164. Y.-L. Ma, M. Quan, X.-L. Lin, et al., "Biomimetic Recognition of Organic Drug Molecules in Water by Amide Naphthotubes," *CCS Chemistry* 3, no. 4 (2021): 1078–1092.

165. D. A. McNaughton, W. G. Ryder, A. M. Gilchrist, et al., "New Insights and Discoveries in Anion Receptor Chemistry," *Chemistry* 9, no. 11 (2023): 3045–3112.

166. S. Kubik, "Anion Recognition in Water," *Chemical Society Reviews* 39, no. 10 (2010): 3648–3663.

167. P. J. Anzenbacher, A. Prakash, S. M. George, A. R. Sartori, M. Zamkov, and A. N. Tarnovsky, "Overcoming the Hydration and Solvation Problem in Ion Recognition and Binding: The Biomimetic Approach," *Accounts of Chemical Research* 58, no. 17 (2025): 2792–2803.

168. A. G. Vidulich and R. L. Kay, "The Dielectric Constant of Water Between 0° and 40°," *The Journal of Physical Chemistry* 66, no. 2 (1962): 383–383.

169. C. A. Hunter, "Quantifying Intermolecular Interactions: Guidelines for the Molecular Recognition Toolbox," *Angewandte Chemie International Edition* 43, no. 40 (2004): 5310–5324.

170. S. Kubik, "When Molecules Meet in Water-Recent Contributions of Supramolecular Chemistry to the Understanding of Molecular Recognition Processes in Water," *ChemistryOpen* 11, no. 4 (2022): e202200028.

171. F. P. Schmidtchen, "Einschluß von Anionen in Makrotricyclische Quartäre Ammoniumsalze," *Angewandte Chemie* 89, no. 10 (1977): 751–752.

172. G. Müller, J. Riede, and F. P. Schmidtchen, "Host-Guest Bonding of Oxoanions to Guanidinium Anchor Groups," *Angewandte Chemie International Edition* 27, no. 11 (1988): 1516–1518.

173. C. Schmuck, "Carboxylate Binding by 2-(Guanidiniocarbonyl)pyrrole Receptors in Aqueous Solvents: Improving the Binding Properties of

Guanidinium Cations Through Additional Hydrogen Bonds," *Chemistry - A European Journal* 6, no. 4 (2000): 709–718.

174. C. Schmuck and M. Schwegmann, "A Molecular Flytrap for the Selective Binding of Citrate and Other Tricarboxylates in Water," *Journal of the American Chemical Society* 127, no. 10 (2005): 3373–3379.

175. P. Blondeau, M. Segura, R. Perez-Fernandez, and J. de Mendoza, "Molecular Recognition of Oxoanions Based on Guanidinium Receptors,"*Chemical Society Reviews* 36, no. 2 (2007): 198–210.

176. M. J. Langton, S. W. Robinson, I. Marques, V. Felix, and P. D. Beer, "Halogen Bonding in Water Results in Enhanced Anion Recognition in Acyclic and Rotaxane Hosts," *Nature Chemistry* 6, no. 12 (2014): 1039–1043.

177. A. Brown and P. D. Beer, "Halogen Bonding Anion Recognition," *Chemical Communications* 52, no. 56 (2016): 8645–8658.

178. A. Borissov, I. Marques, J. Y. C. Lim, V. Felix, M. D. Smith, and P. D. Beer, "Anion Recognition in Water by Charge-Neutral Halogen and Chalcogen Bonding Foldamer Receptors," *Journal of the American Chemical Society* 141, no. 9 (2019): 4119–4129.

179. D. A. Dougherty, "The Cation−$\pi$ Interaction," *Accounts of Chemical Research* 46, no. 6 (2012): 885–893.

180. D. Quinonero, C. Garau, C. Rotger, et al., "Anion–$\pi$ Interactions: Do They Exist?," *Angewandte Chemie International Edition* 41, no. 18 (2002): 3389–3392.

181. C. Zhai, A. Mariscal, and W. Liu, "Molecular Recognition in Water by Synthetic Hydrogen-Bonding Receptors," *Trends in Chemistry* 7, no. 2 (2025): 70–84.

182. L. Escobar and P. Ballester, "Molecular Recognition in Water Using Macrocyclic Synthetic Receptors," *Chemical Reviews* 121, no. 4 (2021): 2445–2514.

183. J. Dong and A. P. Davis, "Molecular Recognition Mediated by Hydrogen Bonding in Aqueous Media," *Angewandte Chemie International Edition* 60, no. 15 (2021): 8035–8048.

184. C. Tanford, *The Hydrophobic Effect: Formation of Micelles and Biological Membranes*, 2nd edn (Wiley, 1980), 1980.

185. F. Biedermann, W. M. Nau, and H. J. Schneider, "The Hydrophobic Effect Revisited—Studies With Supramolecular Complexes Imply High-Energy Water as a Noncovalent Driving Force," *Angewandte Chemie International Edition* 53, no. 42 (2014): 11158–11171.

186. J. Kalia and R. T. Raines, "Hydrolytic Stability of Hydrazones and Oximes," *Angewandte Chemie International Edition* 47, no. 39 (2008): 7523–7526.

187. R. G. Pearson, "Hard and Soft Acids and Bases," *Journal of the American Chemical Society* 85, no. 22 (1963): 3533–3539.

188. B. Bocca, G. Forte, F. Petrucci, et al., "Monitoring of Chemical Elements and Oxidative Damage in Patients Affected by Alzheimer's Disease," *Annali dell'Istituto Superiore di Sanità* 41, no. 2 (2005): 197–203.

189. G. Arakeri, S. G. Patil, D. N. Ramesh, S. Hunasgi, and P. A. Brennan, "Evaluation of the Possible Role of Copper Ions in Drinking Water in the Pathogenesis of Oral Submucous Fibrosis: A Pilot Study," *British Journal of Oral and Maxillofacial Surgery* 52, no. 1 (2014): 24–28.

190. N. Roohani, R. Hurrell, R. Kelishadi, and R. Schulin, "Zinc and Its Importance for human Health: An Integrative Review," *Journal of Research in Medical Sciences* 18, no. 2 (2013): 144–157.

191. M. Jaishankar, T. Tseten, N. Anbalagan, B. B. Mathew, and K. N. Beeregowda, "Toxicity, Mechanism and Health Effects of Some Heavy Metals," *Interdisciplinary Toxicology* 7, no. 2 (2014): 60–72.

192. C. Exley and E. R. House, "Aluminium in the Human Brain," *Monatshefte für Chemie - Chemical Monthly* 142, no. 4 (2011): 357–363.

193. K. Berend, L. H. van Hulsteijn, and R. O. Gans, "Chloride: The Queen of Electrolytes?," *European Journal of Internal Medicine* 23, no. 3 (2012): 203–211.

194. M. Whiteman, S. Le Trionnaire, M. Chopra, B. Fox, and J. Whatmore, "Emerging Role of Hydrogen Sulfide in Health and Disease: Critical Appraisal of Biomarkers and Pharmacological Tools," *Clinical Science* 121, no. 11 (2011): 459–488.

195. J. O. Lundberg, M. T. Gladwin, A. Ahluwalia, et al., "Nitrate and Nitrite in Biology, Nutrition and Therapeutics," *Nature Chemical Biology* 5 (2009): 865–869.

196. V. K. Bansal, "Serum Inorganic Phosphorus," in *Clinical Methods: The History, Physical, and Laboratory Examinations*, 3rd ed., ed. H. K. Walker, W. D. Hall, and J. W. Hurst, (Springer, 1990).

197. H. G. Wood and J. E. Clark, "Biological Aspects of Inorganic Polyphosphates," *Annual Review of Biochemistry* 57 (1988): 235–260.

198. R. M. Madjar, G. Vasile Scăețeanu, and M. A. Sandu, "Nutrient Water Pollution From Unsustainable Patterns of Agricultural Systems, Effects and Measures of Integrated Farming," *Water* 16, no. 21 (2024): 3146.

199. C. R. Kirman, A. M. Belknap, A. F. Webster, and S. M. Hays, "Biomonitoring Equivalents for Cyanide," *Regulatory Toxicology and Pharmacology* 97 (2018): 71–81.

200. S. Guth, S. Hüser, A. Roth, et al., "Toxicity of Fluoride: Critical Evaluation of Evidence for human Developmental Neurotoxicity in Epidemiological Studies, Animal Experiments and In Vitro Analyses," *Archives of Toxicology* 94, no. 5 (2020): 1375–1415.

201. M. V. Balli, F. Biedermann, L. Prodi, and P. Picchetti, "Supramolecular Chemistry for Optical Detection and Delivery Applications in Living Plants," *Chemical Society Reviews* 54, no. 17 (2025): 7769–7869.

202. T. Pradhan, H. S. Jung, J. H. Jang, T. W. Kim, C. Kang, and J. S. Kim, "Chemical Sensing of Neurotransmitters," *Chemical Society Reviews* 43, no. 13 (2014): 4684–4713.

203. S. Kasera, L. O. Herrmann, J. del Barrio, J. J. Baumberg, and O. A. Scherman, "Quantitative Multiplexing With Nano-Self-Assemblies in SERS," *Scientific Reports* 4 (2014): 6785.

204. A. R. Bernardo, J. F. Stoddart, and A. E. Kaifer, "Cyclobis(Paraquat-p-Phenylene) as a Synthetic Receptor for Electron-Rich Aromatic Compounds: Electrochemical and Spectroscopic Studies of Neurotransmitter Binding," *Journal of the American Chemical Society* 114 (1992): 10624–10631.

205. O. Molt, D. Rübeling, G. Schäfer, and T. Schrader, "Adrenaline Recognition in Water," *Chemistry – A European Journal* 10, no. 17 (2004): 4225–4232.

206. P. Jancova, P. Anzenbacher, and E. Anzenbacherovaa, "Phase II Drug Metabolizing Enzymes," *Biomedical Papers* 154, no. 2 (2010): 103–116.

207. A. V. Stachulski and X. Meng, "Glucuronides From Metabolites to Medicines: A Survey of the in Vivo Generation, Chemical Synthesis and Properties of Glucuronides," *Natural Product Reports* 30, no. 6 (2013): 806–848.

208. R. L. Gomes, W. Meredith, C. E. Snape, and M. A. Sephton, "Conjugated Steroids: Analytical Approaches and Applications," *Analytical and Bioanalytical Chemistry* 393, no. 2 (2009): 453–458.

209. S. M. Matt and P. J. Gaskill, "Where Is Dopamine and How Do Immune Cells See It?: Dopamine-Mediated Immune Cell Function in Health and Disease," *Journal of Neuroimmune Pharmacology* 15, no. 1 (2020): 114–164.

210. T. Suominen, T. P. Piepponen, and R. Kostiainen, "Permeation of Dopamine Sulfate Through the Blood-Brain Barrier," *PLoS ONE* 10, no. 7 (2015): e0133904.

211. D. S. Goldstein, K. J. Swoboda, J. M. Miles, et al., "Sources and Physiological Significance of Plasma Dopamine Sulfate," *The Journal of Clinical Endocrinology & Metabolism* 84, no. 7 (1999): 2523–2531.

212. P. Toniolo, K. L. Koenig, B. S. Pasternack, et al., "Reliability of Measurements of Total, Protein-Bound, and Unbound Estradiol in Serum," *Cancer Epidemiology and Prevention Biomarkers* 3, no. 1 (1994): 47–50.

213. F. Biedermann and H. J. Schneider, "Experimental Binding Energies in Supramolecular Complexes," *Chemical Reviews* 116, no. 9 (2016): 5216–5300.

214. G. R. Desiraju, "The C−H···O Hydrogen Bond: Structural Implications and Supramolecular Design," *Accounts of Chemical Research* 29 (1996): 441–449.

215. D. Herschlag, M. M. Pinney, and H. Bonds, "Hydrogen Bonds: Simple After All?," *Biochemistry* 57, no. 24 (2018): 3338–3352.

216. L. Rummel and P. R. Schreiner, "Advances and Prospects in Understanding London Dispersion Interactions in Molecular Chemistry," *Angewandte Chemie International Edition* 63, no. 12 (2024): e202316364.

217. R. Eisenschitz and F. London, "Über das Verhältnis der van der Waalsschen Kräfte zu den Homöopolaren Bindungskräften," *Zeitschrift für Physik A Hadrons and nuclei* 60 (1930): 491–527.

218. A. P. Davis, "Biomimetic Carbohydrate Recognition," *Chemical Society Reviews* 49, no. 9 (2020): 2531–2545.

219. Y. Ferrand, M. P. Crump, and A. P. Davis, "A Synthetic Lectin Analog for Biomimetic Disaccharide Recognition," *Science* 318, no. 5850 (2007): 619–622.

220. R. A. Tromans, T. S. Carter, L. Chabanne, et al., "A Biomimetic Receptor for Glucose," *Nature Chemistry* 11, no. 1 (2019): 52–56.

221. E. Klein, M. P. Crump, and A. P. Davis, "Carbohydrate Recognition in Water by a Tricyclic Polyamide Receptor," *Angewandte Chemie International Edition* 44, no. 2 (2004): 298–302.

222. B. Wu, R. Tang, and Y. Tan, "Synthetic Molecular Cage Receptors for Carbohydrate Recognition," *Nature Reviews Chemistry* 9, no. 1 (2025): 10–27.

223. J. M. Lehn, "Supramolecular Chemistry—Scope and Perspectives Molecules, Supermolecules, and Molecular Devices (Nobel Lecture)," *Angewandte Chemie International Edition in English* 27, no. 1 (1988): 89–112.

224. D. E. Balderston, E. Feo, A. Leonescu, et al., "Advances in Applied Supramolecular Technologies 2021–2025," *Chemical Society Reviews* 54, no. 19 (2025): 8888–8924.

225. T. E. Lockwood, T. X. Leong, S. L. Bliese, et al., "idPAD: Paper Analytical Device for Presumptive Identification of Illicit Drugs," *Journal of Forensic Sciences* 65, no. 4 (2020): 1289–1297.

226. K. Kuczynska, P. Grzonkowski, L. Kacprzak, and J. B. Zawilska, "Abuse of Fentanyl: An Emerging Problem to Face," *Forensic Science International* 289 (2018): 207–214.

227. A. P. de Silva, "Bright Molecules for Sensing, Computing and Imaging: A Tale of Two Once-troubled Cities," *Beilstein Journal of Organic Chemistry* 11 (2015): 2774–2784.

228. X. Ma and Y. Zhao, "Biomedical Applications of Supramolecular Systems Based on Host–Guest Interactions," *Chemical Reviews* 115, no. 15 (2015): 7794–7839.

229. M. T. Albelda, J. C. Frias, E. García-España, and H. J. Schneider, "Supramolecular Complexation for Environmental Control," *Chemical Society Reviews* 41, no. 10 (2012): 3859–3877.

230. X. Huang, K. Nakanishi, and N. Berova, "Porphyrins and Metalloporphyrins: Versatile Circular Dichroic Reporter Groups for Structural Studies," *Chirality* 12, no. 4 (2000): 237–255.

231. R. Paolesse, S. Nardis, D. Monti, M. Stefanelli, and C. Di Natale, "Porphyrinoids for Chemical Sensor Applications," *Chemical Reviews* 117, no. 4 (2017): 2517–2583.

232. N. Kari, M. Zannotti, R. Giovannetti, et al., "Sensing Behavior of Metal-Free Porphyrin and Zinc Phthalocyanine Thin Film Towards Xylene-Styrene and HCl Vapors in Planar Optical Waveguide," *Nanomaterials* 11, no. 7 (2021): 1634.

233. J. Mei, N. L. Leung, R. T. Kwok, J. W. Lam, and B. Z. Tang, "Aggregation-Induced Emission: Together We Shine, United We Soar!," *Chemical Reviews* 115, no. 21 (2015): 11718–11940.

234. Y. Cui, Z. M. Chen, X. F. Jiang, J. Tong, and S. Y. Yu, "Self-Assembly and Anion Sensing of Metal–Organic [$M_6$ $L_2$] Cages From Fluorescent Triphenylamine Tri-Pyrazoles With Dipalladium(ii, ii) Corners," *Dalton Transactions* 46, no. 18 (2017): 5801–5805.

235. L. Xu, L. Hu, J. Huang, et al., "Anthracene-Functionalized Metallacage With Fluorescence Response Behavior to Anions," *Synlett* 35, no. 01 (2024): 130–134.

236. M. J. Langton and P. D. Beer, "Sulfate-Selective Binding and Sensing of a Fluorescent [3]Rotaxane Host System," *Chemistry – A European Journal* 18, no. 45 (2012): 14406–14412.

237. C. Xu, Q. G. Tran, D. Liu, C. Zhai, L. Wojtas, and W. Liu, "Charge-Assisted Hydrogen Bonding in a Bicyclic Amide Cage: An Effective Approach to Anion Recognition and Catalysis in Water," *Chemical Science* 15, no. 39 (2024): 16040–16049.

238. L. Jing, E. Deplazes, J. K. Clegg, and X. Wu, "A Charge-Neutral Organic Cage Selectively Binds Strongly Hydrated Sulfate Anions in Water," *Nature Chemistry* 16, no. 3 (2024): 335–342.

239. Y. X. Li, M. Xue, and Y. Yang, "Shape-Persistent Oxa- and Aza-calix[4]Arene Hybrid Molecular Cage and Naked Eye Sensing of Fluoride," *Organic Letters* 23 (2021): 6435–6438.

240. A. Loudet and K. Burgess, "BODIPY Dyes and Their Derivatives: Syntheses and Spectroscopic Properties," *Chemical Reviews* 107, no. 11 (2000): 4891–4932.

241. P. P. Neelakandan, A. Jiménez, and J. R. Nitschke, "Fluorophore Incorporation Allows Nanomolar Guest Sensing and White-light Emission in M4L6 Cage Complexes," *Chemical Science* 5, no. 3 (2014): 908–915.

242. V. López-Corbalán, A. Fuertes, A. L. Llamas-Saiz, M. Amorín, and J. R. Granja, "Recognition of Anion-Water Clusters by Peptide-Based Supramolecular Capsules," *Nature Communications* 15, no. 1 (2024): 6055.

243. M. Chvojka, A. Singh, A. Cataldo, et al., "The Lucigenin Assay: Measuring Anion Transport in Lipid Vesicles," *Analysis & Sensing* 4, no. 2 (2023): e202300044.

244. S. Sudan, D. W. Chen, C. Berton, F. Fadaei-Tirani, and K. Severin, "Synthetic Receptors With Micromolar Affinity for Chloride in Water," *Angewandte Chemie International Edition* 62, no. 9 (2023): e202218072.

245. M. Konopka, P. Cecot, J. M. Harrowfield, and A. R. Stefankiewicz, "Structural Self-Sorting of Pseudopeptide Homo and Heterodimeric Disulfide Cages in Water: Mechanistic Insights and Cation Sensing," *Journal of Materials Chemistry C* 9, no. 24 (2021): 7607–7614.

246. L.-M. Fu, X.-C. Ai, M.-Y. Li, et al., "Role of Ligand-to-Metal Charge Transfer State in Nontriplet Photosensitization of Luminescent Europium Complex," *The Journal of Physical Chemistry A* 114, no. 13 (2010): 4494–4500.

247. C. L. Liu, R. L. Zhang, C. S. Lin, et al., "Intraligand Charge Transfer Sensitization on Self-Assembled Europium Tetrahedral Cage Leads to Dual-Selective Luminescent Sensing Toward Anion and Cation," *Journal of the American Chemical Society* 139, no. 36 (2017): 12474–12479.

248. N. Siraj, B. El-Zahab, S. Hamdan, et al., "Fluorescence, Phosphorescence, and Chemiluminescence," *Analytical Chemistry* 88, no. 1 (2016): 170–202.

249. X. F. Jiang, F. K. Hau, Q. F. Sun, S. Y. Yu, and V. W. Yam, "From {Au I ···Au I }-Coupled Cages to the Cage-Built 2-D {Au I ···Au I } Arrays: Au I ···Au I Bonding Interaction Driven Self-Assembly and Their Ag I Sensing and Photo-Switchable Behavior," *Journal of the American Chemical Society* 136, no. 31 (2014): 10921–10929.

250. C. Dai, B. Gu, S. P. Tang, P. H. Deng, and B. Liu, "Fluorescent Porous Organic Cage With Good Water Solubility for Ratiometric Sensing of Gold(III) Ion in Aqueous Solution," *Analytica Chimica Acta* 1192 (2022): 339376.

251. T. P. Sheng, C. Z. Sun, and F. R. Dai, "Triphenylamine-Functionalized Coordination Cage as a Supramolecular Fluorescence Sensor for Sequen-

tial Detection of Aluminum Ions and Nitrofurantoin," *ACS Applied Materials & Interfaces* 15, no. 24 (2023): 29252–29258.

252. Z. C. Wang, Y. Z. Tan, H. Yu, W. H. Bao, L. L. Tang, and F. Zeng, "A Benzothiadiazole-Based Self-Assembled Cage for Cadmium Detection," *Molecules* 28, no. 4 (2023): 1841.

253. C. García-Simón, M. Garcia-Borràs, L. Gómez, et al., "Self-Assembled Tetragonal Prismatic Molecular Cage Highly Selective for Anionic $\pi$ Guests," *Chemistry – A European Journal* 19 (2013): 1445–1456.

254. A. Prabodh, Y. Wang, S. Sinn, et al., "Fluorescence Detected Circular Dichroism (FDCD) for Supramolecular Host–Guest Complexes," *Chemical Science* 12, no. 27 (2021): 9420–9431.

255. H. Ito and S. Shinoda, "Chirality Sensing and Size Recognition of N-Boc-Amino Acids by Cage-type Dimeric Lanthanide Complexes: Chirality Detection of N-Boc-Aspartate Anions via Luminescence Colour Change," *Chemical Communications* 51, no. 18 (2015): 3808–3811.

256. C. Bravin, G. Mason, G. Licini, and C. Zonta, "A Diastereodynamic Probe Transducing Molecular Length Into Chiroptical Readout," *Journal of the American Chemical Society* 141, no. 30 (2019): 11963–11969.

257. C. Bravin, E. Badetti, F. A. Scaramuzzo, G. Licini, and C. Zonta, "Triggering Assembly and Disassembly of a Supramolecular Cage," *Journal of the American Chemical Society* 139, no. 18 (2017): 6456–6460.

258. L. Cheng, K. Liu, Y. Duan, et al., "Adaptive Chirality of an Achiral Cage: Chirality Transfer, Induction, and Circularly Polarized Luminescence Through Aqueous Host–Guest Complexation," *CCS Chemistry* 3, no. 11 (2021): 2749–2763.

259. F. S. Richardson and J. P. Riehl, "Circularly Polarized Luminescence Spectroscopy," *Chemical Reviews* 77, no. 6 (1977): 773–792.

260. Y. Zhou and J. Yoon, "Recent Progress in Fluorescent and Colorimetric Chemosensors for Detection of Amino Acids," *Chemical Society Reviews* 41, no. 1 (2012): 52–67.

261. H. Zhang, Y. Li, Y. F. Zhang, et al., "Solvato-Controlled Assembly and Structural Transformation of Emissive Poly-NHC-Based Organometallic Cages and Their Applications in Amino Acid Sensing and Fluorescence Imaging," *Chemistry – A European Journal* 29, no. 23 (2023): e202300209.

262. M. Zhang, M. L. Saha, M. Wang, et al., "Multicomponent Platinum(II) Cages With Tunable Emission and Amino Acid Sensing" *Journal of the American Chemical Society* 139, no. 14 (2017): 5067–5074.

263. S. Maji, J. Samanta, and R. Natarajan, "Water-Soluble Triazolium Covalent Cages for ATP Sensing," *Chemistry – A European Journal* 30, no. 15 (2024): e202303596.

264. B. Paul and R. Natarajan, "Metal–Organic Cage Receptors for Encapsulation and Sensing of Bile Acids," *Inorganic Chemistry* 63, no. 18 (2024): 8449–8461.

265. G. Monta-Gonzalez, E. Garrido, E. Climent, C. Vicent, R. Martinez-Manez, and V. Marti-Centelles, "Molecular Cages as Probes in Indicator Displacement Assays: The Case of Scopolamine Detection," *Angewandte Chemie International Edition* 65 (2025): e23575.

266. G. Monta-Gonzalez, D. Bastante-Rodriguez, A. Garcia-Fernandez, P. J. Lusby, R. Martinez-Manez, and V. Marti-Centelles, "Comparing Organic and Metallo-Organic Hydrazone Molecular Cages as Potential Carriers for Doxorubicin Delivery," *Chemical Science* 15, no. 26 (2024): 10010–10017.

267. Z. Meng, F. Yang, X. Wang, et al., "Trefoil-Shaped Metal–Organic Cages as Fluorescent Chemosensors for Multiple Detection of $Fe^{3+}$ , $Cr_2O_7^{2-}$ , and Antibiotics," *Inorganic Chemistry* 62, no. 4 (2023): 1297–1305.

268. L. A. Perez-Marquez, M. D. Perretti, R. Garcia-Rodriguez, F. Lahoz, and R. Carrillo, "A Fluorescent Cage for Supramolecular Sensing of 3-Nitrotyrosine in Human Blood Serum," *Angewandte Chemie International Edition* 61, no. 28 (2022): e202205403.

269. C. Ke, H. Destecroix, M. P. Crump, and A. P. Davis, "A Simple and Accessible Synthetic Lectin for Glucose Recognition and Sensing," *Nature Chemistry* 4, no. 9 (2012): 718–723.

270. W. Liu, Y. Tan, L. O. Jones, et al., "PCage: Fluorescent Molecular Temples for Binding Sugars in Water," *Journal of the American Chemical Society* 143, no. 38 (2021): 15688–15700.

271. M. Wang, V. Vajpayee, S. Shanmugaraju, et al., "Coordination-Driven Self-Assembly of $M_3L_2$ Trigonal Cages From Preorganized Metalloligands Incorporating Octahedral Metal Centers and Fluorescent Detection of Nitroaromatics," *Inorganic Chemistry* 50, no. 4 (2011): 1506–1512.

272. C. L. Liu, L. P. Zhou, D. Tripathy, and Q. F. Sun, "Self-Assembly of Stable Luminescent Lanthanide Supramolecular $M_4L_6$ cages With Sensing Properties Toward Nitroaromatics," *Chemical Communications* 53, no. 16 (2017): 2459–2462.

273. S. Y. Yin, Y. X. Zhu, M. Pan, et al., "Nanosized NIR-Luminescent Ln Metal–Organic Cage for Picric Acid Sensing," *European Journal of Inorganic Chemistry* 2017, no. 3 (2017): 646–650.

274. T. Feng, X. Li, J. Wu, C. He, and C. Duan, "Cavity-Directed Nitroaromatics Sensing Within a Carbazole-Based Luminescent Supramolecular $M_2L_3$ Cage," *Chinese Chemical Letters* 31, no. 1 (2020): 95–98.

275. Q. Tang, Y. Sun, H. Y. Li, J. Q. Wu, Y. N. Liang, and Z. Zhang, "Hexanuclear 3d – 4f Metal–Organic Cages Assembled From a Carboxylic Acid-Functionalized Tris-Triazamacrocycle for Highly Selective Fluorescent Sensing of Picric Acid," *Applied Organometallic Chemistry* 33, no. 4 (2019): e4814.

276. A. B. Sainaba, R. Saha, M. Venkateswarulu, E. Zangrando, and P. S. Mukherjee, "Pt(II) Tetrafacial Barrel With Aggregation-Induced Emission for Sensing," *Inorganic Chemistry* 63, no. 1 (2024): 508–517.

277. X. Li, H. Li, L. Xie, et al., "Phenoxazine-Based Supramolecular Metal-Organic Cage for Picric Acid Detection," *Inorganica Chimica Acta* 557 (2023): 121681.

278. E. Hammel, T. F. Webster, R. Gurney, and W. Heiger-Bernays, "Implications of PFAS Definitions Using Fluorinated Pharmaceuticals," *Iscience* 25 (2022): 104020.

279. A. U. Rehman, M. Crimi, and S. Andreescu, "Current and Emerging Analytical Techniques for the Determination of PFAS in Environmental Samples," *TrEAC* 37 (2023): e00198.

280. N. M. A. Speakman, A. W. Heard, and J. R. Nitschke, "A $Cu^{I}{}_6L_4$ Cage Dynamically Reconfigures to Form Suit[4]Anes and Selectively Bind Fluorinated Steroids," *Journal of the American Chemical Society* 146, no. 15 (2024): 10234–10239.

281. X. Z. Wang, D. W. Chen, F. Fadaei-Tirani, X. P. Zhou, and K. Severin, "Selective Recognition and Extraction of Short-Chain Perfluoroalkyl Carboxylates by a Supramolecular Receptor," *Angewandte Chemie International Edition* 64, no. 22 (2025): e202504880.

282. M. Yamashina, M. M. Sartin, Y. Sei, et al., "Preparation of Highly Fluorescent Host–Guest Complexes With Tunable Color upon Encapsulation," *Journal of the American Chemical Society* 137, no. 29 (2015): 9266–9269.

283. K. Ono, J. K. Klosterman, M. Yoshizawa, K. Sekiguchi, T. Tahara, and M. Fujita, "ON/OFF Red Emission From Azaporphine in a Coordination Cage in Water," *Journal of the American Chemical Society* 131 (2009): 12526–12527.

284. J. Wang, C. He, P. Wu, J. Wang, and C. Duan, "An Amide-Containing Metal–Organic Tetrahedron Responding to a Spin-Trapping Reaction in a Fluorescent Enhancement Manner for Biological Imaging of NO in Living Cells," *Journal of the American Chemical Society* 133, no. 32 (2011): 12402–12405.

285. F. Kamel, "Paths From Pesticides to Parkinson's," *Science* 341, no. 6147 (2013): 722–723.

286. P. K. Maitra, S. Bhattacharyya, P. C. Purba, and P. S. Mukherjee, "Coordination-Induced Emissive Poly-NHC-Derived Metallacage for Pesticide Detection," *Inorganic Chemistry* 63, no. 5 (2024): 2569–2576.

287. D. Wu, A. C. Sedgwick, T. Gunnlaugsson, E. U. Akkaya, J. Yoon, and T. D. James, "Fluorescent Chemosensors: The Past, Present and Future," *Chemical Society Reviews* 46, no. 23 (2017): 7105–7123.

288. F. Broch and A. Gautier, "Illuminating Cellular Biochemistry: Fluorogenic Chemogenetic Biosensors for Biological Imaging," *ChemPlusChem* 85, no. 7 (2020): 1487–1497.

289. D. Kolarski, M. L. Bossi, R. Lincoln, J. C. Fuentes-Monteverde, V. N. Belov, and S. W. Hell, "Supramolecular Complexation of Quenched Rosamines With Cucurbit[7]Uril: Fluorescence Turn-ON Effect for Super-Resolution Imaging," *Journal of the American Chemical Society* 147, no. 32 (2025): 28893–28902.

290. J. Wu, Z. Shi, L. Zhu, et al., "The Design and Bioimaging Applications of NIR Fluorescent Organic Dyes With High Brightness," *Advanced Optical Materials* 10, no. 8 (2022): 2102514.

291. E. Ivens, M. M. D. Cominetti, and M. Searcey, "Junctions in DNA: Underexplored Targets for Therapeutic Intervention," *Bioorganic & Medicinal Chemistry* 69 (2022): 116897.

292. Y. Wang and D. J. Patel, "Guanine residues in d(T2AG3) and d(T2G4) Form Parallel-Stranded Potassium Cation Stabilized G-Quadruplexes With Anti Glycosidic Torsion Angles in Solution," *Biochemistry* 31, no. 35 (1991): 8112–8119.

293. F. W. Smith and J. Feigon, "Quadruplex Structure of Oxytricha Telomeric DNA Oligonucleotides," *Nature* 356 (1992): 164–168.

294. G. N. Parkinson, M. P. H. Lee, and S. Neidle, "Crystal Structure of Parallel Quadruplexes From human Telomeric DNA," *Nature* 417 (2002): 876–880.

295. J. Spiegel, S. Adhikari, and S. Balasubramanian, "The Structure and Function of DNA G-Quadruplexes," *Trends in Chemistry* 2, no. 2 (2020): 123–136.

296. D. L. Ma, Z. Zhang, M. Wang, L. Lu, H. J. Zhong, and C. H. Leung, "Recent Developments in G-Quadruplex Probes," *Chemistry & Biology* 22, no. 7 (2015): 812–828.

297. G. Biffi, D. Tannahill, J. McCafferty, and S. Balasubramanian, "Quantitative Visualization of DNA G-Quadruplex Structures in Human Cells," *Nature Chemistry* 5, no. 3 (2013): 182–186.

298. J. Chen, B. L. Hickey, L. Wang, et al., "Selective Discrimination and Classification of G-Quadruplex Structures With a Host–Guest Sensing Array," *Nature Chemistry* 13, no. 5 (2021): 488–495.

299. A. C. Hotze, N. J. Hodges, R. E. Hayden, et al., "Supramolecular Iron Cylinder With Unprecedented DNA Binding Is a Potent Cytostatic and Apoptotic Agent Without Exhibiting Genotoxicity," *Chemistry & Biology* 15, no. 12 (2008): 1258–1267.

300. J. S. Craig, L. Melidis, H. D. Williams, et al., "Organometallic Pillarplexes That Bind DNA 4-Way Holliday Junctions and Forks," *Journal of the American Chemical Society* 145, no. 25 (2023): 13570–13580.

301. R. Kieltyka, P. Englebienne, J. Fakhoury, C. Autexier, N. Moitessier, and H. F. Sleiman, "A Platinum Supramolecular Square as an Effective G-Quadruplex Binder and Telomerase Inhibitor," *Journal of the American Chemical Society* 130, no. 31 (2008): 10040–10041.

302. H. Yu, X. Wang, M. Fu, J. Ren, and X. Qu, "Chiral Metallo-Supramolecular Complexes Selectively Recognize Human Telomeric G-Quadruplex DNA," *Nucleic Acids Research* 36, no. 17 (2008): 5695–5703.

303. O. Domarco, D. Lotsch, J. Schreiber, et al., "Self-Assembled $Pt_2$ $L_2$ Boxes Strongly Bind G-Quadruplex DNA and Influence Gene Expression in Cancer Cells," *Dalton Transactions* 46, no. 2 (2017): 329–332.

304. X. H. Zheng, Y. F. Zhong, C. P. Tan, L. N. Ji, and Z. W. Mao, "Pt(II) Squares as Selective and Effective Human Telomeric G-Quadruplex Binders and Potential Cancer Therapeutics," *Dalton Transactions* 41, no. 38 (2012): 11807–11812.

305. C. Kaubler, D. Wragg, C. Schmidt, et al., ""Dynamical Docking" of Cyclic Dinuclear Au(I) Bis-N-Heterocyclic Complexes Facilitates Their Binding to G-Quadruplexes," *Inorganic Chemistry* 61, no. 50 (2022): 20405–20423.

306. S. F. Xi, L. Y. Bao, Z. L. Xu, Y. X. Wang, Z. D. Ding, and Z. G. Gu, "Enhanced Stabilization of G-Quadruplex DNA by $[Ni_4L_6]^{8+}$ Cages With Large Rigid Aromatic Ligands," *European Journal of Inorganic Chemistry* 2017, no. 29 (2017): 3533–3541.

307. T. Rodríguez-Prieto, D. Wragg, N. Heiduk, et al., "A Golden Touch in the Design of Multifunctional Porphyrin Metallacages: Host–Guest Chemistry for Drug-Target Interactions," *CCS Chemistry* 6, no. 7 (2024): 1662–1671.

308. B. Woods, D. Dollerer, B. Aikman, et al., "Highly Luminescent Metallacages Featuring Bispyridyl Ligands Functionalised With BODIPY for Imaging in Cancer Cells," *Journal of Inorganic Biochemistry* 199 (2019): 110781.

309. O. Domarco, C. Kieler, C. Pirker, et al., "Subcellular Duplex DNA and G-Quadruplex Interaction Profiling of a Hexagonal Pt II Metallacycle," *Angewandte Chemie International Edition* 58, no. 24 (2019): 8007–8012.

310. G. Yu, T. R. Cook, Y. Li, et al., "Tetraphenylethene-Based Highly Emissive Metallacage as a Component of Theranostic Supramolecular Nanoparticles," *Proceedings of the National Academy of Sciences* 113, no. 48 (2016): 13720–13725.

311. L. C. Gilday, N. G. White, and P. D. Beer, "Triazole- and Triazolium-Containing Porphyrin-Cages for Optical Anion Sensing," *Dalton Transactions* 41, no. 23 (2012): 7092–7097.

312. A. Herrmann, R. Haag, and U. Schedler, "Hydrogels and Their Role in Biosensing Applications," *Advanced Healthcare Materials* 10, no. 11 (2021): e2100062.

313. H. Choi, W. S. Choi, and J. O. Jeong, "A Review of Advanced Hydrogel Applications for Tissue Engineering and Drug Delivery Systems as Biomaterials," *Gels* 10, no. 11 (2024): 693.

314. N. Petelinsek and S. Mommer, "Tough Hydrogels for Load-Bearing Applications," *Advanced Science* 11, no. 12 (2024): e2307404.

315. L. Rijns, M. B. Baker, and P. Y. W. Dankers, "Using Chemistry To Recreate the Complexity of the Extracellular Matrix: Guidelines for Supramolecular Hydrogel–Cell Interactions," *Journal of the American Chemical Society* 146, no. 26 (2024): 17539–17558.

316. C. Hu and K. Severin, "Nanogels with Metal-Organic Cages as Functional Crosslinks," *Angewandte Chemie International Edition* 63, no. 23 (2024): e202403834.

317. O. Calvo-Lozano, L. Hernandez-Lopez, L. Gomez, et al., "Integration of Metal–Organic Polyhedra Onto a Nanophotonic Sensor for Real-Time Detection of Nitrogenous Organic Pollutants in Water," *ACS Applied Materials & Interfaces* 15, no. 33 (2023): 39523–39529.

318. A. V. Zhukhovitskiy, M. Zhong, E. G. Keeler, et al., "Highly Branched and Loop-Rich Gels via Formation of Metal–Organic Cages Linked by Polymers," *Nature Chemistry* 8, no. 1 (2016): 33–41.

319. Y. Wang, Y. Gu, E. G. Keeler, J. V. Park, R. G. Griffin, and J. A. Johnson, "Star PolyMOCs with Diverse Structures, Dynamics, and Functions by Three-Component Assembly," *Angewandte Chemie International Edition* 56, no. 1 (2017): 188–192.

320. J. A. Foster, R. M. Parker, A. M. Belenguer, et al., "Differentially Addressable Cavities Within Metal–Organic Cage-Cross-Linked Polymeric Hydrogels," *Journal of the American Chemical Society* 137, no. 30 (2015): 9722–9729.

321. R. Küng, T. Pausch, D. Rasch, R. Göstl, and B. M. Schmidt, "Mechanochemical Release of Non-Covalently Bound Guests From a Polymer-Decorated Supramolecular Cage," *Angewandte Chemie International Edition* 60, no. 24 (2021): 13626–13630.

322. R. Küng, A. Germann, M. Krusmann, et al., "Mechanoresponsive Metal-Organic Cage-Crosslinked Polymer Hydrogels," *Chemistry – A European Journal* 29, no. 18 (2023): e202300079.

323. M. Irie, "Diarylethenes for Memories and Switches," *Chemical Reviews* 100 (2000): 1685–1716.

324. Y. Gu, E. A. Alt, H. Wang, X. Li, A. P. Willard, and J. A. Johnson, "Photoswitching Topology in Polymer Networks With Metal–Organic Cages As Crosslinks," *Nature* 560, no. 7716 (2018): 65–69.

325. A. V. Zhukhovitskiy, J. Zhao, M. Zhong, et al., "Polymer Structure Dependent Hierarchy in PolyMOC Gels," *Macromolecules* 49, no. 18 (2016): 6896–6902.

326. B. T. Nguyen, A. B. Grommet, A. Tron, M. C. A. Georges, and J. R. Nitschke, "Heat Engine Drives Transport of an $Fe^{II}{}_4L_4$ Cage and Cargo," *Advanced Materials* 32, no. 19 (2020): e1907241.

327. M. Burnworth, L. Tang, J. R. Kumpfer, et al., "Optically Healable Supramolecular Polymers," *Nature* 472, no. 7343 (2011): 334–337.

328. Z. Zhang, Z. Zhao, L. Wu, et al., "Emissive Platinum(II) Cages With Reverse Fluorescence Resonance Energy Transfer for Multiple Sensing," *Journal of the American Chemical Society* 142, no. 5 (2020): 2592–2600.

329. S. J. Hu, X. Q. Guo, L. P. Zhou, et al., "Guest-Driven Self-Assembly and Chiral Induction of Photofunctional Lanthanide Tetrahedral Cages," *Journal of the American Chemical Society* 144, no. 9 (2022): 4244–4253.

330. K. Wu, J. Tessarolo, A. Baksi, and G. H. Clever, "Guest-Modulated Circularly Polarized Luminescence by Ligand-to-Ligand Chirality Transfer in Heteroleptic Pd II Coordination Cages," *Angewandte Chemie International Edition* 61, no. 35 (2022): e202205725.

331. H. Zhu, L. Pesce, R. Chowdhury, et al., "Stereocontrolled Self-Assembly of a Helicate-Bridged $Cu^{I}{}_{12}L_4$ Cage That Emits Circularly Polarized Light," *Journal of the American Chemical Society* 146, no. 4 (2024): 2379–2386.

332. J. F. Chen, Q. X. Gao, H. Yao, et al., "Recent Advances in Circularly Polarized Luminescence of Planar Chiral Organic Compounds," *Chemical Communications* 60, no. 53 (2024): 6728–6740.

333. D. Li, Z. Jiang, X. Liu, and Y. Cheng, "Recent Advances in Application of Circularly Polarized Luminescence Probes Toward Bioimaging Technology," *Chemical & Biomedical Imaging* 4 (2025): 144–166, https://doi.org/10.1021/cbmi.5c00091.

334. P. Kovacic and R. Somanathan, "Nitroaromatic Compounds: Environmental Toxicity, Carcinogenicity, Mutagenicity, Therapy and Mechanism," *Journal of Applied Toxicology* 34, no. 8 (2014): 810–824.

335. S. B. Haderlein, K. W. Weissmahr, and R. P. Schwarzenbach, "Specific Adsorption of Nitroaromatic Explosives and Pesticides to Clay Minerals," *Environmental Science & Technology* 30, no. 2 (1996): 612–622.

336. K. Wirdefeldt, H. O. Adami, P. Cole, D. Trichopoulos, and J. Mandel, "Epidemiology and Etiology of Parkinson's Disease: A Review of the Evidence," *European Journal of Epidemiology* 26 (2011): 1–58.

337. E. Bible, "High Serum Levels of the Pesticide Metabolite DDE—A Potential Environmental Risk Factor for Alzheimer Disease," *Nature Reviews Neurology* 10, no. 125 (2014): 125.

338. N. Jones, "Risk of Dementia and Alzheimer Disease Increases With Occupational Pesticide Exposure," *Nature Reviews Neurology* 6 (2010): 353.

339. K. Wiklund, J. Dich, and L. E. Holm, "Risk of Malignant Lymphoma in Swedish Pesticide Appliers," *British Journal of Cancer* 56 (1987): 505–508.

340. M. G. Evich, M. J. B. Davis, J. P. McCord, et al., "Per- and Polyfluoroalkyl Substances in the Environment," *Science* 375, no. 6580 (2022): eabg9065.

341. A. C. Kalita and R. Murugavel, "Fluoride Ion Sensing and Caging by a Preformed Molecular D4R Zinc Phosphate Heterocubane," *Inorganic Chemistry* 53, no. 7 (2014): 3345–3353.

342. C. S. Kwan, A. Walther, A. S. Mikherdov, J. J. Holstein, C. Drechsler, and G. H. Clever, "Dual Cation/Anion Binding in Crown Ether-Based Coordination Cages," *Journal of the American Chemical Society* 148, no. 3 (2025): 3230–3239.

343. S. Hollstein and M. von Delius, "The Dynamic Chemistry of Orthoesters and Trialkoxysilanes: Making Supramolecular Hosts Adaptive, Fluxional, and Degradable," *Accounts of Chemical Research* 57, no. 4 (2024): 602–612.

344. T. Marchetti, L. Goldin, B. M. W. Roberts, et al., "Near-Quantitative Formation of Imines in Water With Allosteric Control," *Journal of the American Chemical Society* 148 (2026): 4615–4621.

345. H. C. Ates, P. Q. Nguyen, L. Gonzalez-Macia, et al., "End-to-End Design of Wearable Sensors," *Nature Reviews Materials* 7, no. 11 (2022): 887–907.

346. C. Jiang, G. Wang, R. Hein, N. Liu, X. Luo, and J. J. Davis, "Antifouling Strategies for Selective in Vitro and In Vivo Sensing," *Chemical Reviews* 120, no. 8 (2020): 3852–3889.

347. Y. Geng, W. J. Peveler, and V. M. Rotello, "Array-Based "Chemical Nose" Sensing in Diagnostics and Drug Discovery," *Angewandte Chemie International Edition* 58, no. 16 (2019): 5190–5200.

348. Y. Zhang, S. Gao, H. Li, et al., "Design Principles of Nanosensors for Multiplex Detection of Contaminants in Food," *Small* 21, no. 26 (2025): e2412271.

349. S. Stewart, M. A. Ivy, and E. V. Anslyn, "The Use of Principal Component Analysis and Discriminant Analysis in Differential Sensing Routines," *Chemical Society Reviews* 43, no. 1 (2014): 70–84.

350. V. Croué, S. Goeb, G. Szalóki, M. Allain, and M. Sallé, "Reversible Guest Uptake/Release by Redox-Controlled Assembly/Disassembly of a Coordination Cage," *Angewandte Chemie International Edition* 55, no. 5 (2016): 1746–1750.

351. G. Szalóki, V. Croué, V. Carré, et al., "Controlling the Host-Guest Interaction Mode Through a Redox Stimulus," *Angewandte Chemie International Edition* 56, no. 51 (2017): 16272–16276.

352. K. Yazaki, S. Noda, Y. Tanaka, Y. Sei, M. Akita, and M. Yoshizawa, "An $M_2$ $L_4$ Molecular Capsule With a Redox Switchable Polyradical Shell," *Angewandte Chemie International Edition* 55, no. 48 (2016): 15031–15034.

353. S. Bera, N. Goujon, M. Melle-Franco, D. Mecerreyes, and A. Mateo-Alonso, "A Redox-Active Organic Cage as a Cathode Material With Improved Electrochemical Performance," *Chemical Science* 15, no. 36 (2024): 14872–14879.

354. L. An, P. De La Torre, P. T. Smith, M. R. Narouz, and C. J. Chang, "Synergistic Porosity and Charge Effects in a Supramolecular Porphyrin Cage Promote Efficient Photocatalytic $CO_2$ Reduction**," *Angewandte Chemie International Edition* 62, no. 5 (2023): e202209396.

355. C. Liu, Z. Wang, H. Wang, and J. Jiang, "Recent Advances in Porous Organic Cages for Energy Applications," *Chemical Science* 15, no. 46 (2024): 19188–19211.

356. H. Y. Lin, Y. T. Wang, X. Shi, H. B. Yang, and L. Xu, "Switchable Metallacycles and Metallacages," *Chemical Society Reviews* 52, no. 3 (2023): 1129–1154.

357. V. Amendola, M. Boiocchi, B. Colasson, et al., "Redox Active Cage for the Electrochemical Sensing of Anions," *Inorganic Chemistry* 47 (2008): 4808–4816.

358. K. D. Legg and D. M. Hercules, "Electrochemically Generated Chemiluminescence of Lucigenin," *Journal of the American Chemical Society* 91, no. 8 (1968): 1902–1907.

359. J. D. Luttmer and A. J. Bard, "Electrogenerated Chemiluminescence: 34. Photo-Induced Electrogenerated Chemiluminescence and Up-Conversion at Semiconductor Electrodes," *Journal of The Electrochemical Society* 126 (1979): 414–419.

360. A. Fiorani, G. Valenti, M. Iurlo, M. Marcaccio, and F. Paolucci, "Electrogenerated Chemiluminescence: A Molecular Electrochemistry Point of View," *Current Opinion in Electrochemistry* 8 (2018): 31–38.

361. Y. Wang, J. Liu, Y. Niu, et al., "Tetraphenylethene-Based Multicomponent Platinum (II) Metallacages With Tunable Luminescence and Aggregation-Induced Electrochemiluminescence Properties," *Advanced Optical Materials* 11, no. 15 (2023): 2202940.

362. J. Tong, Y. Cao, Y. W. Zhang, et al., "Chiral-at-Cage Carboranes for Circularly Polarized Luminescence and Aggregation-Induced Electro-

chemiluminescence," *Angewandte Chemie International Edition* 61, no. 45 (2022): e202209438.

363. L. Turcani, R. L. Greenaway, and K. E. Jelfs, "Machine Learning for Organic Cage Property Prediction," *Chemistry of Materials* 31, no. 3 (2018): 714–727.

364. M. H. Du, Y. Dai, L. P. Jiang, et al., "Exploration and Insights on Topology Adjustment of Giant Heterometallic Cages Featuring Inorganic Skeletons Assisted by Machine Learning," *Journal of the American Chemical Society* 145, no. 42 (2023): 23188–23195.

365. Q. Yuan, F. T. Szczypinski, and K. E. Jelfs, "Explainable Graph Neural Networks for Organic Cages," *Digital Discovery* 1, no. 2 (2022): 127–138.

366. A. R. Basford, S. K. Bennett, M. Xiao, et al., "Streamlining the Automated Discovery of Porous Organic Cages," *Chemical Science* 15, no. 17 (2024): 6331–6348.

367. P. Kalhor, N. Jung, S. Bräse, C. Wöll, M. Tsotsalas, and P. Friederich, "Functional Material Systems Enabled by Automated Data Extraction and Machine Learning," *Advanced Functional Materials* 34, no. 20 (2023): 2302630.

368. Y. Luo, S. Bag, O. Zaremba, et al., "MOF Synthesis Prediction Enabled by Automatic Data Mining and Machine Learning**," *Angewandte Chemie International Edition* 61, no. 19 (2022): e202200242.

369. J. A. Stebani, I. Iribarren Aguirre, G. A. Siddiqui, D. Wragg, A. Gagliardi, and A. Casini, "Computational Workflow to Unravel the Structural Dynamics of Supramolecular Metallacages in Solution," *Journal of Chemical Theory and Computation* 21, no. 23 (2025): 12278–12288.

## Biographies

**Rabia Zahid** completed her Master's degree in Physics at the Bonn–Cologne Graduate School of Physics and Astronomy (BCGS), University of Bonn, Germany, and her Bachelor's degree in Physics at Forman Christian College, Pakistan. She is currently a PhD candidate in Chemistry at the Institute of Nanotechnology (INT), Karlsruhe Institute of Technology (KIT), Germany, supervised by Dr. Pierre Picchetti and co-supervised by Prof. Stefanie Dehnen, with funding from the Fonds der Chemischen Industrie (Chemical Industry Fund, FCI). Her research focuses on the synthesis of hybrid organic–inorganic nanomaterials with enzyme-like properties, harnessing supramolecular chemistry for biomedical applications.

**Martina Viola** is a postdoctoral researcher at the Biointerface Laboratory of Empa, with expertise in chemistry, biomaterials and biofabrication. During her Ph.D. at UMC Utrecht within the Marie Curie COFUND–Horizon 2020 program, she worked on silk fibroin modification for biofabrication and regenerative medicine, focusing on polymer synthesis, hydrogel engineering and 3D printing for musculoskeletal applications. As a postdoc, she develops bioadhesive and antimicrobial hydrogels for corneal ulcer treatment and, since 2025, has collaborated with Dr. Pierre Picchetti (KIT) on hybrid DNA–polymer hydrogels functionalized with organosilica nanoparticles for targeted drug delivery.

**Maria Vittoria Balli** is currently pursuing her PhD under the supervision of Prof. Luca Prodi, in the Luminescent Nanomaterials and Sensors for Health and Environment research group of the University of Bologna. Her research focuses on the investigation and development of innovative luminescence- and electrochemiluminescence-based biosensors for healthcare applications. As part of the European Union's Horizon Europe EIC Pathfinder Open Programme project "ECLIPSE", she was a visiting researcher at the Institute of Nanotechnology (INT) at the Karlsruhe Institute of Technology (KIT) in Germany, where she worked on the design and characterization of cucurbit[*n*]uril-based chemosensors.

**Dr. Guillermo Moreno-Alcántar** obtained his PhD from the Universidad Nacional Autónoma de México (UNAM) in 2018. Soon after, he joined the group of Prof. Luisa De Cola at the prestigious Supramolecular Science and Engineering Institute (ISIS) in Strasbourg, France. In 2021, he was selected as a Carl Friedrich von Siemens Research Fellow of the Alexander von Humboldt Foundation to start his research on gold-containing metallacages as bioactive agents, co-hosted by the groups of Professors Angela Casini and Roland A. Fischer at the Department of Chemistry of the Technical University of Munich (TUM), Germany. In 2023, he joined the SMARTdrugs team as part of the Casini group to pursue the development of metallacage-based theranostic platforms. In 2026, he started his independent research group at CIC biomaGUNE, funded by a Ramón y Cajal grant. The Supramolecular Inorganic Biosystems Lab aims to study inorganic self-assembled structures in living environments for biomedical purposes.

**Pierre Picchetti** obtained his Ph.D. in Chemistry in 2020 in France, from the University of Strasbourg, under the supervision of Prof. Luisa De Cola, where he worked on the development of stimuli-responsive drug nanocarriers for biomedical applications. He subsequently joined the group of Prof. Frank Biedermann at the Institute of Nanotechnology (INT) at the Karlsruhe Institute of Technology (KIT) in Germany as a postdoctoral fellow, working on the design of supramolecular chemosensors for bioanalyte detection. He began his independent research in March 2024 as a group leader (Liebig Fellow, funded by the Fonds der Chemischen Industrie, FCI) at the INT and was appointed a KIT Associate Fellow the following year. His research interests include supramolecular and materials chemistry, with a particular emphasis on developing bottom-up synthesis approaches and the precise engineering of nanomaterials that mimic natural enzymes for applications ranging from catalysis to drug delivery and analyte detection.